RESOLVING ELECTRON TRANSPORT PATHWAYS IN THE SELENATE RESPIRING BACTERIUM *THAUERA SELENATIS.*

Submitted by

Elisabeth Clare Lowe

To the University of Exeter as a thesis for the degree of Doctor of Philosophy in Biological Sciences, July 2008.

I certify that all material in this thesis which is not my own work has been identified and that no material has previously been submitted and approved for the award of a degree by this or any other University.

Elisabeth Clare Lowe

Acknowledgements

I would like to thank Clive Butler for all his help, support, encouragement and enthusiasm, especially during the move to Exeter and my last few months in the lab. Thanks to Ian Singleton for help and enthusiasm during my time in Newcastle. I also owe huge thanks to everyone in Team Butler, past and present, Carys Watts for helping me get started and all the help with the *Thauera* preps, Auntie Helen for being brilliant, Jim Leaver for rugby, beer, tea-offs and 30 hour growth curves and Lizzy Dridge for being a great friend and scientific team member, in and out of the lab.

Thanks also to everyone in M3013 at the start of my PhD and everyone in the Biocat at the end, for lots of help, borrowing of equipment and most importantly, tea. Thanks to AFP for help, tea breaks and motivation, especially during the writing period.

Thank you to everyone who has been generous with their time and equipment, namely Prof. David Richardson at UEA for the redox potentials, Dr Jo Santini at UCL for helpful discussions, Prof. Jeremy Lakey at Newcastle for the SPR and spectra and last but definitely not least, Prof. Rick Lewis at Newcastle for letting me use his lab and equipment. I am very grateful for their help. Thanks also to the BBSRC for funding the committee studentship.

Huge thanks to Jon for being fantastic, supportive and helping me so much with science, writing and keeping me positive, I hope you know how much it means to me.

Finally, massive thanks to my family, Mick, Suze and James, your generosity and love have made this so much easier for me during the ups and downs; your support (not just financial!) has been amazing and I can’t thank you enough.

Abstract

The Gram negative bacterium *Thauera selenatis* is able to respire with selenate as the sole terminal electron acceptor, utilising a periplasmic selenate reductase enzyme to reduce selenate to selenite. Previous characterisation of this enzyme has shown that it is a heterotrimeric molybdo-enzyme (SerABC) of the dimethylsulfoxide reductase family, containing a Mo-*bis* molybdopterin guanine dinucleotide co-factor, Fe-S clusters and a *b*-type haem (Schroder *et al*., 1997, J Biol Chem, **272**: 23765-68, Dridge *et al*., 2007, Biochem J, **408**: 19-28). In order to elucidate the electron transport pathway to selenate reductase, and how it can generate a proton motive force, detailed study was required. Firstly, the redox potential of the *b*-haem of SerC was determined by optical redox titration to be +234 mV. The *serC* gene was cloned and expressed heterologously in *E. coli*, but the protein was incorrectly folded into inclusion bodies, and attempts to refold and reconstitute SerC with haem were unsuccessful. A profile of *c*-type cytochromes in *T. selenatis* was undertaken, and characterisation of a number of cytochromes was carried out. Two cytochromes were purified, cyt*c*7 and cyt*c*4, and cyt*c*4 was shown to be able to donate electrons to SerABC *in vitro*. Protein sequence was obtained by N-terminal sequencing and LC-MS/MS, and assigned cyt*c*4 to the cytochrome c_4 family of dihaem cytochromes. Redox potentiometry combined with UV-visible and electron paramagnetic spectroscopy showed that cyt*c*4 is a dihaem cytochrome with a redox potential of +282 mV and both haems are predicted to have His-Met ligation. To investigate the role of membrane bound cytochromes in selenate respiration, PCR with degenerate primers amplified a partial gene coding for quinol: cytochrome c oxidoreductase (QCR). A microplate growth method was developed to monitor growth of *T. selenatis* under reproducible conditions, and used to analyse the effect of respiratory chain inhibitors on growth under different conditions. Aerobic metabolism was unaffected by QCR inhibitors, while nitrite reduction was totally inhibited, linking nitrite reduction to the generation of a proton motive force by the QCR. The QCR inhibitor myxothiazol partially inhibited selenate respiration, showing that some electron flux is via the QCR, but total inhibition of selenate respiration was achieved by combining myxothiazol with the more general inhibitor 2-n-heptyl-4-hydroxyquinoline N-oxide (HQNO). These data suggest that electron transfer to selenate reductase occurs via a branched pathway, in which one route is inhibited by myxothiazol and the other by HQNO. Electron transfer via a QCR and a dihaem cytochrome c_4 is a novel route for a member of the dimethylsulfoxide reductase family of molybdo-enzymes.

List of abbreviations

Standard abbreviations are used without definition in accordance to the instructions for authors for submission to the Biochemical Journal (www.biochemj.org). The following abbreviations are also provided for the reader.

Å	Angstrom (10^{-10} m)
ANAMMOX	anaerobic ammonium oxidation
Mo-*bis*MGD	molybdopterin guanine dinucleotide
BLAST	basic local alignment search tool
CAPS	N-Cyclohexyl-3-aminopropanesulfonic acid
Clr	chlorate reductase
Ddh	dimethylsulfide dehydrogenase
Dor	DMSO reductase
Ebd	ethylbenzene dehydrogenase
EPR	electron paramagnetic resonance
ETC	electron transport chain
Fdh	formate dehydrogenase
GF	gel filtration
GHz	gigahertz
HCl	hydrochloric acid
HIC	hydrophobic interaction chromatography
HQNO	2-n-Heptyl-4-hydroxyquinoline N-oxide
IPTG	isopropyl β-D-galactopyranoside
K	Kelvin
kDa	kilo Dalton
K_m	Michaelis constant
K_s	substrate affinity constant
LB	Luria-Bertani
M	molar concentration
ma	milliamps
MES	2-Morpholinoethanesulfonic acid
MOPS	3-(N-Morpholino) propanesulfonic acid
mT	millitesla

mW	microwave
MW	molecular weight
MWCO	molecular weight cut-off
μ_{max}	maximum specific growth rate
Nap	periplasmic nitrate reductase
Nar	membrane bound nitrate reductase
nm	nanometre
OD	optical density
PIC	protease inhibitor cocktail
PIPES	piperazine-1,4-*bis*(2-ethanesulfonic acid)
PMF	proton-motive force
rpm	revolutions per minute
S	substrate
Tat	twin-arginine translocase
TBE	Tris-borate-EDTA
TFB	transformation buffer
TMAO	trimethylamine N-oxide
Tor	TMAO reductase
Tris	Tris (hydroxymethyl) aminoethane
V	Volts
V_{max}	maximum velocity
v/v	volume by volume
w/v	weight by volume
w/w	weight by weight
X-gal	5-Bromo-4-chloro-3-indolyl β-D-galactopyranoside

Table of Contents

List of Figures

List of tables

1. Introduction

The ability to generate ATP is essential to life, and can be achieved by a complex system of proteins known as the electron transport chain (ETC). The exact components of this chain vary depending on the organism, but the overall result is the same – generation of ATP from ADP and P_i. The generation of ATP is powered by a proton gradient across a membrane, an idea which is conceptually simple, but in reality requires a great number of proteins and utilises complex redox chemistry. The complexes involved in respiration can consist of a large number of subunits and bind a variety of prosthetic groups. In order to place this work in context, a summary of the electron transfer chain in humans is presented below.

In humans, respiration occurs in the mitochondria, which is thought to have evolved from a symbiotic relationship with an α-proteobacterium capable of aerobic metabolism (Dyall *et al.*, 2004). Carbon sources are oxidized to yield electrons in the form of NADH (reduced nicotinamide adenine dinucleotide) and $FADH_2$ (reduced flavin adenine dinucleotide), high energy electron donors. These donors pass their electrons down a chain of proteins of increasing redox potential, in a process called oxidative phosphorylation, and finally to O_2 which is reduced to H_2O (Nicholls & Ferguson, 2002). The key protein complexes involved in this electron transfer chain are located in and around the mitochondrial inner membrane. While transferring electrons down this chain, these proteins produce a proton (H^+) gradient (PMF – the proton motive force) across the inner membrane which can be used to power ATP synthase, catalysing the formation of ATP (adenosine 5'-triphosphate) from ADP (adenosine 5'-diphosphate). The PMF is composed of two components, the concentration gradient of protons (ΔpH), and also the electrical charge resulting from the charge of the protons ($\Delta\psi$).

There are six main proteins/protein complexes involved in mitochondrial respiration, as well as lipid soluble co-factors called quinones in the membrane, and our understanding of these complexes has been greatly enhanced by structural biology (see figure 1.1). Electron input occurs through two complexes, NADH dehydrogenase and succinate dehydrogenase, which oxidize NADH and succinate respectively, and transfer their electrons to quinone (Q), reducing it to quinol (QH_2). These reduced quinols in the membrane are known as the Q-pool.

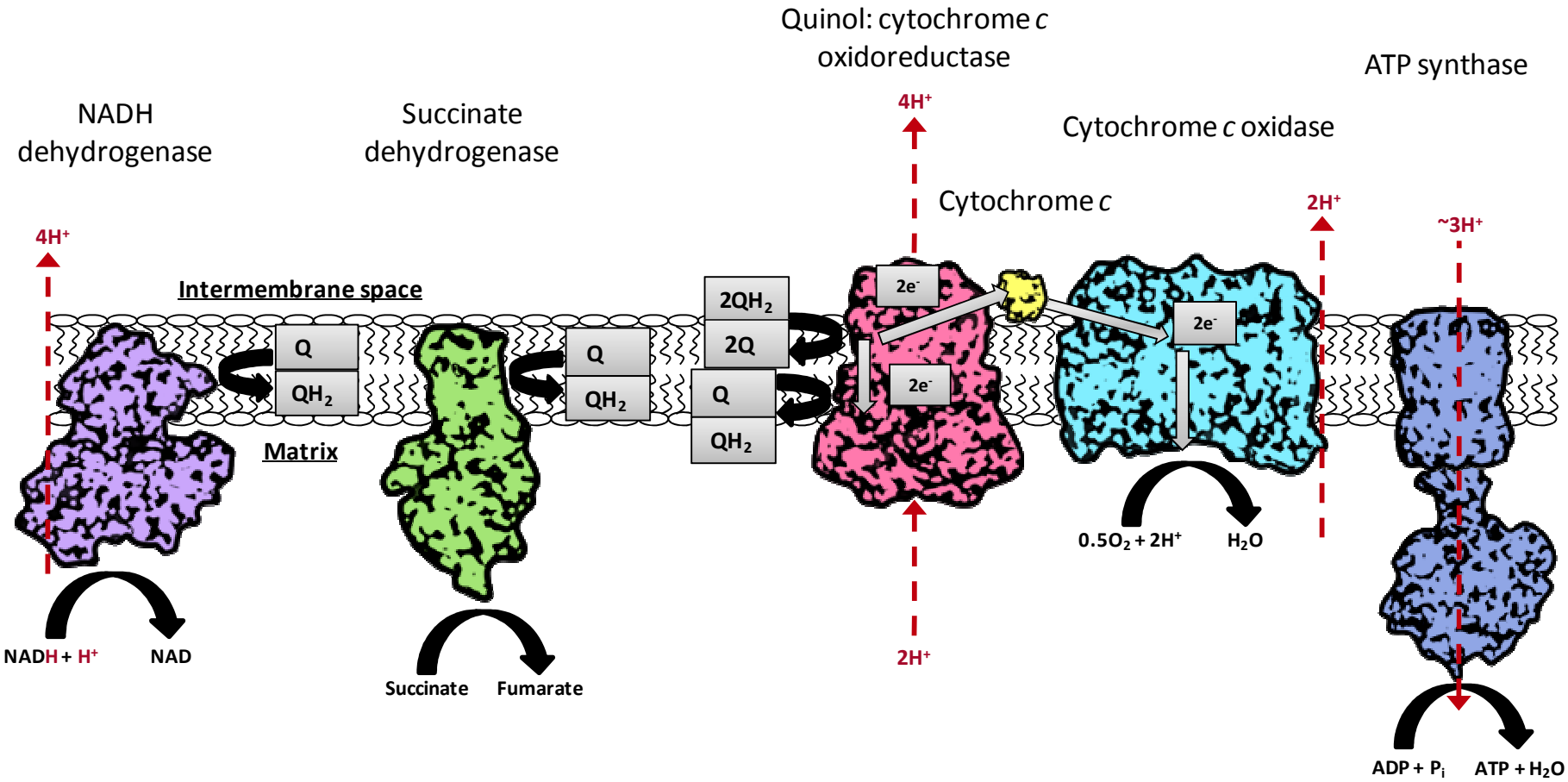
NADH dehydrogenase
Succinate dehydrogenase
Quinol: cytochrome c oxidoreductase
Cytochrome c oxidase
ATP synthase
Cytochrome c
4H+
2H+
~3H+
Intermembrane space
Matrix
Q
QH2
2QH2
2Q
2e-
NADH + H+
NAD
Succinate
Fumarate
0.5O2 + 2H+
H2O
ADP + Pi
ATP + H2O

Figure 1.1: The mitochondrial electron transport chain.

Cartoons of protein complexes are based on the structures deposited in the PDB, codes are as follows: NADH dehydrogenase - 2FUG (the structure of mitochondrial NADH dehydrogenase has not been solved so that of *Thermus thermophilus* was used) (Sazanov & Hinchliffe, 2006), Succinate dehydrogenase – 1YQ3 (Huang *et al.*, 2006), Quinol-cytochrome *c* oxidoreductase – 1KYO (Lange & Hunte, 2002), Cytochrome *c* – 1HRC (Bushnell *et al.*, 1990), Cytochrome *c* oxidase – 1OCC (Tsukihara *et al.*, 1996), ATP synthase – 1QO1 (F_o)(Stock *et al.*, 1999) and 1BMF (F_1)(Abrahams *et al.*, 1994). Q – quinone and QH_2 – quinol.

Electrons are removed from the Q-pool by a dimeric quinol: cytochrome *c* oxidoreductase (QCR) (also known as the cytochrome bc_1 complex) using a process called the Q-cycle. The QCR possesses two *b*-type haem groups of different redox potentials known as b_H (high potential) and b_L (low potential), which occupy sites in the QCR called Q_i and Q_o respectively, as well as a Rieske iron-sulfur cluster and cytochrome c_1. When one molecule of quinol is oxidised by the b_L haem, it yields two electrons, one which is passed on to the Rieske [2Fe-2S] cluster and cytochrome c_1, and the other is passed to the b_H haem to partially reduce a quinone molecule to semiquinone. It also releases two protons into the intermembrane (IM) space. When a second molecule of quinol is oxidised in the same way, this results in another electron being transferred to downstream electron acceptors via the Rieske cluster and cytochrome c_1, as well as one electron moving to the b_H haem so the semiquinone can be fully reduced to quinol. In this way, two molecules of quinol are oxidised, two electrons are transferred to the next step in the ETC, four protons are transferred into the intermembrane space and two are consumed in the matrix by the regeneration of one quinone to quinol. This Q-cycle allows the QCR to act as the mediator between the two electron carrier quinol, and the subsequent one electron carriers such as cytochrome *c*, as well as contributing to the proton gradient across the inner membrane.

The one electron carrier which receives electrons from cytochrome c_1 of the QCR is cytochrome *c*, a soluble protein loosely associated with the membrane. Cytochrome *c* then passes electrons to cytochrome *c* oxidase, which catalyses the reduction of O_2 to H_2O, consuming two matrix protons in the process, as well as translocating two protons into the IM space. Three out of the four main complexes therefore contribute to the PMF by translocating protons into the IM space during electron transfer, thereby generating a proton gradient to be used by ATP synthase.

Mitochondrial ATP synthase consists of two complexes, F_1 and F_o. The F_o complex is intergrated into the membrane and acts as the proton pore, while the F_1 complex is the catalytic centre. ATP is synthesised using a remarkable mechanism of rotary catalysis; F_1 contains three α and three catalytic β subunits arranged alternately, the β subunits have different nucleotide binding affinity induced by the rotation of an asymmetric central stalk (γ), which is in turn powered by the proton flow through the F_o complex. The change in binding affinity leads to catalysis of the formation, and then release of ATP (Boyer, 1997, Stock *et al.*, 2000).

Interestingly, NADH dehydrogenase, QCR and cytochrome *c* oxidase (also known as complexes I, III and IV respectively) have been shown to form various supercomplexes in the mitochondrial membrane, the most common are I + III_2, III_2 + IV_{1-2} and I + III_2 + IV_{1-4}. The supercomplexes are thought to have a role in increasing the rate of electron transfer, and possibly in regulating respiration (for a review, see Boekema and Braun 2007). This supramolecular assembly is not limited to mitochondria however, as complexes consisting of I + III_4 + IV_4 have been discovered in the membrane of the bacterium *Paracoccus denitrificans* (Stroh *et al.*, 2004)

1.1. Bacterial respiration

Humans are obligate aerobes and must use oxygen as their terminal electron acceptor during respiration, whereas prokaryotes possess a great deal more flexibility in their respiratory chains, allowing them to colonise a wide range of environments and survive in extreme conditions. Bacteria are able to use a wide variety of terminal electron acceptors (see Richardson (2000) for a review), including nitrogen oxyanions (Tavares *et al.*, 2006), elemental sulfur and sulfur oxyanions (Lie *et al.*, 1999, McCrindle *et al.*, 2005), halogenated organics (Louie & Mohn, 1999, van de Pas *et al.*, 1999, Futagami *et al.*, 2008), metalloid oxyanions such as selenate and arsenate (Stolz & Oremland, 1999, Stolz *et al.*, 2006), transition metals such as Fe and Mn (Lovley *et al.*, 2004), and radionuclides (Lloyd & Lovley, 2001). Both Gram positive and Gram negative bacteria exhibit a high degree of respiratory flexibility, but this study will concentrate on respiration in the Gram negative bacteria.

The generation of a PMF across the bacterial inner membrane can occur via a redox loop, where substrate oxidation on the ψ+ve (periplasmic) side of the membrane is coupled with reduction of a substrate on the ψ-ve side. The best known example is the formate dehydrogenase (Fdh-N) and nitrate reductase (Nar) loop, studied in *Escherichia coli* and *Paracoccus denitrificans* (see figure 1.2). Fdh-N oxidises formate to CO_2 and H^+ in the periplasm, utilising the two electrons from this reaction to reduce quinone at the cytoplasmic face of the membrane, consuming two cytoplasmic protons in the process. Nar oxidises this diffusible quinol at the periplasmic face of the membrane, and uses the electrons to reduce nitrate to nitrite in the cytoplasm, consuming a further two cytoplasmic protons (Jormakka *et al.*, 2003, Richardson & Sawers, 2002).

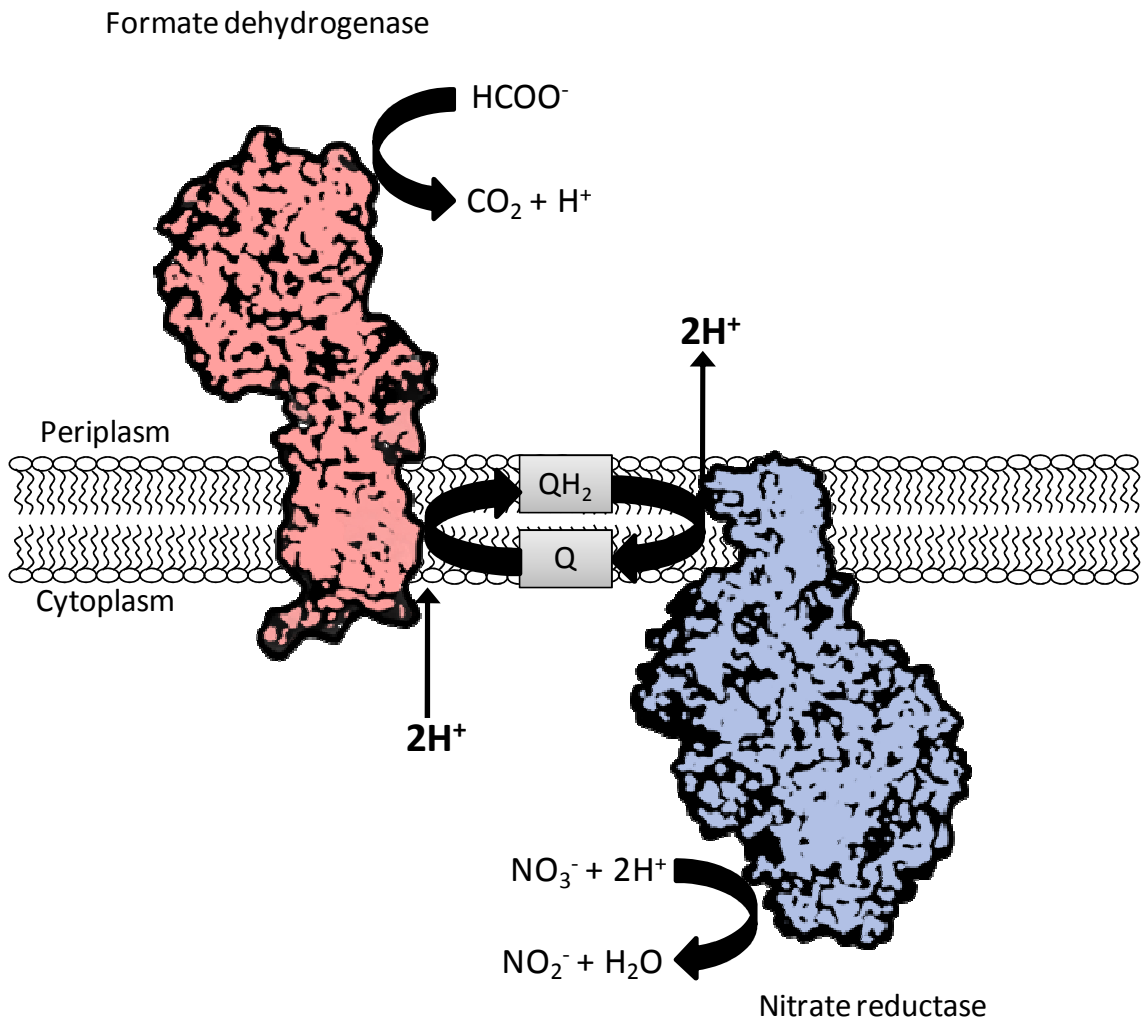

Figure 1.2: The formate dehydrogenase-N – nitrate reductase redox loop.

PDB entries used to generate cartoons of the structures are as follows, formate dehydrogenase-N – 1KQF (Jormakka *et al.*, 2002), membrane bound nitrate reductase – 1Q16 (Bertero *et al.*, 2003). This redox loop generates a PMF by consuming cytoplasmic protons and releasing periplasmic protons during nitrate reduction and formate oxidation respectively.

Alternatively, a PMF can be generated in a similar way to oxidative phosphorylation in the mitochondrial ETC, by linking the reduction of terminal electron acceptors in the periplasm to proton pumping complexes such as the QCR and primary dehydrogenases.

Bacteria vary in the type and number of respiratory complexes they express, and a major difference is the presence or absence of a QCR. The two bacteria mentioned above, *E. coli* and *P. denitrificans* differ here, *E. coli* does not express a QCR, whereas *P. denitrificans* does. Both exhibit a great deal of flexibility in their ETCs (figure 1.3). *P. denitrificans* for example, has three terminal oxidases, two of which are linked to the QCR to generate PMF (Otten *et al.*, 2001). Of these two, one is expressed under high oxygen conditions (cytochrome aa_3 oxidase), whereas the other, higher affinity oxidase is expressed in low oxygen levels (cytochrome cbb_3 oxidase). This allows the bacterium to grow at different oxygen tensions, while keeping the central PMF generating ETC the same (Richardson, 2000).

1.2. Molybdo-enzymes in bacterial respiration

There is a great deal of variety not only in the terminal electron acceptors that bacteria are able to utilise, but in the oxidoreductase enzymes which are used for this reaction. They contain a variety of co-factors to enable the transfer of electrons to their active sites, and to catalyse the reduction of the substrate. A large group of these enzymes use a molybdenum containing co-factor at their active site, as Mo can cycle through three oxidation states (Mo (IV) – Mo (V) – Mo (VI)). In biological systems, Mo is found in two forms, the multinuclear molybdenum centre of nitrogenase enzymes (Howard & Rees, 2006), and in the mononuclear active site of a group of oxidoreductases which transfer an oxygen atom to/from substrate acceptor/donor molecules (Hille, 1996).

Within the mononuclear molybdo-enzymes, the Mo atom is commonly found within a molybdopterin ring (MPT), a tricyclic pterin derivative which co-ordinates the Mo through its sulfur atoms. In a subset of these enzymes, two MPTs are modified by the addition of a guanine-diphosphate to each (Kisker *et al.*, 1998, McEwan *et al.*, 2002). This dinucleotide co-factor is known as molybdopterin guanine dinucleotide or Mo-*bis*(MGD) (see figure 1.4) and was first determined from the crystal structure of *Rhodobacter sphaeroides* dimethylsulfoxide (DMSO) reductase (Schindelin *et al.*, 1996).

A

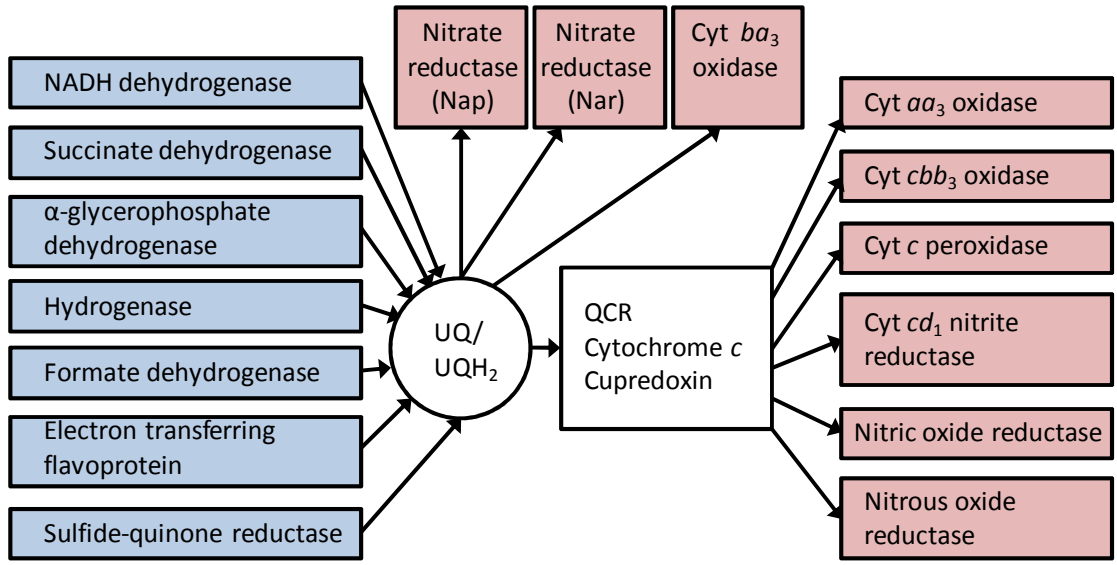

B

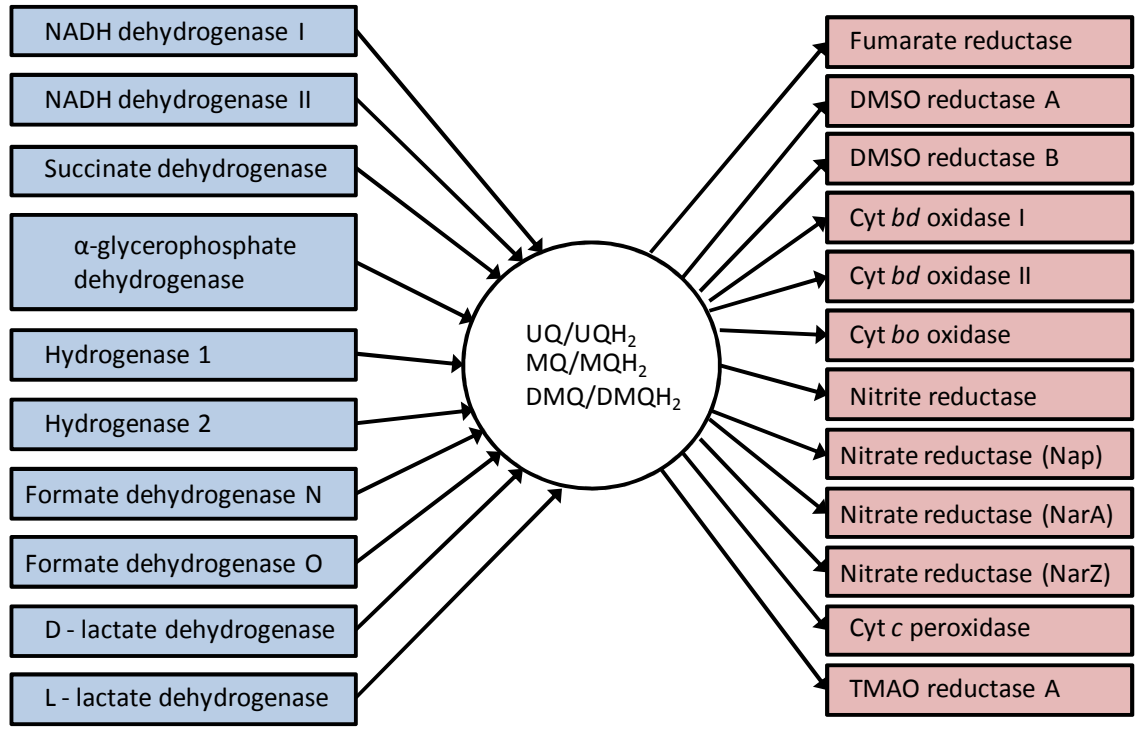

Figure 1.3: Electron transport chains of *P. denitrificans* and *E. coli*.

Blue boxes indicate points of electron input to the Q-pool, pink boxes represent enzymes responsible for electron output from the Q-pool. A: *P. denitrificans*, B: *E. coli*. Images adapted from Richardson, 2000. UQ - ubiquinone, MQ – menaquinone, DMQ – demethylmenaquinone.

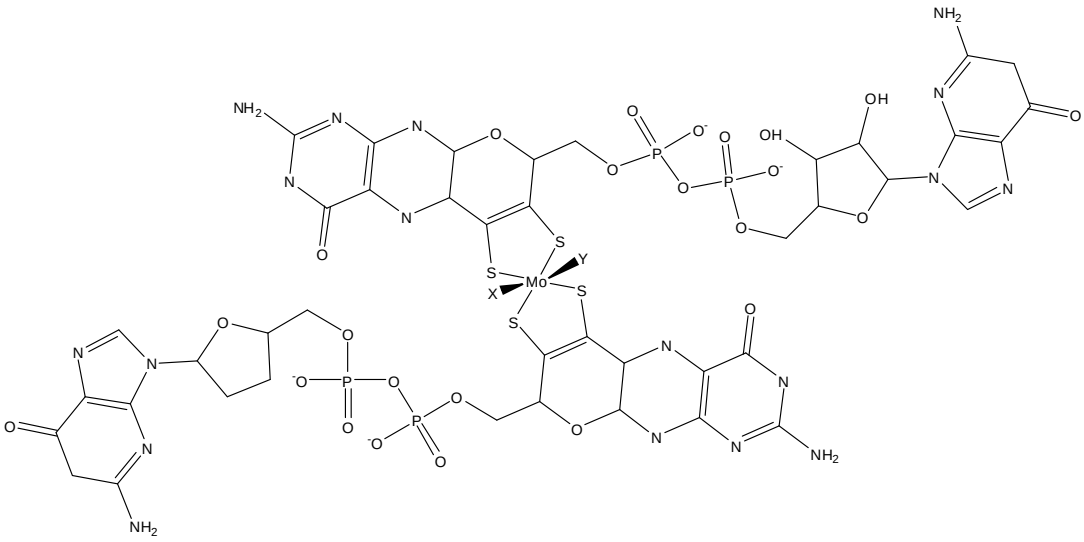

Figure 1.4: The structure of the molybdenum *bis*(MGD) cofactor.
The Mo is co-ordinated by four sulfur atoms, and two additional ligands, X and Y, which vary between the different groups in the DMSO reductase family.

The family containing this co-factor is therefore known as the DMSO reductase family of molybdo-enzymes, and they can be further divided into three types, depending upon differences within the N-terminal region of the catalytic subunit. Type I *bis*MGD enzymes such as periplasmic nitrate reductase, arsenite oxidase and formate dehydrogenase-H (Ellis *et al.*, 2001, Dias *et al.*, 1999, Boyington *et al.*, 1997) contain a cysteine rich motif (C-X_2-C-X_3-C-X_{27}-C) which co-ordinates a [4Fe-4S] cluster, and also a cysteine or selenocysteine side chain which is a ligand to the Mo of the *bis*MGD co-factor (McDevitt *et al.*, 2002b).

Type II *bis*MGD molybdo-enzymes contain a cysteine rich motif similar to that of the type I enzymes, except that the first cysteine may be replaced by a histidine, and an extra residue is found between the His and following Cys (H/C-X_3-C-X_3-C-X_{34}-C). This type of enzyme is exemplified by the membrane bound nitrate reductase (Blasco *et al.*, 2001), chlorate and perchlorate reductases from *Ideonella dechloratans* and *Dechloromonas agitata* (Bender *et al.*, 2005, Thorell *et al.*, 2003), DMSO reductase

from *E. coli* (McCrindle *et al.*, 2005), ethylbenzene dehydrogenase from *Aromatoleum aromaticum* (Kloer *et al.*, 2006), dimethylsulfide dehydrogenase from *Rhodovulum sulfidophilum* (McDevitt *et al.*, 2002b) and selenate reductase from *Thauera selenatis* (Schroder *et al.*, 1997). These type II enzymes have a highly conserved aspartate residue which co-ordinates the Mo either through a monodentate ligand as seen in the structures of ethylbenzene dehydrogenase and NarG (Jormakka *et al.*, 2004, Kloer *et al.*, 2006) or a bidentate ligand as seen in an alternative structure of NarG (Bertero *et al.*, 2003) and are therefore sometimes known as the 'D' group of molybdo-enzymes.

Type III Mo-*bis*MGD enzymes lack the [4Fe-4S] cluster in the catalytic subunit seen in both type I and II enzymes, and have a serine ligand co-ordinating the molybdenum. The trimethylamine oxide and dimethylsulfoxide reductase enzymes from *E. coli* and *Rhodobacter* sp. are examples of this type (McCrindle *et al.*, 2005).

1.3. Electron transfer to DMSO reductase family enzymes

Although there are common features between the enzymes of the DMSO reductase family of molybdo-enzymes, they differ in the topology of their subunits and the route by which electrons are transferred from the Q-pool to the catalytic subunit. They use a variety of membrane bound electron donors, and vary in both the number and orientation of their subunits. A summary of the topology and composition of some of these enzymes is given below and in figure 1.5 (page 27).

1.3.1. Membrane bound nitrate reductase (Nar)

The membrane bound nitrate reductase is found among a wide variety of bacterial species, both Gram positive and Gram negative, including soil bacteria such as *Bacillus subtilis* (Hoffmann *et al.*, 1995), and pathogens such as *Mycobacterium tuberculosis* and *Pseudomonas aeruginosa*, in which it is thought to aid the ability of the bacteria to thrive in the microaerobic environments of lung mucus in cystic fibrosis patients (Palmer *et al.*, 2007). The most comprehensively studied are the enzymes from *E. coli* and *P. denitrificans*. Nar is typically the first enzyme of denitrification (or ammonification), a key process of the inorganic nitrogen cycle. It consists of three subunits (NarGHI), and is found in the inner membrane, with its active site facing the cytoplasm. NarI (~ 19-25 kDa), the membrane spanning subunit contains two *b*-type haems, and is the site of quinol binding and oxidation, passing on electrons to the iron-

sulfur cluster containing subunit NarH (~52-64 kDa), and then on to the catalytic subunit NarG (~112-140 kDa) for the reduction of nitrate to nitrite. As described above, the orientation of NarGHI means that protons are consumed in the cytoplasm, and released in the periplasm, contributing to the PMF, so that nitrate reduction can support growth.

The structure of Nar from *E. coli* (Bertero *et al.*, 2003) has confirmed the presence and co-ordination of the electron transferring prosthetic groups present in NarGHI. The two low-spin haems of NarI (b_P and b_D) have redox potentials of +120 and +20 mV respectively (Blasco *et al.*, 2001) and both have *bis*-histidinyl co-ordination. NarH binds three [4Fe-4S] clusters (FS1-3) and one [3Fe-4S] cluster (FS4), which have redox potentials of +130, -420, -55 and +180 mV (FS1-FS4). The low potential of FS2 is an unusual feature, meaning that the high potential of the nitrate/nitrite couple (+440 mV) must be able to overcome this unfavourable drop in potential. A further [4Fe-4S] cluster (FS0) has been identified in the NarG subunit, with unusual co-ordination of one histidine and three cysteines (Bertero *et al.*, 2003, Jormakka *et al.*, 2004), which has since been shown to be a high-spin cluster with a redox potential of -55 mV (Rothery *et al.*, 2004). The molybdenum of the Mo-*bis*MGD co-factor is co-ordinated by the carboxylate group of an aspartate residue in addition to the four thiolate groups of the pterin co-factor.

1.3.2. Periplasmic nitrate reductase (Nap)

Nap is a periplasmic hetero-dimer consisting of the catalytic subunit NapA (~90 kDa) and the dihaem cytochrome *c* Nap B (~16 kDa). The interaction between these subunits can be strong, as found in *P. denitrificans* and *Rhodobacter sphaeroides* (Arnoux *et al.*, 2003), or weak, as seen in *E. coli* (Jepson *et al.*, 2007) (k_D = 0.5 nM for *R. sphaeroides* compared to 32 µM for *E. coli*). NapA also contains an FS0 iron-sulfur cluster in addition to the Mo-*bis*MGD, as seen in NarG. Electrons are typically passed from NapC, a tetra-haem membrane bound quinol dehydrogenase to NapB and then on to NapA, but an alternative pathway also exists. In *E. coli*, two further proteins termed NapG and NapH are found, both iron-sulfur proteins believed to oxidise ubiquinol and pass electrons to NapC, to allow further transfer to NapAB, while NapC itself oxidises menaquinol (Brondijk *et al.*, 2004). The high resolution structure of NapA from *Desulfovibrio desulfuricans* has shown that the Mo is solely co-ordinated by sulfur

ligands, four from the pterin co-factor, one from a cysteine residue and one sulfur atom, which was previously thought to be OH or water (Najmudin *et al.*, 2008).

Unlike Nar, Nap is not coupled to the generation of a PMF, as it catalyses nitrate reduction in the periplasm, and does not receive its electrons from a proton translocating membrane bound subunit. In *Paracoccus* species it is primarily expressed under aerobic conditions, allowing oxidative metabolism to provide ATP, and is thought to have a role in dissipating energy during growth on reduced carbon substrates (Sears *et al.*, 2000). In *E. coli* it is expressed in anaerobic, nitrate limited conditions and is thought to be important in scavenging nitrate (Richardson *et al.*, 2001). Nap is targeted to the periplasm after protein synthesis, and transported via the Tat (Twin-arginine translocase) system (Berks, 1996), which recognises a specific signal sequence and is involved in transporting fully folded proteins across the membrane (for more detail, see section 1.4.2).

1.3.3. Periplasmic facing nitrate reductase (pNar)

The pNar group of enzymes is very similar to Nar, in that they are membrane bound and possess two subunits in common, NarG and NarH. However, the catalytic site faces the periplasm (or outside of the cytoplasmic membrane in prokaryotes without two membranes), meaning that PMF cannot be generated in the same way as seen in the cytoplasmic facing Nar. These pNar enzymes are most commonly found in the archaea, such as *Haloferax mediterranei* and *Haloarcula marismortui* (Lledo *et al.*, 2004, Yoshimatsu *et al.*, 2007) and possess leader peptides targeting them to the outside of the cytoplasmic membrane via the Tat system (Martinez-Espinosa *et al.*, 2007). The pNarG subunits are smaller than those of the Nar enzymes but the Asp residue responsible for co-ordinating the Mo in Nar is conserved. Other than orientation, the main difference between Nar and pNar enzymes is the lack of a NarI subunit in the pNars. In its place are a variety of other subunits which could possibly function in a similar way to a QCR, with a Q-cycle, allowing periplasmic nitrate reduction to be electrogenic. A gene encoding a dihaem protein (*narC*) with similarity to the dihaem subunit of QCRs has been identified, along with *narB*, a gene predicted to encode a Rieske iron-sulfur protein. A further gene, *Orf7* which shows similarity to soluble *b*-type cytochromes found in other DMSO reductase family enzymes such as ethylbenzene dehydrogenase and selenate reductase, is postulated to receive electrons from this QCR-type enzyme and pass them along to NarGH (Martinez-Espinosa *et al.*, 2007).

1.3.4. DMSO reductase from *E. coli* (Dms)

DMSO reductase catalyses the reduction of dimethylsulfoxide (DMSO) to dimethylsulfide (DMS). In *E. coli*, this enzyme is a heterotrimer (DmsABC), anchored in the cytoplasmic membrane (McCrindle *et al*., 2005). Initially, it was thought that the catalytic subunits were cytoplasmic facing (Sambasivarao *et al.*, 1990), but evidence now shows that they are located on the periplasmic face (Stanley *et al.*, 2002). DmsC (30 kDa), the membrane anchor subunit, oxidises menaquinol and passes electrons to DmsB (23 kDa), which contains four [4Fe-4S] clusters. The catalytic subunit, DmsA (87 kDa) binds the Mo-*bis*MGD co-factor. *E. coli* can respire anaerobically using DMSO as terminal electron acceptor (McCrindle *et al*., 2005), but it is not clear how this periplasmic enzyme contributes to the PMF.

1.3.5. TMAO reductase from *E. coli* and DMSO reductase from *Rhodobacter* species (Tor/Dor)

Trimethylamine-N-oxide (TMAO) can be reduced to trimethylamine by *E. coli* TMAO reductase (TorAC), and DMSO reductase (DorAC) from *Rhodobacter* sp. (this enzyme can catalyse both TMAO and DMSO reduction, but has a higher affinity for DMSO) (McCrindle *et al*., 2005). These enzymes are grouped together here because they have a similar organisation of subunits. A periplasmic catalytic subunit (TorA/DorA) containing the Mo-*bis*MGD co-factor receives its electrons from a membrane bound multi-haem quinol dehydrogenase (TorC/DorC) of the NapC family, although these subunits bind five *c*-type haems, in contrast to the four found in NapC. Both *E. coli* and *Rhodobacter* sp. can utilise TMAO as a terminal electron acceptor, and although initially *Rhodobacter* was thought to use DMSO/TMAO reduction as a way of controlling redox balance when grown on reduced substrates, reduction has since been shown to contribute to the PMF (McEwan *et al.*, 1983).

1.3.6. Chlorate/perchlorate reductase (Clr/Pcr)

Chlorate/perchlorate (ClO_3^-/ClO_4^-) can be reduced to chlorite (ClO_2^-) by a number of reductases, but the bacterium must also possess a chlorite dismutase enzyme to remove toxic chlorite to be able to utilise chlorate as sole electron acceptor. Two bacteria capable of this feat are *Ideonella dechloratans* and *Dechloromonas agitata*. The chlorate reductase from *I. dechloratans* is a periplasmic heterotrimer (ClrABC), which can reduce chlorate but not perchlorate (Thorell *et al.*, 2003). ClrC is a mono *b*-haem

protein (Karlsson & Nilsson, 2005), and is thought to pass electrons to ClrB, the iron-sulfur subunit which is predicted to contain four Fe-S clusters. ClrA binds the Mo-*bis*MGD co-factor. It is not known however, how electrons are transferred from the Q-pool to this soluble enzyme. ClrA has a Tat signal sequence, and ClrB is thought to be translocated with ClrA, whereas ClrC has a Sec dependent signal sequence which targets unfolded proteins to the periplasm.

The perchlorate reductase (PcrABC) from *D. agitata* (and the related *D. aromatica*) has a similar subunit organisation as deduced from genome sequencing, with PcrA binding the molybdenum co-factor, and PcrB binding three [4Fe-4S] clusters and one [3Fe-4S] cluster (Bender *et al.,* 2005). The PcrC subunit however, differs from ClrC as it binds four *c*-type haems instead of one *b*-type as found in ClrC. There is also a downstream gene present which codes for a NapC/NirT type multi-haem cytochrome which could act as the membrane bound electron donor to PcrC.

1.3.7. Ethylbenzene dehydrogenase (Ebd)

A number of the enzymes of the DMSO reductase family catalyse the oxidation of a substrate rather than the reduction, so electrons pass from the catalytic subunit on to downstream acceptors. The ethylbenzene dehydrogenase (Ebd) from *Aromatoleum aromaticum* strain EbN1 is one such enzyme. It catalyses the oxidation of ethylbenzene to 1-(S)-phenylethanol in the periplasm (Kniemeyer & Heider, 2001) and shows high similarity to the chlorate reductases discussed previously. The structure of Ebd has been solved recently (Kloer *et al.,* 2006) and reveals a number of interesting facts. The EbdA subunit has high similarity with NarG and the structure shows that the Mo atom is co-ordinated with an aspartate residue and an oxo group as seen with NarG. The FS0 iron-sulfur cluster is also seen in EbdA. EbdB has the expected four iron-sulfur clusters, three of the [4Fe-4S] type and one [3Fe-4S], and their redox potentials are -15, -400, -8 and +70 mV for FS1-FS4 (Creevey *et al.,* 2008). The EbdC subunit which binds a single *b*-haem, shows unusual co-ordination of the haem by methionine and lysine residues, and has a high midpoint potential, +254 mV, which means that any downstream electron acceptor must also have a high potential, most likely a *c*-type cytochrome (Kloer *et al*., 2006). EbdA possesses a Tat leader sequence as with the others of this group, but unusually, EbdC does not have the Sec leader sequence seen for ClrC, so how it is targeted to the periplasm is unknown.

1.3.8. Dimethylsulfide dehydrogenase (Ddh)

Another of the enzymes which works in a 'reverse' direction to the reductase enzymes previously discussed is the DMS dehydrogenase (DdhABC) from *Rhodovulum sulfidophilum* which oxidizes DMS to DMSO. It is homologous to the Ebd and Clr enzymes, and the composition of subunits is the same. The redox potentials of some of the Fe-S clusters were recently determined and show the same pattern as those those determined for Nar and Ebd (Creevey *et al.*, 2008). The potentials of FS1-FS4 are +175, -337, +66 and +92 mV respectively. The potential of the haem was determined to be +324 mV, and it is thought that the electron acceptor is a cytochrome c_2, with a midpoint potential of +357 mV (McDevitt *et al.*, 2002b, Yoshida *et al.*, 2001). The lysine and methionine residues which are ligands to the haem in EbdC are conserved in the DdhC sequence.

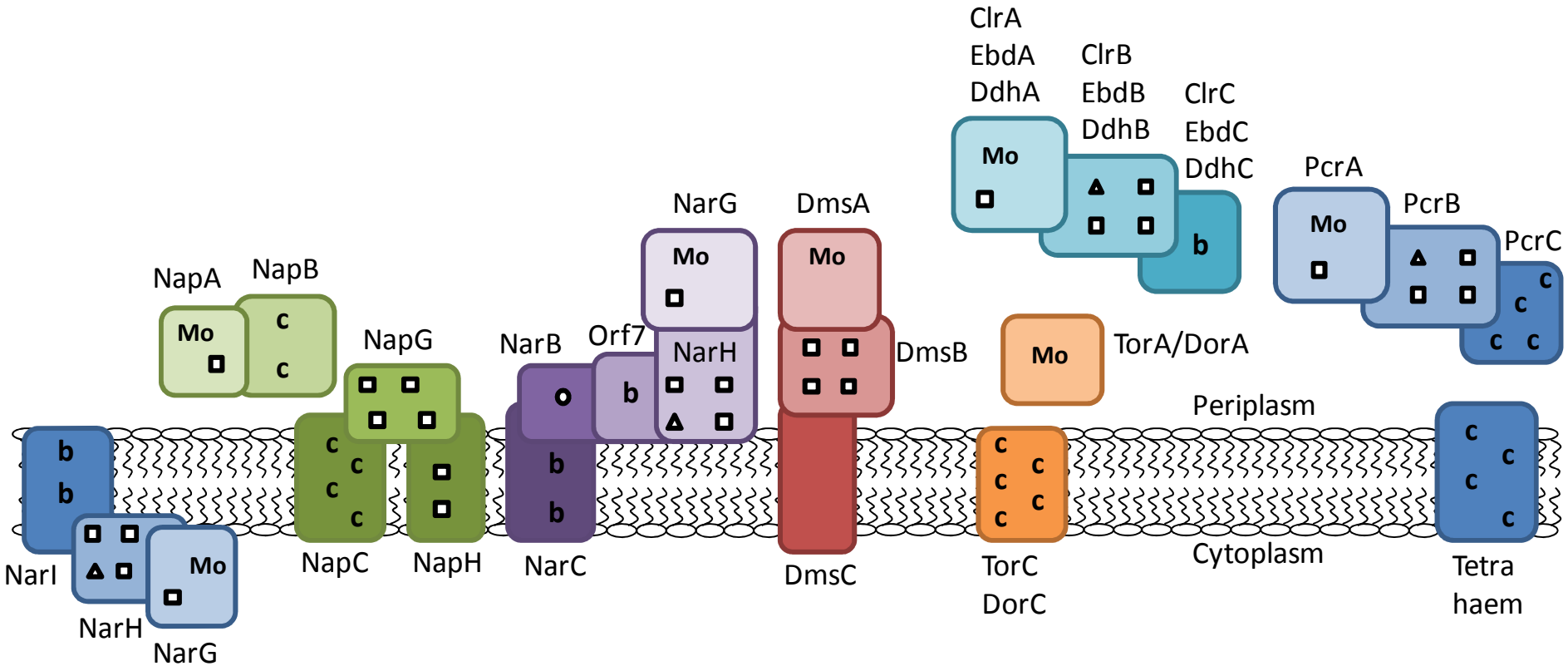

Figure 1.5: Topology of the DMSO reductase family of molybdo-enzymes.

Subunit organisation and cofactor composition of some molybdo-enzymes of the DMSO reductase family. Mo: Mo-*bis*MGD co-factor, b and c: *b* and *c*-type haems, squares: [4Fe-4S] clusters, triangles: [3Fe-4S] clusters, circles: Rieske [2Fe-2S] clusters.

1.4. Assembly of molybdo-enzymes

The molybdo-enzymes discussed here are complex proteins containing a variety of redox co-factors, and it is logical that their assembly and localisation to the correct membrane/compartment is an intricate process. Two export systems are implicated in their transport, the Sec and Tat systems, and each enzyme is expressed along with a chaperone type protein thought to aid folding and insertion of co-factors. All three parts of this process will be covered in more detail here.

1.4.1. The Sec system

The general secretory pathway (Sec) has been well characterised (Driessen *et al.*, 1998, Pugsley, 1993) and involves translocation of unfolded proteins from the cytoplasm through a membrane spanning pore called the translocase (figure 1.6a). SecB, a cytosolic chaperone binds the unfolded preproteins to protect them from degradation, and is recognised by SecA, part of the translocase complex, transferring the preprotein from SecB to SecA. The protein then passes through the translocase (SecYEG) in an ATP dependent process, N terminal first, and folds in the periplasm. This system is used to transport some subunits of the molybdo-enzymes discussed previously, namely those which contain *b* or *c*-type haem. The process by which soluble cytochromes *b* bind their haems is not well known, but the complex process involved in cytochrome *c* maturation has been studied in detail (Thony-Meyer, 2002, Stevens *et al.*, 2004). Cytochrome *c* maturation will be described further in section 1.5.2.

1.4.2. The Tat system

Complex proteins containing a number of co-factors need assembly in the cytoplasm, resulting in fully folded proteins which cannot be transported by the Sec system. In that case, proteins can be exported via the Twin-arginine translocase pathway (Tat), a Δp-dependent process which moves fully folded proteins across the cytoplasmic membrane (Berks, 1996, Santini *et al.*, 1998, Sargent *et al.*, 1998, Weiner *et al.*, 1998) (figure 1.6b). The system is so-called because it recognises a specific N-terminal signal sequence containing a twin arginine motif (S/T-R-R-x-F-L-K). The signal sequence consists of a basic n-region, a hydrophobic h-region and a hydrophilic c-region which is recognised by the signal peptidase. The twin arginine motif is found at the boundary of the n and h-regions (Berks *et al.*, 2005, Berks *et al.*, 2000). In *E. coli*, the minimal components of the Tat system are TatA, TatB and TatC. Initially, the signal peptide is

bound by the TatBC complex in the membrane, specifically the TatC protein (Alami *et al.*, 2003). The TatBC complex then associates with TatA in the membrane, an interaction which is dependent on Δp. A pore is predicted to open in TatA of up to 70 Å (Berks *et al*., 2000), allowing passage of the folded protein, which has its signal peptide cleaved when it reaches the periplasm by the peptidase LepB (Berks *et al*., 2005). The periplasmic molybdo-enzymes discussed above generally possess a single Tat leader sequence on the 'A' subunit (eg. ClrA, DdhA, EbdA) which somehow leads to both the A and B subunits both being translocated across the membrane. This form of translocation has been termed the 'hitchhiker mechanism' (Rodrigue *et al.*, 1999).

1.4.3. Chaperones for molybdo-enzymes

The operons containing genes for the molybdo-enzymes typically also contain a small soluble cytoplasmic protein which is predicted to act as a chaperone for protein folding and co-factor insertions. NarJ, the chaperone associated with the membrane bound nitrate reductase has been studied in the most detail, and has been shown to be essential for insertion of the Mo-*bis*MGD co-factor and production of a stable enzyme (Blasco *et al.*, 1998). Recently, NarJ has been shown to co-ordinate the insertion of FS0, assembly of subunits including the *b*-haems of NarI, and anchoring of the enzyme to the membrane (Lanciano *et al.*, 2007). The structures of several of these chaperones have been solved, TorD from *Shewanella massilia* (Tranier *et al*., 2003), DmsD from *Salmonella typhimurium* (Qiu *et al.*, 2008), and AF0173 from *Archaeoglobus fulgidus* (Kirillova *et al.*, 2007), the chaperone of a predicted pNar enzyme. A predicted signal peptide binding site has been identified on the surface of AF0173 (Kirillova *et al*., 2007).

A

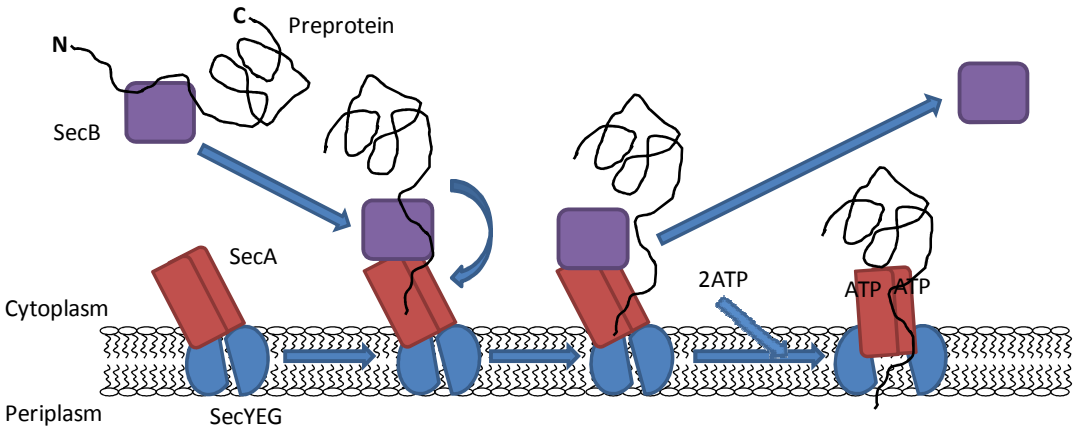

B

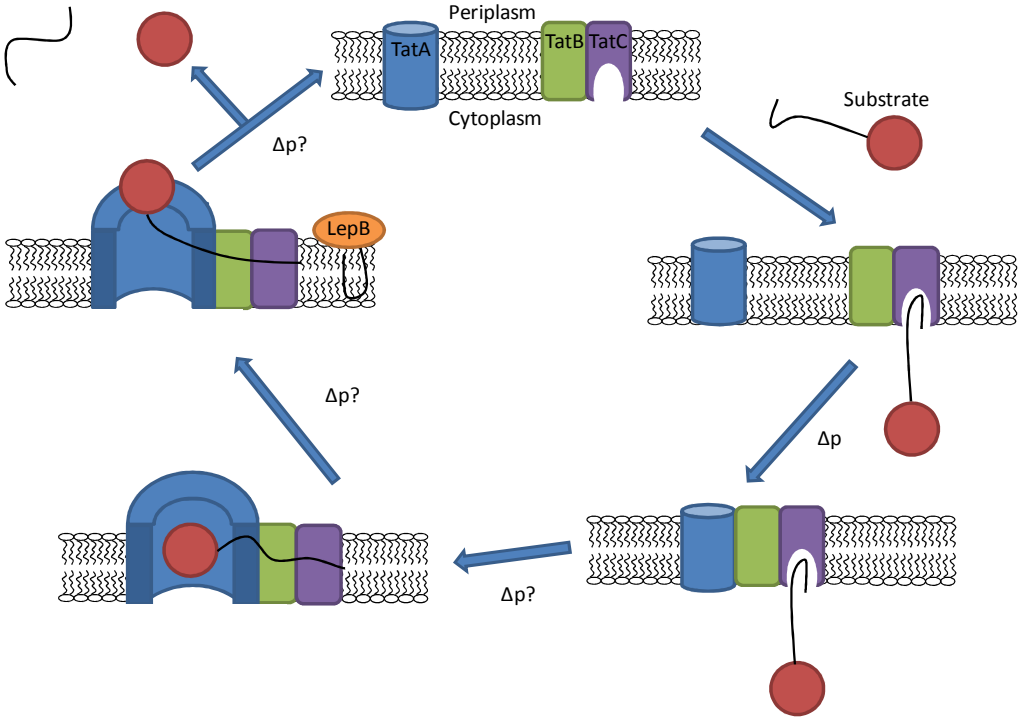

Figure 1.6: Protein translocation systems.

A: The Sec system, adapted from Driessen *et al*., 1998. The unfolded preprotein binds to SecB, which is recognised by the membrane bound SecA. The preprotein is transferred to SecA, and passes through the SecYEG translocase complex in an ATP dependent manner. B: The Tat system, adapted from Berks *et al*., 1995. The assembled substrate protein binds to TatC through its signal peptide, leading to the Δp dependent association of TatBC with TatA. Binding of the target protein to TatC is inhibited by the TorD family of chaperones to ensure the protein is folded and cofactors are inserted prior to translocation. The protein is translocated through the membrane by TatA, and the signal sequence cleaved by the peptidase LepB in the periplasm.

1.5. Redox co-factors

In addition to the Mo-*bis*MGD co-factor bound by the DMSO reductase family, we have seen that a number of other metal centres are present in each of these enzymes, namely iron-sulfur clusters and both *b* and *c*–type cytochromes. In order to understand the role of these co-factors, a further description is necessary.

1.5.1. Iron-sulfur clusters

Iron-sulfur clusters can accept and donate a single electron, and exist in several forms: [Fe-S], [2Fe-2S], [3Fe-4S] and [4Fe-4S] (see figure 1.7). The simplest form of iron-sulfur cluster, [Fe-S] has one Fe co-ordinated by the sulfur atoms of four cysteine residues (figure 1.5a). There are two types of [2Fe-2S] clusters, one co-ordinated by four cysteines (figure 1.5b), and the alternative Rieske cluster (figure 1.5c), which is co-ordinated by two cysteines and two histidines. The 'true' Rieske proteins also have an additional two cysteine residues which form a disulfide and influence the redox potential of the cluster, allowing it to function at higher potentials. This kind of Rieske cluster is found in the QCR and also the NarB subunit of some pNar enzymes (Martinez-Espinosa *et al.*, 2007). Both [4Fe-4S] (figure 1.5e) and [3Fe-4S] (figure 1.5d) clusters can be found in the molybdo-enzymes described in this work, as well as the unusual [4Fe-4S] cluster found in the catalytic subunits of the type II DMSO reductase family, FS0, which is co-ordinated by three cysteines and one histidine.

1.5.2. Cytochromes

Cytochromes are proteins which contain a porphyrin ring co-ordinating an octahedral iron atom (see figure 1.8). The ring system is conjugated, leading to delocalisation of electrons, and the Fe atom can convert between reduced and oxidised forms (Fe^{2+} and Fe^{3+}), accepting and donating an electron. The type of cytochrome (*a*, *b*, *c* and *d*) is defined by the side chains which are present on the haem ring (see figure 1.6). The haem iron is co-ordinated by four nitrogen atoms from the porphyrin ring, leaving two further co-ordination sites on the Fe, which can be co-ordinated by residues from the protein such as histidine, methionine and lysine. Sometimes, the sixth position is unoccupied by a fixed protein ligand and can be co-ordinated by molecules such as water and oxygen and hydroxide (OH^-). Typically, those haems which are penta-co-ordinate can have a catalytic role.

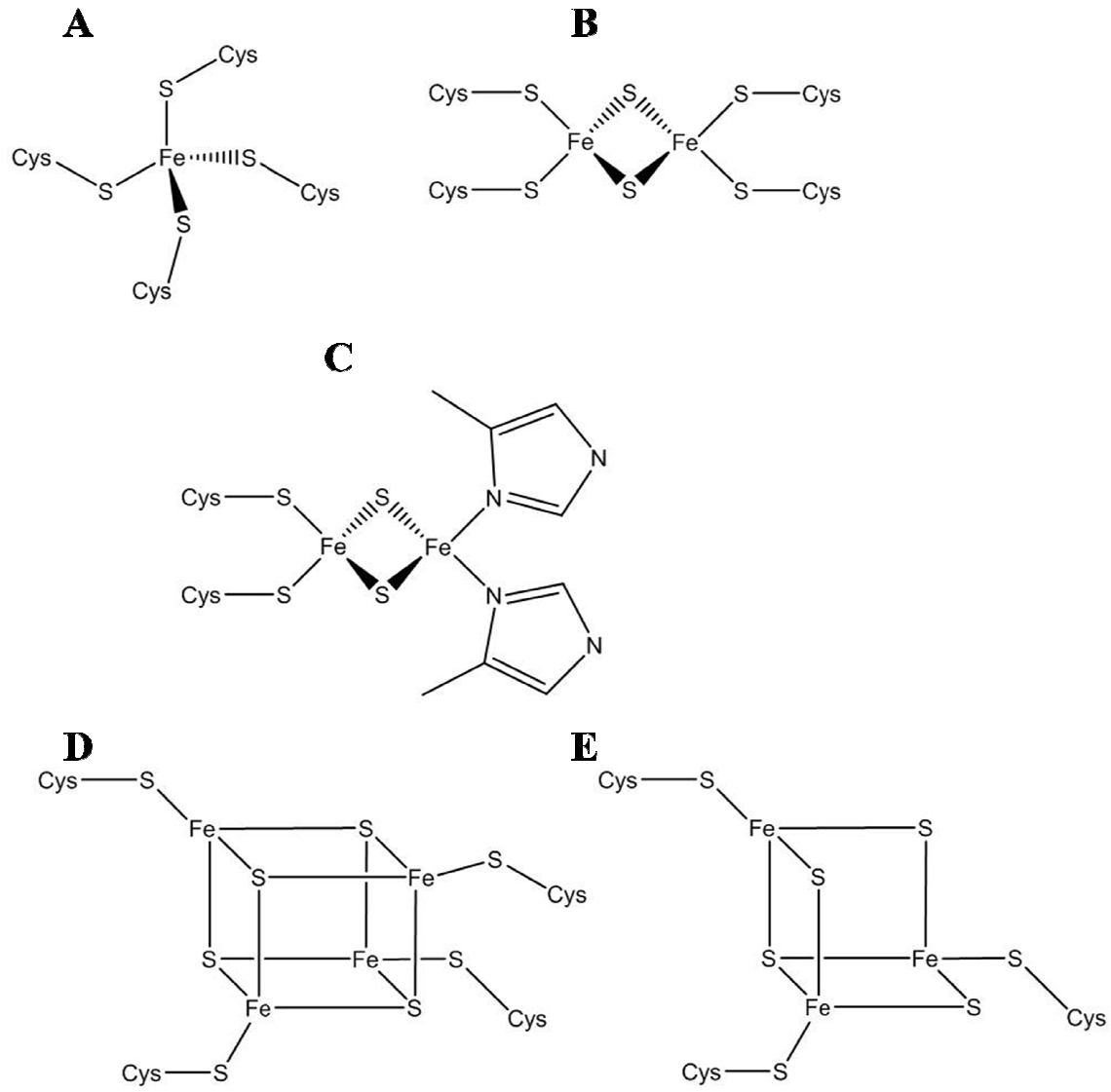

Figure 1.7: The structures of iron-sulfur clusters.

A: [Fe-S], B: [2Fe-2S], C: Rieske [2Fe-2S], D: [4Fe-4S] and E: [3Fe-4S]. (Nicholls & Ferguson, 2002)

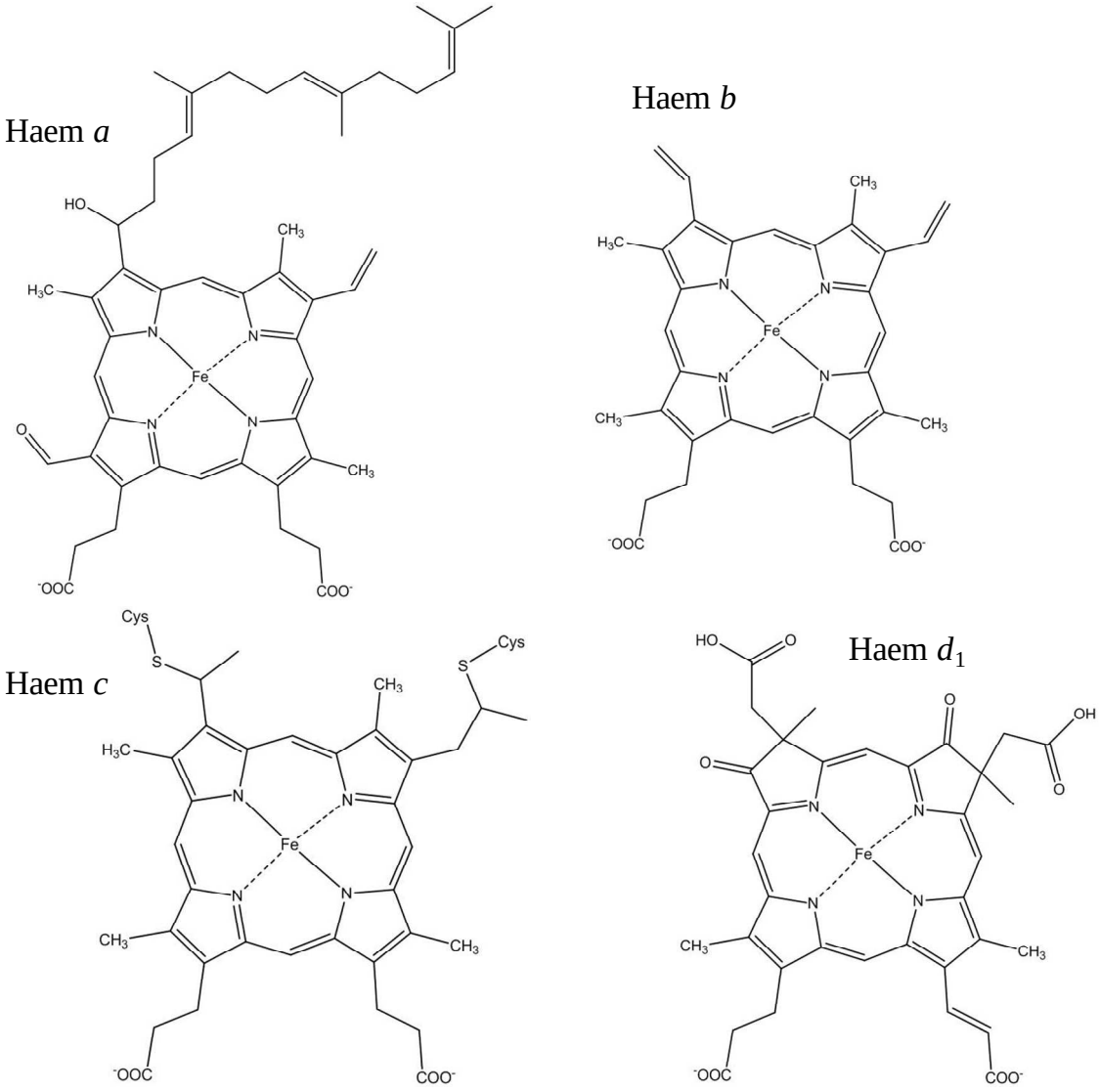

Figure 1.8: The structures of common types of haem.
(Allen *et al*., 2005)

Haem *a* is found in some cytochrome oxidase enzymes such as that in the mitochondrial ETC, where two *a*-type haems are present, haems *a* and a_3. It is substituted with an isoprenoid chain, and is not covalently bound to the protein, but is attached through co-ordination of the Fe by a residue side chain. The hydrophobic isoprenoid chain can also serve to anchor the haem in the protein. In the case of cytochrome oxidase, the iron of haem *a* is co-ordinated by two histidine residues and that of haem a_3 is co-ordinated by one. Haem a_3 is in a binuclear centre with copper (Cu_B), and catalyses the reduction of oxygen to water (Nicholls & Ferguson, 2002).

Cytochromes *b* are more common than those containing haem *a*, and are particularly prevalent amongst membrane proteins of the ETC, such as the QCR and NarI. Again, they are not covalently attached to the protein, and their axial ligands can vary. Haemoglobin and myoglobin are well known proteins which bind heme *b*, and co-ordinate it through a conserved histidine residue.

Cytochromes *c* are the only family of cytochromes which covalently bind the haem group to the protein. This is accomplished through a conserved CXXCH motif, where the two cysteine residues bind the vinyl groups of the haem and the histidine typically becomes the fifth ligand to the iron. Cytochromes *c* vary dramatically in size and number of haems, it is not known exactly why cytochromes *c* gain an advantage from covalent attachment of the haem, but theories include increased stability and allowing muti-haem *c*-type cytochromes to cluster a large number of haems within a relatively small polypeptide chain (Allen *et al.*, 2005).

The highly unusual d_1 haem is only found in one enzyme, the cytochrome cd_1 nitrite reductase, found in the bacterial periplasm. This enzyme catalyses the reduction of nitrite to nitric oxide, and receives its electrons from the QCR via a *c*-type cytochrome or copper protein (Moir *et al.*, 1993). It is not known why this saturated, derivatised ring structure is necessary to reduce nitrite instead of the more common haem *c*, but suggestions involve aiding the release of NO after catalysis, and possessing a redox potential which makes the further reduction of NO to hydroxylamine unfavourable (Allen *et al*., 2005).

A number of systems exist in different organisms for the maturation of cytochromes *c*. The most common among the Gram-negative bacteria is the Ccm system, or System I (Thony-Meyer, 2002), which is composed of eight proteins (CcmABCDEFGH). The haem and polypeptide are both synthesised separately in the cytoplasm, the apoprotein is exported to the periplasm via the Sec system, while the haem is exported via an unknown mechanism. CcmA and B compose an ABC transporter which transports an unknown, but essential substrate for maturation of the cytochrome. CcmE is a haem chaperone which transiently binds the haem through a histidine residue, aided by CcmC, before transferring the haem to the apoprotein. The transfer of haem to the apoprotein is assisted by CcmF. CcmD is a membrane bound protein thought to stabilise other Ccm proteins in the membrane (Ahuja & Thony-Meyer, 2005). Both the apoprotein and haem are reduced before attachment, which is thought to involve the CcmG and H proteins, as well as the disulfide bond proteins (Dsb) (Thony-Meyer, 2002, Stevens *et al.*, 2005).

1.6. Nitrogen oxyanions as respiratory substrates

Inorganic nitrogen exists in oxidation states ranging from +5 (nitrate) to -3 (ammonium) and the oxidative and reductive processes which cycle in between these states are carried out predominantly by microbes. Several processes make up the nitrogen cycle, including denitrification (reduction of nitrate to N_2 gas), nitrification (oxidation of ammonia to nitrate), nitrogen fixation (converting N_2 gas into ammonia for assimilation), ammonification (conversion of nitrate into ammonia), and anaerobic ammonium oxidation (ANAMMOX) (converting ammonium and nitrite into N_2) (see figure 1.9a).

Denitrification involves sequential reduction of nitrate to N_2, through nitrite, nitric oxide and nitrous oxide. It is generally carried out anaerobically, as each of the enzymes involved in this process can contribute to the PMF and conserve energy (Richardson, 2000) and is carried out by a large number of diverse bacteria (Richardson & Watmough, 1999). Reduction of nitrogen oxyanions has a role in pathogenesis, for example in the gastro-intestinal pathogen *Campylobacter jejuni*. *C. jejuni* is an obligate aerobe which expresses both a nitrate (Nap) and nitrite reductase (Nrf), thought to aid survival in the micro-aerobic conditions of infection (Pittman & Kelly, 2005, Sellars *et al.*, 2002). In fact, *C. jejuni* strains lacking either Nap or Nrf have been shown to be impaired in their ability to colonise host organisms (Weingarten *et al.*, 2008).

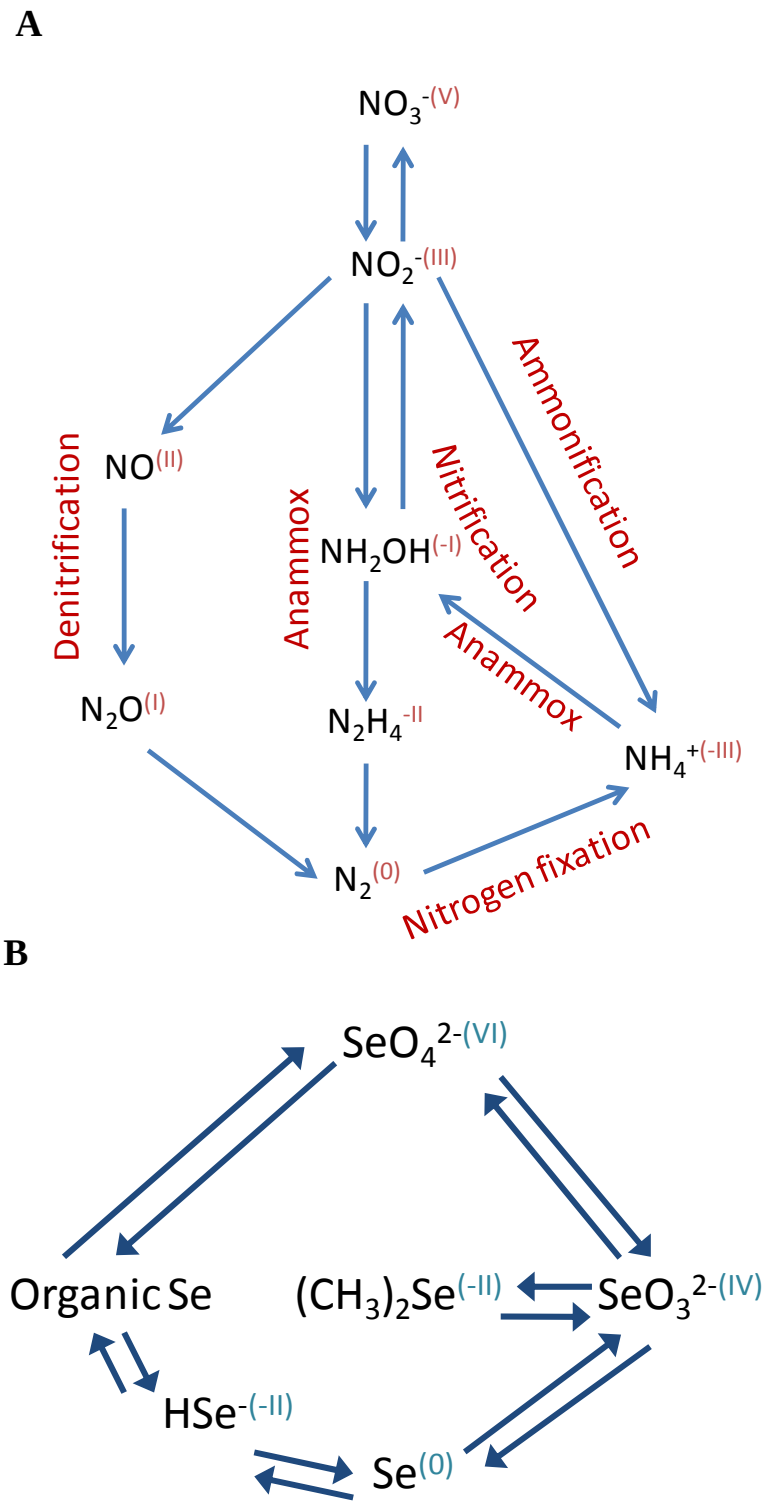

Figure 1.9: The nitrogen and selenium cycles.

A: The inorganic nitrogen cycle, adapted from Gonzalez *et al.*, (2006). The oxidation state of each compound is given in pink. NO_3^- - nitrate, NO_2^- - nitrite, NH_4^+ - ammonium, N_2 - nitrogen, N_2H_4 - hydrazine, NH_2OH - hydroxylamine, N_2O – nitrous oxide, NO – nitric oxide. B: The selenium cycle, adapted from Stolz *et al.*, (2006). The oxidation state of each compound is given in blue. SeO_4^{2-} - selenate, SeO_3^{2-}- selenite, Se - selenium, $(CH_3)_2Se$ - dimethyl selenide, HSe^- - hydrogen selenide.

Nitrification is generally performed by soil-living bacteria. The initial oxidation of ammonia to nitrite in nitrification is typically carried out by bacteria of the *Nitrosomonas* genus, while the final oxidation of nitrite to nitrate is carried out by the *Nitrobacter* genus (Richardson, 2000). Nitrogen fixation and ammonification both convert substrates into ammonia which can then be assimilated into organic nitrogen, essential for biosynthesis of proteins and nucleic acids. Nitrogen fixation is commonly carried out by symbiotic bacteria such as *Rhizobium* which live in root nodules of leguminous plants and possess the nitrogenase enzyme for converting N_2 and hydrogen into ammonia. The most recently discovered part of the N-cycle, anaerobic oxidation of ammonia (ANAMMOX) is carried out by a very slow-growing consortium of bacteria which oxidise ammonia, use nitrite as electron acceptor and CO_2 as carbon source, producing nitrogen gas as the product (Jetten *et al.*, 2005).

1.7. Selenium oxyanions as respiratory substrates

Selenium is a trace element with an abundance of less than 0.0001% of the Earth's crust, and is found in fossil fuels and alkaline soils. Weathering, together with anthropogenic activities has contributed to the accumulation of selenium in certain environments. The use of pesticides, combustion of coal, glass manufacturing and even anti-dandruff shampoo are all contributors to selenium enrichment (Stolz & Oremland, 1999) and in cases it can accumulate to micro molar concentrations. Selenium exists in the environment in four oxidation states, the toxic oxyanions selenate (VI) and selenite (IV), selenide (-II), and insoluble elemental selenium (0) (see figure 1.9b). Selenide is found incorporated into proteins in the form of selenocysteine or selenomethionine, as well as in volatile forms such as dimethyl selenide. Elemental selenium is mostly found in anoxic environments, whereas selenate and selenite are prevalent in oxic areas (Stolz *et al.*, 2006). The incorporation of selenium into proteins makes it an essential element; however it is also toxic at higher concentrations as it replaces sulfur in proteins, for example altering cysteine residues to selenocysteine and disrupting vital sulfhydryl groups. Toxicity symptoms in humans include nausea, vomiting, and loss of hair and fingernails (Vinceti *et al.*, 2001). Bacteria have a requirement for selenium (Stolz *et al.*, 2006), in fact it is so essential that the genome of the bacterium *Aeromonas hydrophila* encodes the *selABC* genes for insertion of selenocysteine, for only one expressed selenoprotein, formate dehydrogenase-H (Seshadri *et al.*, 2006). How the bacteria acquire this selenium is less clear, specific uptake systems for selenate and selenite have

been proposed – in pathogenic bacteria, it could be speculated that Se scavenged from the host organism is a potential source.

The ability to reduce selenate and selenite to elemental selenium (which is visible as a brick red precipitate in solution) is widespread throughout the bacterial domain (Stolz *et al*., 2006, Stolz & Oremland, 1999). Many can reduce selenate/selenite as a detoxification mechanism, but must use an alternative electron acceptor or a fermentable carbon source for respiration. This group includes *Enterobacter cloacae* SLD1a-1 (Losi & Frankenberger, 1997) and *Pseudomonas stutzeri* (Lortie *et al.*, 1992). The majority of bacteria that reduce selenium oxyanions for respiration rather than detoxification use selenate rather than selenite, only *Bacillus selenitireducens* and *Aquificales sp*. have been shown to respire with selenite (Switzer Blum *et al.*, 1998, Takai *et al.*, 2002). Selenate respiration however, is more widespread and bacteria capable of this include *Thauera selenatis* (Macy *et al.*, 1993), *Sulfospirillium barnesii* (Oremland *et al.*, 1994), *A. hydrophila* (Knight & Blakemore, 1998) and *Sedimenticola selenatireducens* (Narasingarao & Haggblom, 2006), as well as a number of environmental isolates.

1.8. Selenate and selenite reduction

The enzymes responsible for selenate reduction have only been characterised in a few organisms, namely *T. selenatis* (see section 1.9) (Schroder *et al.*, 1997), *E. cloacae* SLD1-a1 (Ridley *et al.*, 2006b) and *A. hydrophila* (Leaver, 2008). It has been suggested that selenate reduction may be catalysed by nitrate reductases, and in fact selenate reductase activity has been detected in the Nar and Nap enzymes of *Ralstonia eutropha*, *P. denitrificans* and *P. pantotrophus* (Butler *et al.*, 1999, Sabaty *et al.*, 2001).

E. cloacae SLD1a-1 was isolated from selenium contaminated water in the San Joaquin valley, California (Losi & Frankenberger, 1997, Macy *et al.*, 1989, Yee & Kobayashi, 2008). In *E. cloacae* SLD1a-1 selenate reduction cannot support growth but is reduced when the organism is grown in the presence of an alternative electron acceptor such as nitrate or oxygen (Ridley *et al.*, 2006b). The selenate reductase was shown to be located in the cytoplasmic membrane, facing the periplasm (Watts *et al.*, 2003), and consists of a heterotrimeric protein with subunits 100, 55 and 36 kDa. This membrane bound selenate reductase contains molybdenum, *b*-haem and non-haem iron, suggesting Fe-S clusters (Ridley *et al.*, 2006b), and has activity for chlorate but not nitrate. It has

recently been shown that the selenate reductase may confer a selective advantage to *E. cloacae* SLD1a-1 when growing in nitrate depleted environments where selenate is present (Leaver *et al.*, 2008). The authors showed using anaerobic continuous culture experiments, that washout of cells when nitrate is depleted is delayed by the addition of selenate, so although selenate reduction is not sufficient to support growth, it may be sufficient to maintain cell viability in the absence of nitrate.

Selenate reduction in *A. hydrophila* can support slow growth (Knight & Blakemore, 1998), and selenate activity has been localised to the cytoplasmic membrane. The selenate reductase has been purified and shown to have both nitrate and selenate activity, and N-terminal sequence analysis as well as molybdenum EPR showed it to be a Nap-type nitrate reductase, which unusually, is associated with the membrane (Leaver, 2008).

In contrast to selenate reduction, very little is known about selenite reduction. Selenite reduction is inhibited by nitrate and nitrite in *E. cloacae* SLD1a-1, suggesting that selenite reduction is carried out by a nitrite reductase (Butler *et al*., unpublished). A similar situation is postulated in *T. selenatis*, where mutants lacking the ability to reduce selenite also lacked nitrite reductase activity (Demolldecker & Macy, 1993). It has also been suggested that in some cases, selenite could be reduced by an abiotic mechanism involving the tripeptide glutathione (GSH), and production of an unstable GS-Se-persulfide which then dismutates into elemental selenium and glutathione (Kessi & Hanselmann, 2004). It is not known however, if any of the organisms mentioned here express glutathione as part of their anti-oxidant system, although it is abundant among the proteobacteria.

The reduction of selenite necessarily leads to the production of elemental Se, which interestingly, has been shown to result in the formation of selenium ‘nanospheres’ in a number of bacteria (Losi & Frankenberger, 1997, Oremland *et al.*, 2004) both inside the cell, and extracellularly. The particles are generally in the order of 0.2-0.4 µm, and can be purified away from the bacteria. Spectroscopic analysis has shown that they are unlike Se formed by chemical reduction, and their physical properties vary between species (Oremland *et al*., 2004). It is not yet known, however, how intracellular Se particles are exported to the extracellular environment, which would seem to be a difficult task given the size of the nanospheres.

1.9. *Thauera selenatis*

T. selenatis is perhaps the best characterised of the selenate respiring bacteria, certainly from a biochemical point of view. It is a Gram negative, rod shaped, β-proteobacteria which is capable of using selenate as an electron acceptor for anaerobic respiration. It can also utilise a variety of carbon sources including acetate, lactate, pyruvate, benzoate and amino acids, although acetate is the preferred carbon source (Macy *et al*., 1993). As well as selenate respiration, *T. selenatis* can grow aerobically or with nitrate as terminal electron acceptor. During selenate respiration, elemental selenium is the final product, giving a distinctive deep red colour to the growth medium. Electron microscopy images have shown that *T. selenatis* also produces extracellular selenium nanoparticles, which seem to occur in chains associated with the bacterium (see figure 1.10).

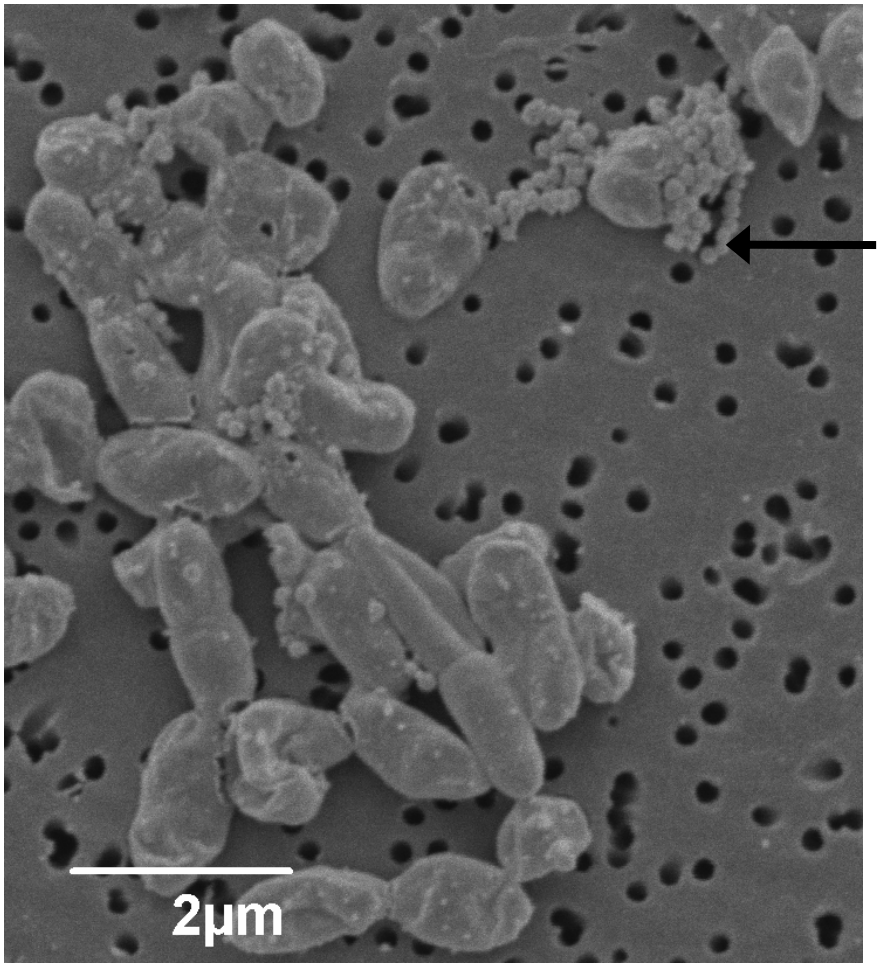

Figure 1.10: Electron microscopy image of *T. selenatis* grown under selenate respiring conditions.
Image taken at the University of Exeter, by G. Wakely, EM department. The black arrow indicates chains of Se nanospheres.

Initially it was shown that the enzymes responsible for nitrate and selenate reduction were distinct, the nitrate reductase activity is localised to the membrane whereas the selenate reductase activity is found in the periplasm (Rech & Macy, 1992). Further work then isolated this selenate reductase and found it to be a heterotrimeric molybdo-enzyme, composed of SerA, SerB and SerC (96, 40 and 23 kDa respectively). It was found to contain molybdenum, iron and acid labile sulfur, as well as a *b*-type haem (Schroder *et al*., 1997). It was also thought to be specific for the reduction of selenate with a K_m of 16 µM and V_{max} of 40 µmol/min/mg of protein (Schroder *et al*., 1997), although recent work shows it also possesses chlorate reductase activity at a lower affinity (K_m = 5.7 mM) (Dridge, 2007). Interestingly, although *T. selenatis* is a mesophilic bacterium with a optimum growth temperature of 30ºC, selenate reductase retains high activity even at 60ºC (Dridge, 2007).

The genes encoding the selenate reductase were sequenced (Krafft *et al.*, 2000) and showed that the selenate reductase is a member of the type II DMSO reductase family of molybdo-enzymes, with homology to ethylbenzene dehydrogenase and chlorate reductase. The catalytic subunit, SerA, contains the Mo-*bis*MGD co-factor, as well as a predicted FS0 iron-sulfur cluster. SerB contains four Fe-S clusters, and SerC is thought to bind the *b*-haem (figure 1.11a and b). A fourth gene, *serD* was also sequenced which is predicted to be an assembly chaperone for the selenate reductase. SerA and B are thought to be targeted to the periplasm via the Tat system, as SerA posesses a Tat leader sequence containing the twin-arginine motif. SerC has a typical periplasmic signal sequence which would direct it via the Sec system.

Recent spectroscopic characterisation of SerABC confirmed the presence of three [4Fe-4S] (FS1-3) clusters and one [3Fe-4S] (FS4) cluster with redox potentials of +183, -356, -51 and +118 mV (FS1-4) , as well as detecting EPR signals for the Mo (V) and haem *b* (Dridge *et al.*, 2007). The redox potentials determined here are comparable to those seen in NarH (Blasco *et al*., 2001), EbdB, and DdhB (Creevey *et al*., 2008) (figure 1.11c). The high redox potential of the haem *b* in DdhC (+324 mV) and EbdC (+254 mV), both homologous to SerC raises the question of whether a similarly high potential could be expected in this case, although it must be noted that both Ebd and Ddh work in the opposite direction to Ser, as oxidases rather than reductases. The high potential of the selenate/selenite couple (+475 mV) does mean that a high potential haem subunit would not be energetically unfavourable.

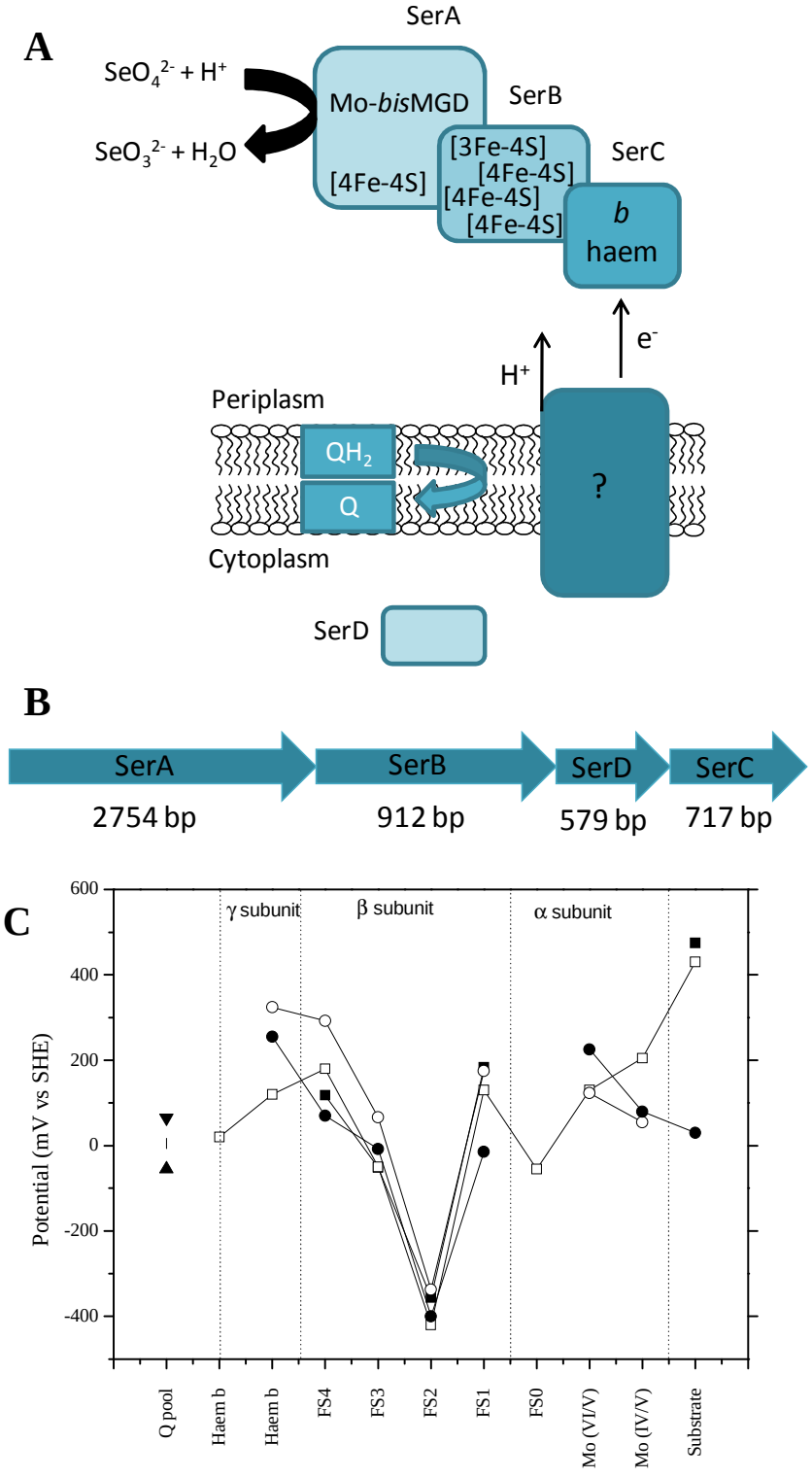

Figure 1.11: Enzyme topology, gene cluster organisation and redox potentials of selenate reductase from *T. selenatis*.

A: Subunit composition and co-factors of selenate reductase. B: Gene cluster organisation and size for *serABDC*. C: Redox potentials of known co-factors for SerABC and homologous enzymes. ■ = SerABC, □ = NarGHI, ○ = DdhABC, ● = EbdABC.

The data shown in figure 1.11c shows that the enzymes share a common feature, a very low potential [4Fe-4S] cluster (FS2) in the β subunit. This must rely on the high potential of the substrate in the case of Ser and Nar, or that of the *b*-haem in the case of Ebd and Ddh.

The pathway by which selenate reductase receives its electrons is unknown, as is the mechanism by which selenate reduction can be electrogenic and contribute to a PMF. McEwan *et al*., (2002) propose that SerABC is the only member of the DMSO reductase family which could receive electrons from a QCR via a high-potential cytochrome *c*, due to the high potential of the selenate/selenite couple. This possibility has not yet been examined further, and it is not known whether *T. selenatis* possesses a QCR like *Paracoccus* species, or resembles the QCR-lacking *E. coli* in its respiratory chain. In either case, the periplasmic location of SerABC means that the electron transport chain is likely to involve both a membrane bound quinol oxidase of some kind, and a soluble electron 'shuttle'. The genome of *T. selenatis* has not yet been sequenced, so we are unable to gain clues about the identity of these proteins from studying genomic data.

It has been suggested that reduction of selenite to selenium in *T. selenatis* is carried out by a nitrite reductase (Demolldecker & Macy, 1993), and studies of *Thauera* species have revealed that *T. selenatis* has genes (*nirS*) coding for a cd_1-type nitrite reductase but not a copper (*nirK*) or cytochrome *c* type (*Nrf*) (Song & Ward, 2003). This enzyme is linked to the QCR in *P. pantotrophus*, and should therefore provide a PMF, but it has previously been stated that *T. selenatis* is unable to grow with selenite as the sole electron acceptor (Macy *et al.*, 1989).

1.10. Aims of the project

The introduction has given an overview of the known electron transport chains to DMSO reductase family molybdo-enzymes, and it is clear that there is considerable diversity among these pathways. It has become apparent that the electron transport chain to selenate reductase in *T. selenatis* is poorly understood and there are a number of key questions to be answered:

- How similar is the selenate reductase C subunit to those in related enzymes such as ethylbenzene dehydrogenase and dimethylsulfide dehydrogenase? Is the redox potential of the haem lower, given that the selenate reductase works in the opposite direction? The SerC subunit will be cloned and expressed in order to provide SerC to study interactions with potential electron donors.

- What is the soluble electron donor to SerC? A profile of the *c*-type cytochromes expressed during selenate respiration will be undertaken, suitable candidates will be characterised, and their effectiveness in donating electrons to selenate reductase will be assessed.

- Which membrane bound proteins are involved in selenate respiration? The identity of membrane bound components of the selenate respiratory chain will be investigated using inhibitors of the electron transport chain to probe their effect on growth of *T. selenatis* under various conditions.

2. Materials and methods

2.1. Bacterial strains and cultures

All strains used in this study are outlined in Table 2.1. All strains were maintained as glycerol stocks by mixing 1 ml of growing culture with 1 ml 60 % glycerol and flash-freezing in liquid nitrogen, before storing at -80°C. *E. coli* JM109 and *E. coli* BL21 (DE3) strains were cultured aerobically in Luria-Bertani (LB) broth with agitation at 180 rpm, or on LB plates containing 15% w/v agar, both at 37°C. Antibiotics and other supplements were added, where appropriate, at the following concentrations: ampicillin, 100 μg ml^{-1}; X-gal, 80 μg ml^{-1}; isopropyl β-D thiogalactopyranoside (IPTG), 1 mM.

T. selenatis was cultured anaerobically at 30°C in Hungates minimal salts medium (see appendix). Prior to inoculation, the minimal media was supplemented with vitamin solution and SL8 trace elements solution (see appendix) at 10 ml L^{-1}, 1 ml L^{-1} of 15% (w/v) $CaCl_2.H_2O$ and 1 ml L^{-1} of 40% (w/v) $MgCl_2.6H_2O$. Sodium acetate was added at 10 mM to act as a carbon source, and either sodium selenate or potassium nitrate was used as the electron acceptor, also at a final concentration of 10 mM. Supplemented media was prepared in bottles sealed with rubber septa, and sparged with oxygen-free nitrogen (OFN) gas to ensure the media was anaerobic prior to inoculation. Starter cultures (500 ml) used selenate as the sole electron acceptor and were inoculated from glycerol stocks. These were cultured until they reached exponential growth phase, OD_{600nm} 0.6-0.8, and then subcultured into larger anaerobic flasks, typically 10 L Duran bottles for large scale protein purification. The large-scale cultures were grown to late exponential phase (OD_{600nm} ~ 0.8) before harvesting by centrifugation (see sections 2.2 and 2.3). For aerobic growth, *T. selenatis* was cultured in 500 ml of Hungates minimal medium in 1 L flasks, with agitation at 180 rpm, at 30°C. Sodium acetate, vitamins, and mineral solution were added as described above.

In order to monitor the effects of changing culture conditions and inhibitors on the growth of *T. selenatis*, a method utilising microtitre plates was developed, allowing multiple replicates of various conditions. A 500 ml bottle of Hungates medium was prepared as described above, without the addition of selenate or other electron acceptor. The bottle was sealed with rubber septa and sparged with OFN for at least 1 hour. Each well of a 96-well microtitre plate had 250 μl of the degassed media added to it, and

electron acceptor added in varying concentrations from degassed stock solutions. Inhibitors were added to wells as required from stock solutions. Wells were inoculated with 1 µl washed cells from an exponential phase *T. selenatis* culture (1 ml of cells at OD_{600nm} 0.6-0.7 were harvested by centrifugation at 12,000 x *g*, 2 minutes, and resuspended in 1 ml of the degassed media). Inoculated plates were incubated in a FLUOstar Optima microplate reader (BMG Labtech, Aylesbury, UK) attached to a nitrogen cylinder to keep the plate in an anaerobic atmosphere. The plate reader kept the plate at a constant temperature of 30°C, and OD_{600nm} values were measured in each well every 15 minutes using the kinetics measuring program, with 5 seconds shaking before each reading. Each plate had 6 wells without the addition of bacteria to ensure no contaminants were growing, and to act as a baseline, and 6 wells with 'normal' growing conditions for *T. selenatis* to check the culture was growing typically and for comparison.

P. pantotrophus was cultured in DSMZ minimal media #356 (see appendix) with the addition of trace element SL-10 solution at 10 ml L^{-1}. Succinate was used as carbon source and potassium nitrate as electron acceptor, both at final concentrations of 10 mM.

Table 2.1: Strains of organisms used within this study

STRAINS	CHARACTERISTICS	REFERENCE
E. coli JM109	*end*A1, *rec*A1, *gyr*A96, *thi*, *hsd*R17, (r_k^- m_k^+), *rel*A1, *sup*E44, Δ (*lac-pro*AB), [F', *tra* D36, *pro*AB, *lacI*^{q}ZΔM15]	Promega, Southampton, UK.
E. coli BL21 (DE3)	F^-, *dcm*, *omp*T, *hsd*S (r_B^- m_B^-), *gal*, λ(DE3)	Stratagene, Agilent Technologies UK Ltd, Cheshire, UK
Thauera selenatis (ATCC55363)	Selenate respiring, β-subclass of proteobacteria	Macy *et al*, 1993.
Paracoccus pantotrophus (formerly *Thiosphaera pantotropha*) (ATCC31522)	Denitrifying, α-subclass of proteobacteria	Robertson and Kuenen, 1983. Rainey *et al*, 1999

2.2. Preparation of the periplasmic fraction from *T. selenatis*

Cells grown to late exponential phase (OD_{600nm} 0.6-0.8) were harvested by centrifugation at 6,300 x *g*, for 20 minutes at 4°C, then resuspended in 1/100 of the original culture volume of 10 mM Tris-HCl, pH 8.0. The cells were then centrifuged at 4,400 x *g*, 15 minutes, 4°C, and weighed, before resuspending in spheroplasting buffer (0.75 M sucrose, 30 mM Tris-HCl, pH 8.0) at 0.45 g ml^{-1} (wet weight). The resuspended cells were stirred gently on ice for 10 minutes, with the addition of lysozyme (Sigma-Aldrich Company Ltd, Dorset, UK) to 0.4 mg ml^{-1}. Two volumes of ice cold EDTA (15 mM, pH 8.0) were added slowly over 10 minutes, and the solution was allowed to stir for a further 10 minutes. 0.5 ml of Protease inhibitor cocktail (Sigma-Aldrich) was also added at this time. After stirring, the suspension was incubated at 37°C until flocculation was observed, indicating the formation of spheroplasts. The spheroplasts were removed by centrifugation (25,000 x *g*, 20 minutes, 4°C) and the resulting supernatant (periplasmic fraction) was retained.

2.3. Preparation of soluble and membrane fractions from *T. selenatis*

Cells were harvested by centrifugation (6,300 x *g*, 20 minutes, 4°C), and resuspended in 30 mM Tris-HCl, pH 8.5 in 1/100 of the original culture volume. The cells were broken open using sonication for 30s on, 30s off for a total of 10 minutes for a typical 10 L original culture volume. Unbroken cells were removed by centrifugation at 6,300 x *g*, 4°C, for 10 minutes, and the resulting cell lysate supernatant was centrifuged at 100,000 x *g*, 4°C for 1 hour in an ultracentrifuge. The soluble protein fraction (supernatant) was stored at -20°C and the membrane pellet was resuspended in 5-10 ml of 30 mM Tris-HCl, pH 8.5 then stored at -20°C.

2.4. Purification of SerABC

Periplasmic fraction was prepared as in section 2.2. The periplasmic fraction was initially fractionated by ammonium sulfate precipitation. Solid ammonium sulfate was added to the periplasmic fraction to 30% saturation (as calculated by reference to an ammonium sulfate precipitation table) over 30 minutes while stirring on ice. The solution was stirred for a further 30 minutes, then centrifuged to remove precipitated protein (25,000 x *g*, 15 minutes, 4°C). The supernatant was retained and ammonium sulfate added to increase saturation from 30-50%, as described previously. The solution was centrifuged again (25,000 x *g*, 18 minutes, 4°C) and the supernatant retained as

before. One further ammonium sulfate cut to increase the saturation from 50-80% was carried out followed by a final centrifugation (25,000 x *g*, 20 minutes, 4ºC). The supernatant from this final centrifugation was discarded, and the pellet was resuspended in 50 mM PIPES buffer, pH 6.0, 1 M ammonium sulfate. This was loaded onto a 5 ml Phenyl Sepharose HP (high performance) hydrophobic interaction column (GEHealthcare, Amersham, UK) equilibrated with the same buffer. Bound proteins were eluted by applying a 50 ml linear gradient of 1-0 M ammonium sulfate in 50 mM PIPES, pH 6.0. Protein concentration of fractions was monitored by absorbance at 280 nm, and selenate reductase activity was assayed using the microtitre plate method described in section 2.8. Those fractions with selenate reductase activity were pooled and concentrated using a 15 ml 10 kDa molecular weight cut off (MWCO) centrifugal concentrator (Millipore). The concentrate was applied to a Superdex 200 16/60 gel filtration column (bed volume 120 ml) (GEHealthcare) equilibrated with 50 mM PIPES, pH 6.0, and eluted in the same buffer. The protein was concentrated as described above and stored at -80°C.

2.5. Purification of cytochrome *c*4

Soluble protein from a 10 L culture prepared as described in section 2.3 was loaded onto a Q-Sepharose Fast-Flow anion exchange column (70 ml bed volume) (GEHealthcare) pre-equilibrated with 3 column volumes of 30 mM Tris-HCl, pH 8.5. The column was washed with a further column volume of buffer to remove unbound proteins. Cyt*c*4 was eluted using a 300 ml gradient of 0-300 mM NaCl in 30 mM Tris-HCl, pH 8.5. Protein concentration was monitored using absorbance at 280 nm and presence of cytochromes was monitored using absorbance at 410 nm. The fractions containing cyt*c*4 as determined by SDS-PAGE were pooled and concentrated using a 15 ml 10 kDa MWCO centrifugal concentrator at 4000 x *g*. The concentrated protein was loaded in 2 ml aliquots onto a Superdex 200 16/60 gel filtration column (GEHealthcare) equilibrated with 2 column volumes of 30 mM Tris-HCl, pH 8.5 and eluted in the same buffer. The fractions containing cyt*c*4 were pooled and loaded onto a 1 ml MonoQ anion exchange column (GEHealthcare) equilibrated with 30 mM Tris-HCl, pH 8.5 and eluted with a gradient of 0-1 M NaCl in 30 mM Tris-HCl, pH 8.5. As a final purification step, the fractions containing cyt*c*4 were pooled and transferred to dialysis tubing (6 kDa MWCO) (Fisher), the protein was then dialysed overnight at 4°C, with gentle stirring, into 30 mM Tris-HCl, pH 8.5, containing 1 M ammonium sulfate. The dialysed protein was then bound to a 25 ml Fast-Flow Phenyl Sepharose column

(GEHealthcare) pre-equilibrated with 1 M ammonium sulfate in 30 mM Tris-HCl, pH 8.5, and subsequently eluted with a gradient of 1-0 M ammonium sulfate. The fractions containing cyt*c*4 were judged pure by SDS-PAGE analysis, then concentrated as before and stored at 4°C for short term use, or -80°C for longer term storage. All chromatography procedures were carried out using an AKTAPrime purification system at room temperature, except for the MonoQ column which was run on an AKTABasic (GEHealthcare).

2.6. Purification of cytochrome *c*7

The soluble fraction from a 2 L culture was prepared as described in section 2.3. This soluble fraction was concentrated using a 15 ml 10 kDa MWCO centrifugal concentrator (Millipore) to a final volume of 5 ml, and then loaded onto a Superdex 200 16/60 gel filtration column pre-equilibrated with 20 mM Tris-HCl, pH 8.0. Proteins were eluted in the same buffer. Fractions were monitored for presence of protein using the absorbance and at 280 nm for presence of cytochrome using the absorbance at 410 nm. Fractions containing cyt*c*7 were identified by SDS-PAGE analysis, pooled, and concentrated in a 5 ml, 5 kDa MWCO concentrator.

2.7. Oxyanion reductase activity assays

A standard assay was carried out in a 3 ml cuvette containing 2.8 ml 50 mM phosphate buffer, pH 7.5, 30 µl 100 mM methyl viologen (final concentration 1 mM) and 100 µl cell fraction. The volume of cell fraction was sometimes changed dependent on activity, and the volume of phosphate buffer adjusted accordingly to keep the total volume consistent. The cuvette was sealed with a rubber septa, and sparged with OFN for 10 minutes. A stock solution of 0.5 M sodium dithionite was made and also sparged with OFN. Dithionite was titrated into the cuvette using a 10 µl Hamilton syringe until the OD_{600nm} of the solution was ~2.5. The OD_{600nm} was monitored using a spectrophotometer until a stable base line was achieved for 100 seconds, then substrate added (typically a final concentration of 20 mM). The cuvette was inverted several times to mix and replaced in the spectrophotometer, and the OD_{600nm} monitored to measure the oxidation of methyl viologen.

2.8. Microtitre plate assay

The microtitre plate assay for oxyanion reductase activity was adapted from that developed by Ridley *et al*., (2006a). Briefly, incubation buffer containing 50 mM phosphate buffer, pH 7.5, and 1.5 mM methyl viologen was degassed with OFN and 180 µl was added to the wells of a 96 well microtitre plate. 5 µl of protein fraction and 4 µl 0.5 M degassed sodium dithionite were subsequently added to each well and mixed using a pipette tip. 20 mM sodium selenate was added to initiate the reaction, and the oxidation of methyl viologen from a deep blue colour to clear was monitored by eye to determine rapidly which fractions contained selenate reductase activity. Control wells were also set up, either without protein or without substrate, for comparative purposes.

2.9. Electronic absorption spectroscopy

UV-visible spectra of protein samples were recorded on a Varian Cary 4E UV/Vis spectrophotometer between 350-700 nm. Reduced samples were achieved by adding excess sodium dithionite solution, and oxidised samples by the addition of potassium ferricyanide.

2.10. Electron transfer assay

To determine whether purified cytochromes were able to donate electrons to SerABC *in vitro*, a solution of approximately 5 µM cytochrome in 50 mM phosphate buffer (pH 7.5) was degassed in a sealed cuvette. A weak solution (10 mM) of sodium dithionite was also degassed and then titrated into the cuvette using a 10 µl Hamilton syringe, until the cytochrome was fully reduced, as determined by wavelength scanning UV-visible spectroscopy (350-700 nm). SerABC and selenate were added to final concentrations of 1 µM and 20 mM respectively, and re-oxidation of the cytochrome monitored by recording the spectra. Cytochromes were similarly tested for selenate and selenite reductase activity by incubation with the relevant substrate but no SerABC.

2.11. Electron paramagnetic resonance spectroscopy

To prepare the sample for electron paramagnetic resonance (EPR), purified cyt*c*4 was oxidised by the addition of potassium ferricyanide, and excess oxidant was removed using a PD-10 desalting column (GEHealthcare). Cyt*c*4 was concentrated to 10 mg ml^{-1} and frozen in an EPR tube by immersion in liquid nitrogen. EPR spectra were measured using a Bruker (Bruker BioSpin Limited, Coventry, UK) EMX spectrometer equipped

with an ER4112HV liquid helium flow cryostat system. Conditions of measurement are detailed in appropriate figure legends.

2.12. Determination of pI by isoelectric focusing

Isoelectric focusing (IEF) was carried out to determine the pI of cyt*c*4. Purified protein was run on a PhastGel™ IEF 4.0-6.5 gel, using the PhastSystem™ (GEHealthcare). Low pI Kit, pH 2.5-6.5 markers (GEHealthcare) were also run for comparison. The IEF gel was run according to manufacturers' instructions. Gels were stained in the PhastSystem™ development chamber using a program as detailed below. Gels were fixed in 20% trichloroacetic acid for 5 minutes at 20°C, washed in methanol: acetic acid: deionised water (3:1:6) for 2 minutes at 20°C and stained in 0.02% PhastGel Blue R, 0.1% (w/v) $CuSO_4$ in wash solution for 10 minutes at 50°C. Finally, gels were destained in the wash solution for a further 10 minutes at 50°C. The pI of the protein was calculated with reference to the pI standard marker.

2.13. Optical redox titration

Redox titrations were carried out at the University of East Anglia, Norwich. Optical spectra of the samples were measured on a Hitachi U-3310 spectrophotometer between 350-700 nm. Protein samples in 30 mM Tris-HCl pH 7.5 were added to a stirred cuvette constantly sparged with OFN to minimise oxidation from air. Redox mediators as listed in table 2.2 were added at a final concentration of 6 μM each, and the potential measured using an electrode. The electrode was initially calibrated with reference to a saturated solution of quinhydrone (295 mV vs. SHE). A degassed solution of 5 mM sodium dithionite was prepared and added in 1 μl steps, recording the potential, and the spectra at each step. Once the sample was fully reduced, 3 mM potassium ferricyanide was titrated in similarly to re-oxidise the sample. The fraction of protein reduced at each potential was calculated and fitted to a Nernstian equation using the curve fitting program TableCurve 2D (Systat Software Inc.). The Nernst equation is shown below (equation 1). Here, E_h denotes the potential relative to the standard hydrogen half cell (SHE), E_0 is the standard redox potential of the B_{ox}/B_{red} couple, R is the ideal gas constant, T is the temperature in Kelvin, F is the Faraday constant and n is the number of electrons transferred in the reaction.

$$E_h = E_0 + \frac{RT}{nF} \ln \frac{[B_{ox}]}{[B_{red}]} \qquad [1]$$

Table 2.2: Redox mediators used in optical redox titrations	
Mediator	Reduction potential vs. SHE
2, 3, 5, 6 tetramethyl-p-phenylendiamine	+250 mV
1, 2 napthoquinone	+107 mV
Phenozinemethosulfate	+80 mV
Phenylethosulfate	+55 mV
Juglone	+30 mV
Duroquinone	+5 mV
Menadione	-70 mV

2.14. SDS-PAGE

SDS-PAGE gels were cast using mini-PROTEAN 3 (Bio-Rad) gel casting equipment. All gels were 15% acrylamide (see appendix) and run in Tris-HCl-glycine-SDS buffer (see appendix) at 200 V for 45 minutes before staining to visualise protein bands. The molecular weight marker run for comparison on gels was Invitrogen (Invitrogen Ltd, Paisley, UK) SeeBlue® PreStained Standard or Low Molecular Weight protein marker (GEHealthcare).

Alternatively, protein samples were run on pre-cast Nu-PAGE® Novex 10% Bis-Tris-HCl gels (Invitrogen), using the Invitrogen Nu-PAGE® gel running equipment. Samples were prepared by mixing with 4 x Nu-PAGE® LDS Sample Buffer and Nu-PAGE® Sample Reducing Agent as appropriate. Samples were heated at 70°C before loading onto the gel (unless the gel was to be stained for haem, see section 2.16) and the gels run in 1 x Nu-PAGE® SDS (MES) running buffer. Electrophoresis was carried out at 200 V, 125 mA for 45 minutes and the gel subsequently stained as detailed below.

2.15. Staining SDS-PAGE gels

Gels were stained for total protein using Invitrogen SimplyBlue™ SafeStain. The gels were covered with the stain, and heated in the microwave on full power for 1 minute, then allowed to stain for 10 minutes. Excess stain was washed off, and gels were destained by covering with water and microwaving for a further minute. Gels were scanned once protein bands could be clearly seen and stored as jpeg images.

Haem staining is dependent on the peroxidase activity of haem groups, and links this ability to a coloured substrate for easy detection. The method described here is based on one developed by Goodhew *et al*., (1986). Samples to be stained for *c*-type cytochromes were not heated before running on the gel, to ensure the haem stayed attached to the protein during electrophoresis. Gels were washed in deionised water after electrophoresis, and then equilibrated with 70 ml 0.25 M sodium acetate, pH 5.0 for 15 minutes. This step was carried out in an opaque box with a lid to prevent light interfering with the staining procedure. 15 mg of 3, 3', 5, 5' tetramethylbenzidine was dissolved in 15 ml methanol, in the dark, and then added to the gel in the opaque box, ensuring the box was covered. After 10 minutes further equilibration, 200 µl of hydrogen peroxide was added to the gel and allowed to develop in the dark for at least 15 minutes. Blue-green bands on the gel indicated the presence of *c*-type cytochromes. Images of the gels were taken as described above.

2.16. Preparation of sample for N-terminal sequence analysis

The PVDF membrane for blotting (Amersham Hybond–P™) was soaked in methanol for 5 minutes, and then transferred to a petri dish containing blotting buffer (see appendix) with the addition of 50% methanol and DTT (where mentioned, DTT is added at 2 mg 100 ml^{-1}, unless stated otherwise). The membrane was then transferred to another dish containing blotting buffer with DTT and allowed to soak until required.

An SDS-PAGE gel was run as described previously, and rinsed in ultra-pure water containing DTT. The gel was then soaked in blotting buffer with DTT for 10 minutes with a buffer change after 5 minutes. The blotting apparatus was cleaned with deionised water and methanol, and the transblotting sandwich was set up, consisting of 3 layers of 3 mm blotting paper, the membrane for blotting, the SDS gel and 3 further layers of 3 mm blotting paper. The blotting paper was pre-soaked in blotting buffer. Electroblotting was carried out at 150 mA for 1 hour at room temperature. After blotting the membrane was washed in ultra-pure water containing DTT and then stained with 2g L^{-1} Coomassie Blue R in 5:4:1 methanol:water:acetic acid, and destained in the same solvent. The destained membrane was rinsed in water and DTT and then soaked in ultra-pure water with DTT for 10 minutes. The protein band of interest was excised for sequencing, which was carried out by the Pinnacle proteomics lab at Newcastle University, using a LF3000 gas/liquid phase Edman protein microsequencer.

2.17. Native-PAGE

In order to cast non-denaturing (native) gels, the casting equipment was cleaned thoroughly to remove all traces of SDS, and the gel mixture made up as detailed in the appendix. Native gels were cast in a single layer, no stacking gel was used. Samples were mixed with 2 x native loading buffer (see appendix) before loading, and gels were run in native running buffer (Tris-HCl-glycine, see appendix). Native gels were stained in the same way as SDS gels.

2.18. Protein concentration assay

This protein assay is based on the Bradford dye-binding assay (Bradford, 1976). Protein assay dye reagent was diluted 1 in 5 with deionised water and filtered (0.22 μM, Whatman). To create a standard curve, bovine serum albumin (BSA) stock solution (1 mg ml^{-1}) was diluted to appropriate concentrations (as recommended by manufacturer) and mixed with 1 ml of the diluted protein assay dye reagent. The standards were left for at least 5 minutes before reading their absorbance at 595 nm. Different concentrations of the unknown samples were set up (100%, 50% and 10%) and 5 μl of each mixed with 1 ml of diluted protein assay dye reagent, again leaving to stand for 5 minutes before reading absorbance at 595 nm. All samples and standards were prepared in duplicate. Protein concentration was determined by reference to the BSA standard curve.

2.19. Surface plasmon resonance

Surface plasmon resonance (SPR) was carried out using a Biosensor BIAlite™ machine (GEHealthcare), and a Series S Sensor chip CM5. The chip was equilibrated in HBS buffer (see appendix) at a flow rate of 5 μl $minute^{-1}$. Both flow cells were activated using a 1:1 ratio of ethyl-3(dimethylaminopropyl)carbodiimide:N-hydroxysuccinamide (EDC:NHS) and one binding partner (SerABC or cyt*c*4) was bound to one flow cell. Both flow cells were then blocked by washing over 35 μl of 1M ethanolamine, pH 8.5, to stop any other proteins binding to the chip. The other binding partner was then washed over both flow cells to look for a difference in binding between the bound flow cell and the reference cell.

2.20. Tryptic digest

Native cytochrome *c*4 was digested in solution using Trypsin Gold (Promega) according to manufacturers' instructions. Briefly, Trypsin Gold in 50 mM acetic acid was mixed with cytochrome *c*4 (in 30 mM Tris-HCl, pH 8.5) in a ratio of 1:20 w/w protease:protein. The mixture was incubated at 37°C for 1 hour, and analysed by SDS-PAGE.

2.21. Crystallisation trials

Crystallisation of purified protein was initially performed using commercially available screens from Qiagen, using the sitting-drop vapour-diffusion method. Each experiment was set up using a Mosquito nanolitre pipetting robot (TTP Labtech Ltd, Royston, UK) and MRC crystallisation plates containing 100 µl of 96 conditions from the PACT, JCSG+ and Classics screens. The robot was programmed to pipette 100 nl of protein into the sample well of each of the 96 wells of the crystallisation plate followed by 100 nl of each crystallant. The plates were then sealed with clear self-adhesive sealing films and equilibrated at 20°C.

Conditions in which crystals were seen were optimised by refining the composition of the crystallant solution, to generate crystals suitable for X-ray diffraction experiments. Suitable crystals were transferred to a cryoprotectant if required, mounted in a litho-loop on a SPINE specification mount (Molecular Dimensions Ltd, Newmarket, UK) and flash-frozen in liquid nitrogen. Crystals were screened for diffraction using a Rigaku micro-focus X-ray generator and an R-axis IV++ image plate detector.

2.22. Genomic DNA extraction

Genomic DNA was extracted from *T. selenatis* using the GenElute™ Bacterial Genomic DNA Miniprep Kit (Sigma), according to manufacturers' instructions. DNA purified in this way was used for downstream applications such as PCR.

2.23. Polymerase chain reaction (PCR)

Forward and reverse primers for PCR were obtained from MWG Oligonucleotides. Primer sequences can be found in Table 2.3, with restriction enzyme sites in red. The DNA polymerase used for PCR was 1.1 x Thermo-Start Master Mix (ABgene, Epsom, UK), or Phusion™ High-Fidelity polymerase (New England Biolabs, Hitchin, UK).

PCR was carried out using an Eppendorf Mastercycler EpGradient machine. PCR products were run on agarose gels to check product size (see section 2.26).

Table 2.3: Sequences of primers used within this study

Primer name	Sequence (5' to 3')
***bc*$_1$ fwd**	TGG CCT TCG CCT CGG TCG AGC ATA TCA TGC
***bc*$_1$ rev**	TGG CGT AGA AGG GCA GGA AAT ACC ATT CCG
SerC fwd	ACT GGG AGA ATT CAT ATG AGA ACA TCC AGC
SerC rev	AGC CCG GTT CTC GAG TCA GAA GTT CAG CTG
Cyt*c*4 fwd1	GGC CCA CCG GCA TGY AAR AAG GAA GGC ATC
Cyt*c*4 rev1	TCG CCG GTC TTG CCG TGG CAT TCC AGG CAT
Cyt*c*4 rev2	CTT GTA GTG CTG GCC GGC GAT TAC CGG GTA GAA

2.24. Agarose gel electrophoresis

Agarose gel electrophoresis was used to separate DNA products by size. Agarose gels were made from 1% w/v agarose in TBE buffer (tris-HCl-borate-EDTA, see appendix), with 0.5 μg ml^{-1} ethidium bromide for visualising DNA bands under UV light. Samples were mixed with 6 x blue/orange loading dye (Promega) before loading onto the gel and Quick-Load 1 kb DNA ladder (NEB) was also run on the gel to calculate the size of DNA fragments. The gel was run at 100 V, 200 mA for 1-1.5 hours, depending on the size of fragments to be separated, and the fragments visualised using a UV light box.

2.25. Extraction of DNA from agarose gels

DNA fragments to be purified were removed from the gel with a scalpel and extracted from the gel slices using the QIAquick Gel Extraction Kit protocol. Extraction efficiency was checked by running small amounts of the purified samples on an agarose gel. DNA was quantified by measuring absorbance of the sample at 260 nm, where 1 $A_{260\ nm}$ unit of double stranded DNA represents a concentration of 50 μg ml^{-1}. DNA samples were stored at -20°C.

2.26. Restriction digests

Restriction enzymes for digests were purchased from Promega, and reactions carried out according to manufacturers' protocols. Typically, DNA was digested for 1 hour, incubated at 37°C. Restriction enzyme recognition sequences are included in Table 2.3.

2.27. Ligations

T4 DNA ligase (Promega) was used to ligate DNA fragments into cloning or expression vectors. The DNA concentration of both insert and vector was measured at 260 nm, varying ligation ratios of insert:vector were set up, and incubated overnight at 4°C, before the ligated construct was transformed into an appropriate *E. coli* strain (see section 2.29).

2.28. Competent cell preparation

Competent cells for transformations were prepared using an adaptation of the method of Hanahan (1985). A single colony from an LB agar plate was used to inoculate a flask containing 25 ml LB, which was cultured overnight at 37°C. Two millilitres of this overnight culture was used to inoculate a 200 ml flask of LB containing 20 mM $MgSO_4$, which was grown at 37°C with agitation (180 rpm) to exponential phase (OD_{600nm} 0.4-0.6). At this point the cells were harvested by centrifugation (6,300 x *g*, 10 minutes, 4°C), resuspended in 100 ml ice-cold TFB1 (see appendix) and left on ice for 5 minutes. The cells were harvested by centrifugation as before, resuspended gently in 10 ml TFB2 (see appendix) and left on ice for a further hour. The cells were then aliquotted, flash-frozen in liquid nitrogen and stored at -80°C.

2.29. Transformation into *E. coli* strains

Competent cells were thawed on ice and 50 µl aliquots gently mixed with the DNA to be transformed, then incubated on ice for 20 minutes. In the case of ligations, the 20 µl reaction was split into 16 µl and 4 µl to vary the amount of DNA transformed. In the case of purified plasmids, 2 µl was added to the competent cells.

After the incubation on ice, the cells were heat-shocked at 42°C for 45 seconds, and then returned to incubate on ice for a further 2 minutes. 950 µl of LB medium was added to each reaction, and the cells then incubated at 37°C for 90 minutes, with agitation. Cells were harvested by centrifugation (12,000 x *g*, 2 minutes) and

resuspended in 100 µl LB. The resuspended cells were spread onto LB agar plates containing the appropriate antibiotic and supplements, and the plates incubated at 37°C overnight.

2.30. Plasmid purification

Plasmids were purified from overnight cultures using the Eppendorf Fast Plasmid Kit, following the manufacturers' protocol. Extracted plasmids were stored at -20°C.

2.31. DNA sequencing of plasmid constructs

DNA to be sequenced was first precipitated; 2 volumes of ice-cold 100% ethanol, and 5 M potassium acetate to a final concentration of 0.25 M were added to the DNA, and mixed by vortexing. This solution was stored overnight at -80°C, and the precipitated DNA subsequently harvested by centrifugation (12,000 x *g*, 20 minutes). The supernatant was aspirated and the DNA pellet washed with 200 µl of 70% ethanol. DNA was harvested as previously described, and the pellet dried at 30°C before sending for sequencing.

2.32. Expression tests

A single colony of *E. coli* BL21 (DE3) containing the pSerC expression plasmid was inoculated into 10 ml of LB broth containing ampicillin and grown to an $OD_{600\ nm}$ of 0.4-0.6, then induced with 1 mM IPTG for 3 hours at 37ºC. One millilitre of cells was harvested by centrifugation at 4,000 x *g* for 5 minutes and resuspended in 200 µl of SDS-PAGE loading buffer and boiled for 5 minutes to lyse cells and denature proteins. The lysate was analysed by SDS-PAGE.

2.33. Large-scale expression

A single colony of *E. coli* BL21 (DE3) containing the pSerC expression plasmid was inoculated into 100 ml of LB broth containing ampicillin and cultured overnight. The overnight culture was used to inoculate 2 x 1 L flasks of LB ampicillin to an $OD_{600\ nm}$ of 0.02. The cultures were grown at 37ºC and induced with 1 mM IPTG when they reached an $OD_{600\ nm}$ of 0.4-0.6. Cells were induced for 3 hours before harvesting by centrifugation at 4,000 x *g* for 15 minutes. The pellet was resuspended in 30 ml of 20 mM Tris-HCl pH 8.5 and centrifuged again at 4,000 x *g* for 15 minutes. This pellet was stored at -80ºC until required.

2.34. Purification of inclusion bodies

The cell pellet was resuspended in 30ml of 20 mM Tris-HCl pH 8.5, 1 mM DTT, 1 mM AEBSF (serine protease inhibitor) and sonicated for 5 minutes with a cycle of 1 second on, 1 second off. Cells lysate was clarified by centrifugation at 25,000 x *g* for 30 minutes at 4ºC. The supernatant was discarded and the pellet was resuspended in 30 ml ice-cold 50 mM Tris-HCl pH 8.5, 100 mM NaCl, 0.5 % Triton X-100 then centrifuged at 25,000 x *g* for 30 minutes at 4ºC. The pellet was washed in 50 mM Tris-HCl pH 8.5, 100 mM NaCl and centrifuged as before. The washed inclusion body pellet was solubilised in denaturation buffer (6 M guanidine HCl, 50 mM Tris-HCl pH 8.5, 100 mM NaCl, 10 mM EDTA) at 4ºC overnight on a benchtop shaker.

2.35. Protein refolding

One ml of solubilised, denatured protein was incubated with DTT to a final concentration of 10 mM for 1 hour at room temperature. For rapid dilution refolding, this reduced protein solution was added dropwise to 100 ml of ice-cold refolding buffer (50 mM Tris-HCl pH 8.5, 100 mM NaCl, 10 mM DTT, 0.4 M arginine) with stirring. The concentration of the denatured protein solution was determined, and a 2-fold excess of hemin chloride was added to the refolding buffer before addition of protein. Hemin chloride solution was prepared by dissolving 10 mg of hemin chloride in 1 ml DMSO followed by rapid vortexing, and centrifuging at 14,000 x *g* for 10 minutes. The haem concentration of the supernatant was determined spectrophotometrically using the extinction coefficient $\varepsilon_{385\ nm} = 56\ cm^{-1}\ mM^{-1}$ (Karlsson & Nilsson, 2005). The refolding solution was stirred overnight at 4ºC. The solution was centrifuged to remove aggregated protein at 20,000 x *g* for 10 minutes. For refolding via dialysis, 1 ml of protein was sealed in dialysis tubing (6 kDa MWCO) (Fisher), and dialysed into refolding buffer containing 6 M urea for 3 hours at 4ºC. This dialysis was repeated, reducing the concentration of urea by 2 M in each step. The final dialysis into 0 M urea was carried out overnight.

3. Investigation of the *b*-haem binding subunit SerC

3.1. Introduction

The water soluble, periplasmic selenate reductase of *T. selenatis* contains a number of metal centres; the catalytic molybdenum co-factor, iron-sulfur centres and a *b*-haem. The presence of a *b*-type haem in the periplasm is unusual, and found only among a few of the type-II molybdo-enzyme family, such as chlorate reductase from from *I. dechloratans*, ethylbenzene dehydrogenase from *A. aromaticum*, and DMS dehydrogenase from *R. sulphidophilum.* The ethylbenzene dehydrogenase enzyme (Ebd) is the only one for which structural information is available, and the *b*-haem containing γ subunit which is homologous to SerC provides some interesting information (Kloer *et al.*, 2006). The unusual haem co-ordination by methionine and lysine residues has only been seen in this structure.

When the sequence of SerC is input into the BLAST alignment tool, few similar sequences are found. These include the gamma subunits from the chlorate reductase, ethylbenzene dehydrogenase and DMS dehydrogenase, as well as from several uncharacterised molybdo-enzymes identified in microbial genomes. The similarity between SerC and ClrC is much higher (76% identity) than with EbdC (28%) and DdhC (32%), although the methionine and lysine residues shown to co-ordinate the haem in EbdC (Kloer *et al.*, 2006) are among the conserved residues (figure 3.1). A protein from the recently sequenced *Sulfurihydrogenibium* sp. YO3AOP1 (SYO3AOP1_1177) with similarity (33% identity) to SerC is identified from the BLAST search, along with a homologous protein from *Hydrogenivirga* sp. 128-5-R1-1, although the genome sequence of *Hydrogenivirga* has not been completed, and the C-terminus of the protein is labelled incomplete. *Sulfurihydrogenibium* species are thermophiles which can use molecular hydrogen or sulfur compounds as electrons donors, and electron acceptors including nitrate, selenate and arsenate (Takai *et al.*, 2003). Interestingly, the N-terminal domain of the protein has identity to SerC, while a longer C-terminal domain includes a CXXCH motif predicted to bind a *c*-type cytochrome (see figure 3.2). The N-terminal domain retains the Met and Lys residues thought to be involved in *b*-haem binding, which raises the question of whether this protein binds both *b* and *c*-type haem, a highly unusual occurence. The gene encoding this protein is in an operon consisting of an

alpha subunit containing a Tat leader sequence, which has homology to SerA, NarG and DdhA, and a beta subunit also showing high identity with the Fe-S subunits of the type II DMSO reductase family. The alpha subunit lacks the 'QT' motif which has been used as an indicator of nitrate reductase activity (Martinez-Espinosa *et al.*, 2007), but contains the conserved aspartate residue which co-ordinates the Mo in the type II DMSO reductase family. Given that *Sulfurihydrogenibium* sp. can respire selenate, this could be a putative selenate reductase. When the C-terminal domain (~150 residues) of SYO3AOP1_1177 is used as the query sequence, it shows similarity (although low) to a number of cytochromes *c*, including the cytochrome c_1 subunit of quinol: cytochrome *c* oxidoreductases (QCR). Could this protein be a fusion between a cytochrome *b* and a donor/acceptor *c*-type cytochrome? It has already been shown that the DdhC subunit donates electrons to a downstream cytochrome c_2 (McDevitt *et al.*, 2002a, Yoshida *et al.*, 2001), but nothing is known about the way in which SerC receives its electrons. This unusual protein adds weight to the argument that a *c*-type cytochrome could be the donor to SerC. It is important therefore, to study the SerC subunit more closely, investigate how its redox potential compares to those found in homologous enzymes, and how it may interact with upstream electron donors. To obtain SerC for these studies, two approaches were taken, firstly to purify native SerABC from *T. selenatis* cultures, and secondly to clone and express SerC hetrologously to obtain SerC separately from the A and B subunits, to search for possible interacting electron donors.

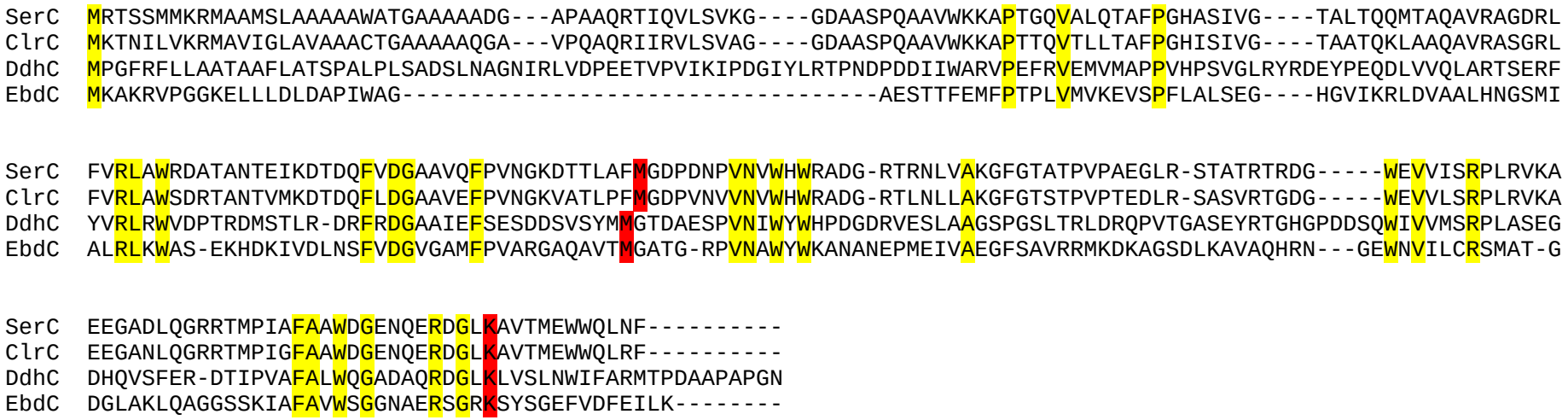

Figure 3.1: Sequence alignment of SerC and related proteins.

SerC – selenate reductase from *T. selenatis*, ClrC – chlorate reductase from *I. dechloratans*, DdhC – dimethylsulfide dehydrogenase from *R. sulfidophilum*, EbdC – ethylbenzene dehydrogenase from *A. aromaticum*. Conserved residues are highlighted yellow, methionine and lysine residues which are predicted/known to co-ordinate the *b*-haem are in red.

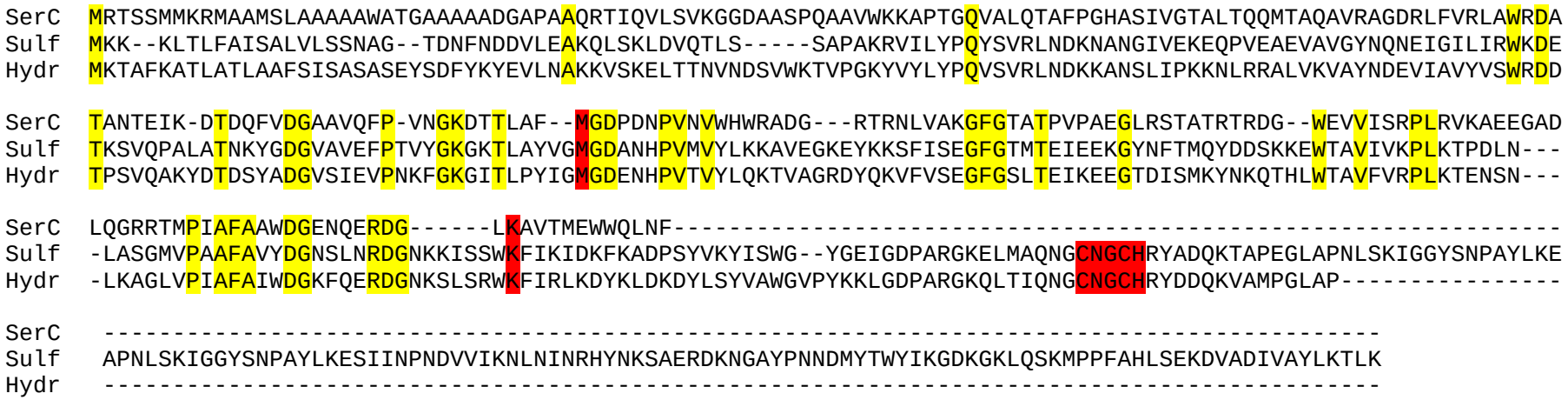

Figure 3.2: Alignment between SerC and class I *c*-type cytochromes from *Sulfurihydrogenibium* sp. YO3AOP1 and *Hydrogenivirga* sp. 128-5-R1-1. For reference, the cytochrome from *Sulfurihydrogenibium* sp. has the locus tag SYO3AOP1_1177 and that from *Hydrogenivirga* sp. has HG1285_11757. Conserved residues are highlighted in yellow, the methionine and lysine residues predicted to be involved in *b*-haem co-ordination in SerC are highlighted red, as is the CXXCH motif of the *c*-type cytochromes.

3.2. Purification of selenate reductase

In order to study the properties of the SerC subunit, selenate reductase enzyme was purified from the periplasm of *T. selenatis* selenate respiring cultures based on a protocol previously described by Schroder *et al.,* (1997). From 10 L batch cultures, the periplasmic fraction was prepared as described in section 2.2 resulting in a final volume of 35 ml, which was subjected to ammonium sulfate precipitation. Selenate reductase activity was tracked using a qualitative microplate assay (Ridley *et al.,* 2006a) (described in section 2.8) and the enzyme was shown to precipitate out between 50-80% ammonium sulfate. This precipitate was resuspended in 4 ml of 50 mM PIPES buffer pH 6.0 containing 1 M ammonium sulfate, and applied to a 1 ml HiTrap Phenyl Sepharose column equilibrated in the same buffer. Bound proteins were eluted in 0.5 ml fractions by reducing the amount of ammonium sulfate in the buffer from 1-0 M over 40 ml (figure 3.3a). Those fractions containing selenate reductase activity were identified by microtitre plate assay as before. Active fractions (elution volume 16-24 ml) were pooled and concentrated to 2 ml using a 15 ml centrifugal concentrator with a 30 kDa molecular weight cut-off (MWCO). SerABC was then further purified by gel filtration (GF) chromatography. A Superdex 200 16/60 column was equilibrated with 50 mM PIPES pH 6.0 and the pooled protein applied to the column, 1 ml fractions were collected (figure 3.3b) and analysed for SerABC via plate assay as described previously. Activity was detected in fractions containing elution volumes 71-79 ml so these were pooled and concentrated to a final volume of 250 µl then stored at -80ºC until required. SDS-PAGE analysis of samples at each stage of the purification was carried out to assess the purity of the enzyme (figure 3.4). The final concentrated sample was estimated to be ~ 80% pure, further purification was attempted but although higher purity was obtained, selenate reductase activity was lost. The specific activity of the concentrated enzyme was measured using methyl viologen cuvette assays, and was determined to be 0.12 µmol SeO_4^{2-} min^{-1} mg^{-1}. A *c*-type cytochrome of approximately 25 kDa was found to co-purify with the selenate reductase enzyme until the GF step, where it eluted around 97 ml (figure 3.3b and figure 3.4, lane 9). This cytochrome could be a potential electron donor to SerC, a possibility that will be discussed more fully in chapter 4.

A

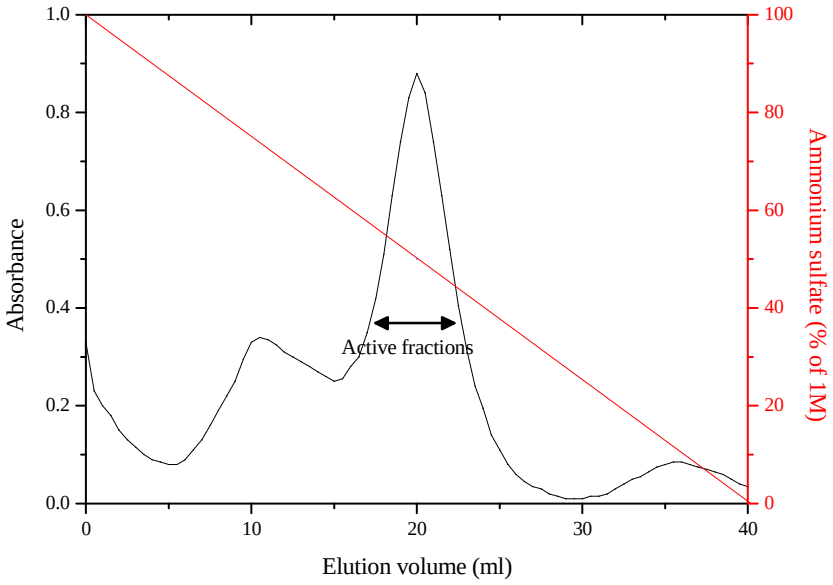

B

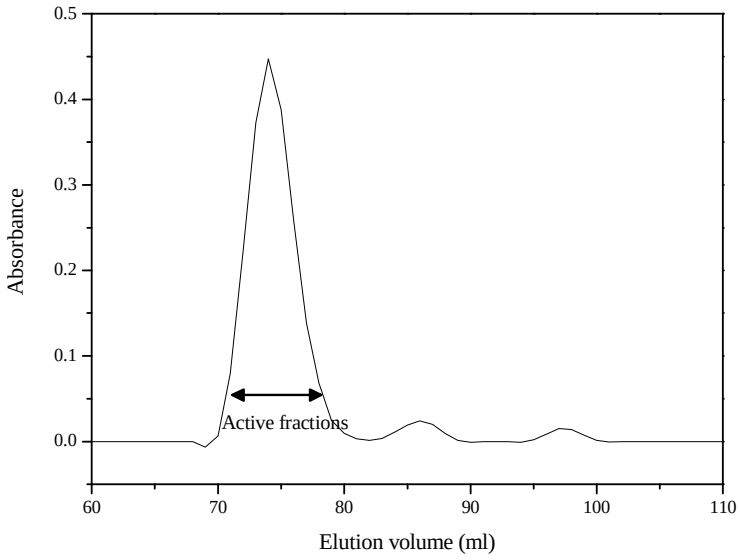

Figure 3.3: Purification of the selenate reductase from *T. selenatis*.

A: Absorbance of eluted fractions (280 nm) from the Phenyl Sepharose column (black) and increasing gradient of buffer without ammonium sulfate (red). B: Absorbance of eluted fractions (280 nm) from Superdex 200 gel filtration column. Active fractions as indicated are those which showed selenate reductase activity using the microplate method.

A

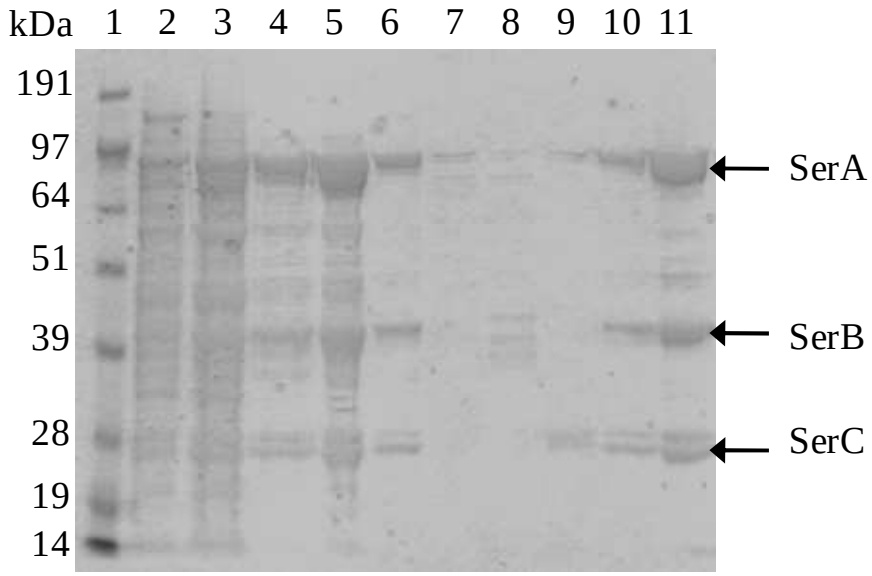

B

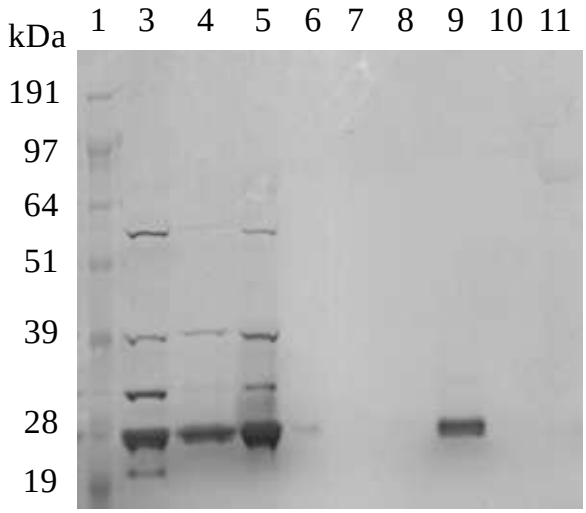

Figure 3.4: SDS-PAGE analysis of the purification of selenate reductase from *T. selenatis*.

Expected sizes for SerA, B and C are ~ 96, 40 and 23 kDa respectively. A: Gel stained for total protein, B: Haem stained gel. Lane 1 – Invitrogen SeeBlue Plus2 prestained standard. Lane 2 – Periplasm. Lane 3 – resuspended pellet from 80% ammonium sulfate cut. Lane 4 – fraction corresponding to elution volume 20 ml from the Phenyl Sepharose column. Lane 5 – protein loaded onto GF column. Lanes 6-9 – GF fractions corresponding to 74, 79, 86 and 97 ml. Lane 10 – pooled active fractions from GF column. Lane 11 – pooled and concentrated active fractions from GF. Lane 2 is missing from gel B due to a gel-loading problem.

3.3. Spectroscopic characterisation of SerC

The UV-visible spectrum of purified SerABC was recorded on 'as prepared' and reduced samples (see figure 3.5) to check for the presence of the haem in SerC. The reduced enzyme showed absorbance maxima at 424, 528 and 558 nm, characteristic of a *b*-haem, and these values agree with data published previously (Schroder *et al.*, 1997).

3.4. Determination of the redox potential of SerC

The redox potential of a protein is the point at which half of the protein is in an oxidised state and half is reduced, and is a measure of the tendency of the haem to accept or donate electrons. A brief summary of redox chemistry, adapted from Dutton (1978) is given below. The redox potential of a couple can be written as a half cell equation (equation [2]), where *n* is the number of electrons transferred, and is measured relative to the standard hydrogen half cell (abbreviated to SHE) which is H_2 gas at 1 atm pressure in equilibrium with a 1 M solution of H^+ at pH 0 (equation [3]), and is given a value of 0 V at any temperature.

$$A_{red} = A_{ox} + ne^- \qquad [2]$$

$$\tfrac{1}{2}H_2 = H^+ + e^- \qquad [3]$$

The complete cell reaction must include another half cell, as written in equation [4], and the equilibrium constant of the reaction, K_{eq} can be described by equation [5].

$$A_{red} + B_{ox} = A_{ox} + B_{red} \qquad [4]$$

$$K_{eq} = \frac{[A_{ox}][B_{red}]}{[A_{red}][B_{ox}]} \qquad [5]$$

The free energy of the reaction under standard conditions is called ΔG^o, and is equal to $-RT \ln K_{eq}$, where R is the ideal gas constant, and T is the temperature in Kelvin. For non-standard conditions, the equation can be rewritten as seen in equation [6].

$$\Delta G = \Delta G° + RT \ln \frac{[A_{ox}][B_{red}]}{[A_{red}][B_{ox}]} \qquad [6]$$

ΔG can be converted to electrical potential units using the equation $\Delta G = -nF\,\Delta E$, where F is the Faraday constant, or conversion factor. If this equation is substituted into equation [6], and rearranged, we can produce equation [7].

$$E_{(B)} - E_{(A)} = E_{0(B)} - E_{0(A)} + \frac{RT}{nF}\ln\frac{[B_{ox}]}{[B_{red}]} - \frac{RT}{nF}\ln\frac{[A_{ox}]}{[A_{red}]} \qquad [7]$$

If we state that A is the SHE half cell, which has a value of 0 V, equation [7] can be simplified; $[A_{ox}] = [A_{red}]$, therefore $RT/nF \ln [A_{ox}]/[A_{red}] = 0$, and $E_{(A)} = E_{0(A)}$, which is 0 V by definition. The B half cell is then relative to the SHE, and the simplified equation is known as the Nernst equation (equation [8]).

$$E_h = E_0 + \frac{RT}{nF}\ln\frac{[B_{ox}]}{[B_{red}]} \qquad [8]$$

E_0 is defined as the standard redox potential of the B couple, under standard conditions, and E_h denotes the fact that the potential is measured relative to the SHE. For biological couples, the measurement of a redox couple is unlikely to occur under standard conditions (pH 0, unit activity) so E_0 is replaced with E_{mx}, where m stands for midpoint potential, and x is the pH at which the redox determination is carried out.

For cytochromes, the concentration of reduced/oxidised protein can be measured spectrophotometrically by monitoring the spectrum of the protein at a specific wavelength (usually in the Soret or α-band region of the spectrum) and the redox potential of the solution, while small amounts of oxidant or reductant are added. The purified SerABC complex was used to determine the midpoint potential of SerC. The redox potential of the haem was determined by optical redox titration with mediators, according to the method of Dutton (1978), as described in section 2.13, by monitoring the absorbance of the haem at 558 nm (adjusted with reference to an isosbestic point at 575 nm) during sequential oxidation and reduction. The absorbance was monitored at the α-band wavelength rather than that of the Soret band, as the redox mediators used do not absorb in the α-band region, but might interfere at Soret band wavelengths. The fraction of protein reduced at each measured potential was calculated and then plotted as a function of redox potential (see figure 3.6). The Nernst curve corresponding to n=1 electrons was fitted to the data using TableCurve 2D (Systat Software Inc.), which gave a midpoint potential of +234±5 mV.

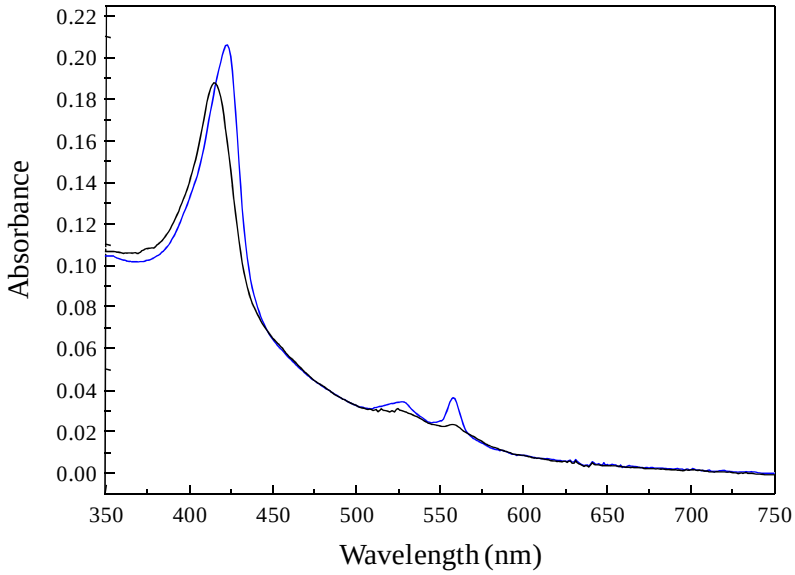

Figure 3.5: UV-visible absorbance spectra of SerABC.

2 µM SerABC in 50 mM PIPES pH 6.0, 'as prepared' (black line) and reduced with sodium dithionite (blue).

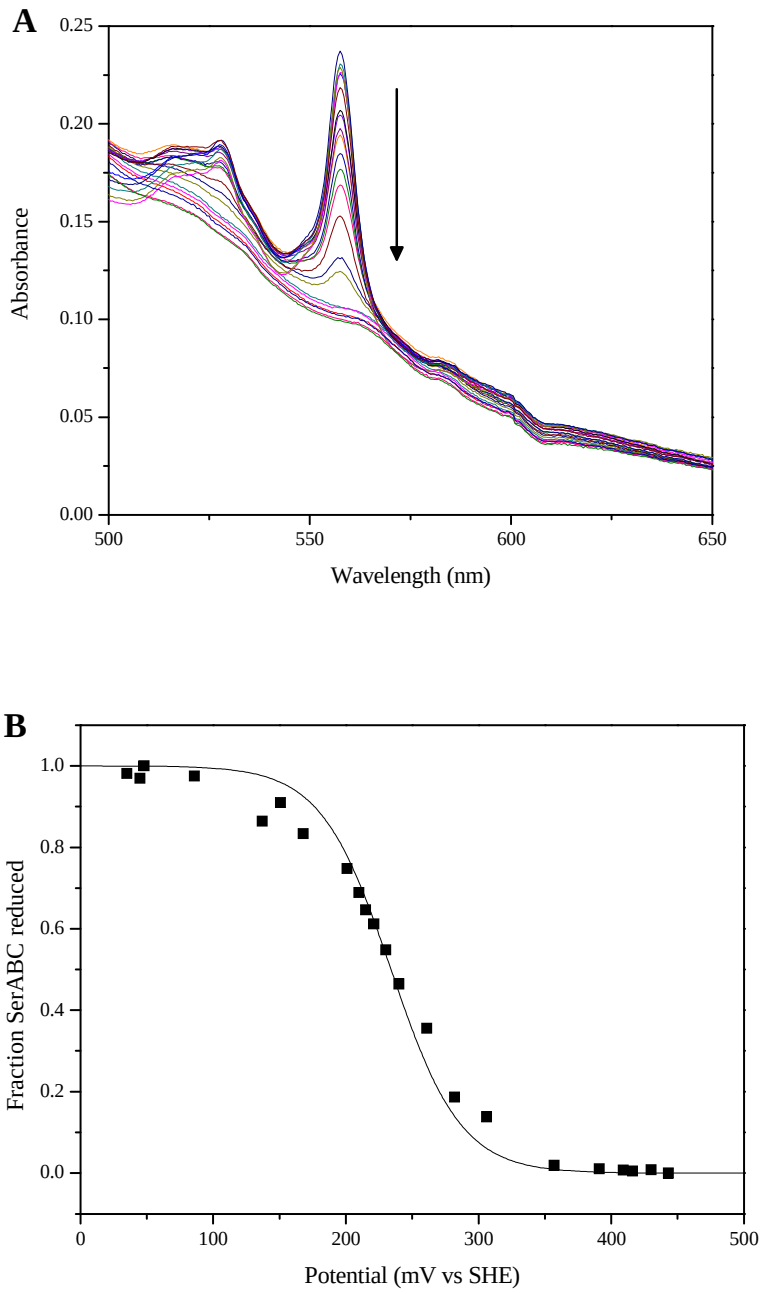

Figure 3.6: Optical redox titration of the *b*-haem of SerC

A: α and β region of SerC spectra during titrations. Black arrow indicates increasing redox potential. B: Fraction of cytochrome reduced as calculated with reference to absorbance at 558 nm, as a function of redox potential. Nernst curve for n=1 electrons is also shown. Titration was carried out with 2.5 µM protein in 30 mM Tris pH 7.5, at 21ºC.

3.5. PCR and cloning of the *serC* gene

In order to produce larger amounts of SerC to study its interaction with electron donors such as *c*-type cytochromes, cloning of the *serC* gene and heterologous expression in *E. coli* was attempted (see figure 3.7). Primers were designed to amplify the *serC* gene from purified *T. selenatis* genomic DNA including the signal sequence predicted to target the protein to the periplasm through the Sec export machinery (Krafft *et al.*, 2000). The primers incorporated restriction sites for the enzymes *Nde*I and *Xho*I in forward and reverse primers respectively to allow insertion into the expression plasmid pET22b (Novagen). For sequence of primers, see table 2.3. PCR produced a fragment of approximately 0.7 kb (figure 3.8a) which was excised from the gel and purified. This DNA fragment was digested with *Nde*I and *Xho*I, and ligated overnight into similarly digested pET22b. The ligation was transformed into *E. coli* JM109 cells producing four colonies which were each cultured in 5 ml LB ampicillin overnight. Plasmids were purified from these four overnight cultures, and diagnostic digestion with *Nde*I and *Xho*I was carried out to confirm insertion of the gene (see figure 3.8b). Digested plasmid from colonies 1, 3 and 4 showed bands of the expected sizes at 5.4 kb (corresponding to linearised pET22b) and ~0.7 kb (corresponding to *serC*). Plasmids were sent for sequencing to confirm insertion of the correct gene, *serC* was correctly inserted into plasmids 3 and 4, and these plasmids were designated pSerC3 and 4.

3.6. Expression of SerC

In comparison to *c*-type cytochromes, the mechanism by which cytochromes *b* are assembled is unknown. It is not known whether a separate maturation system is necessary or if no additional proteins are required. The cytochrome *c* maturation (Ccm) system in *E. coli* which assembles *c*-type cytochromes is only expressed anaerobically, but membrane bound *b*-type haems including the bo_3 oxidase can be expressed under aerobic conditions, suggesting the Ccm system may not be involved (Thony-Meyer, 1997). The situation regarding soluble *b*-haems is unknown as they are much less common than membrane bound *b*-haems, although the periplasmic cytochrome b_{562} can be expressed in *E. coli* mutants lacking the ability to synthesise *c*-type cytochromes (Goldman *et al.*, 1996). The haem of the EbdC subunit is buried in a hydrophobic pocket (Kloer *et al.*, 2006), making it unlikely that the haem can be inserted after protein folding, but the manner in which the *b*-haem and apoprotein are brought together is unknown.

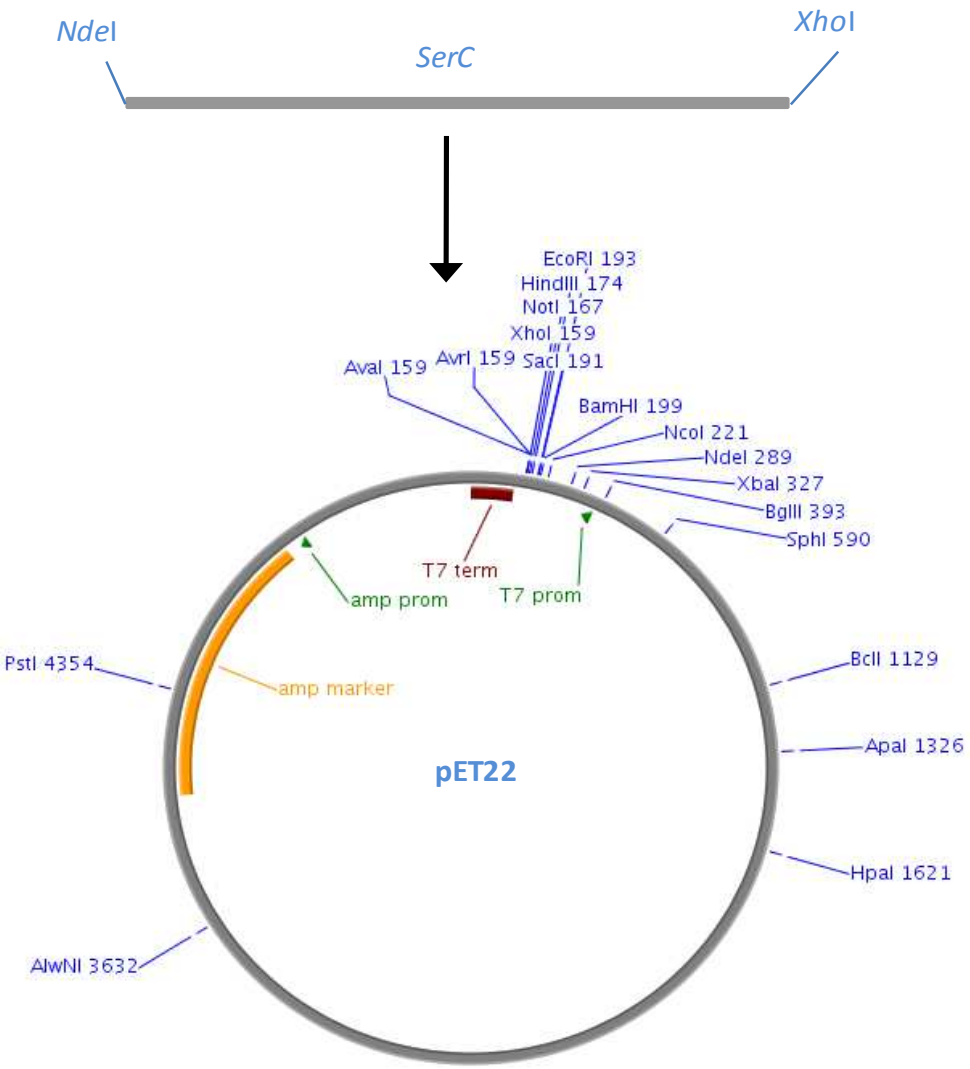

Figure 3.7: Cloning strategy for *serC* gene.

Plasmid map was created using the online tool PlasMapper (Dong *et al.*, 2004). http://wishart.biology.ualberta.ca/PlasMapper/.

A

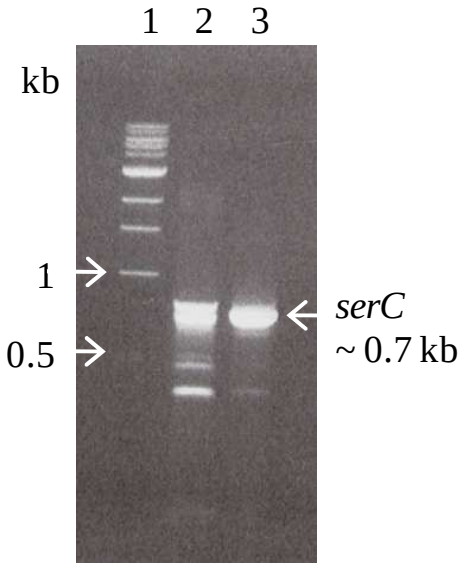

B

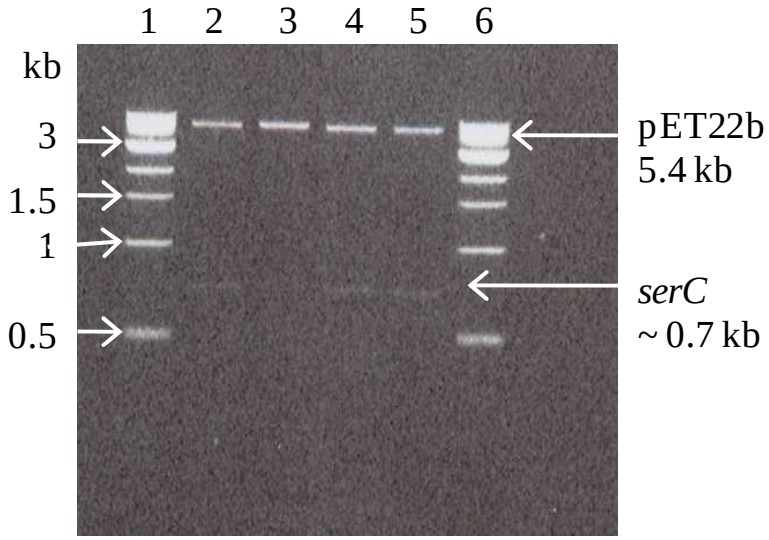

Figure 3.8: PCR and cloning of *serC* from *T. selenatis*.

A: agarose gel showing PCR of *serC* from genomic DNA. Lane 1 – NEB Quick-load 1 kb ladder. Lane 2 – PCR annealing temperature of 55ºC. Lane 3 – PCR annealing temperature of 60 ºC. B: agarose gel of plasmids from transformants, digested with *Nde*I and *Xho*I. Lanes 1 and 6 – NEB Quick-load 1 kb ladder. Lanes 2-5 – plasmid from colonies 1-4 respectively.

As the periplasmic cytochrome b_{562} can be expressed aerobically, it was thought that aerobic expression of SerC was the best way to proceed. The two pSerC plasmids were transformed into the expression strain *E. coli* BL21 (DE3), and small scale expression tests in 10 ml culture volumes were carried out to see which of the plasmids expressed most efficiently. After inducing protein expression for 3 hours at 37ºC, whole cells were lysed in SDS-PAGE loading buffer and the lysate analysed by SDS-PAGE. Both cultures showed an over-expressed protein at around 28 kDa (see figure 3.9a), slightly above the expected size of SerC, but this could be due to the periplasmic leader sequence being uncleaved. pSerC3 was chosen as the plasmid to use for further large-scale expression, as there was no expression of SerC in the uninduced sample, whereas pSerC4 showed somewhat 'leaky' expression, producing protein even in the absence of IPTG.

3.7. Large-scale expression of SerC

SerC was expressed in *E. coli* BL21 (DE3) in 1 L cultures, aerobically at 37ºC as described in section 2.33. While washing the cells, a white layer was observed in the cell pellet, indicative of inclusion body formation. These were purified as described in section 2.34, by washing with a buffer containing 0.5% Triton X-100 detergent to solubilise and remove any cell membrane before denaturing in 6 M guanidine HCl. The denatured protein was analysed by SDS-PAGE (figure 3.9b) and shown to contain a large amount of the 28 kDa protein expected to be unprocessed SerC. As the SerC is predicted to be in its unprocessed state, it will not have been exported to the periplasm and therefore is unlikely to contain haem. The lack of brown colour in the protein sample confirmed this, and so the denatured protein needed to be reconstituted with haem. Attempts to produce soluble SerC by expressing at lower temperatures (18, 25 or 30ºC) and altering the concentration of IPTG (0.1 mM and 0.5 mM) were unsuccessful.

A

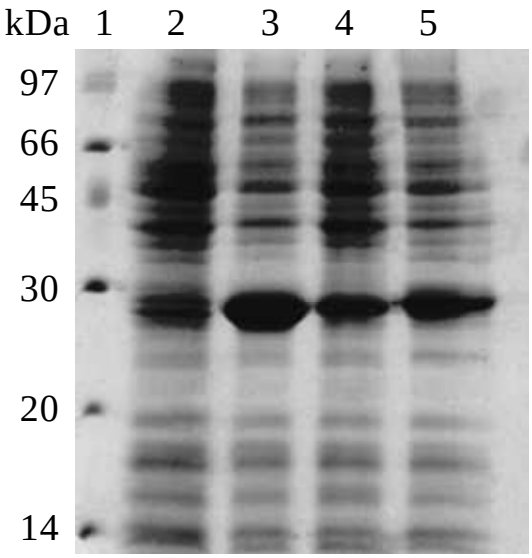

B

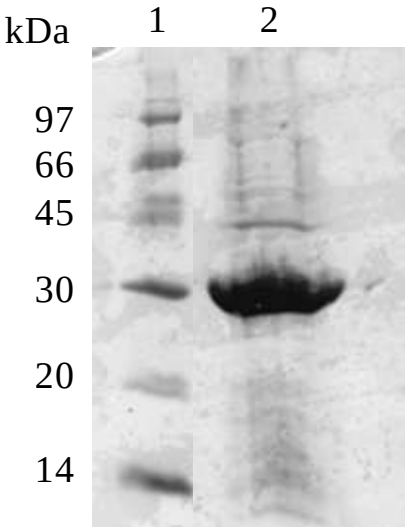

Figure 3.9: Expression of SerC in *E. coli*.

A: SDS-PAGE gel of total protein from *E. coli* BL21 (DE3) cultures containing the plasmids pSerC3 or pSerC4. Lane 1 – Low molecular weight marker (GEHealthcare). Lane 2 – pSerC3 uninduced. Lane 3- pSerC3 induced. Lane 4 – pSerC4 uninduced. Lane 5 – pSerC4 induced. B: SDS-PAGE gel of solubilised, denatured inclusion bodies from large scale expression of SerC. Lane 1 – Low molecular weight marker (GEHealthcare). Lane 2 – solubilised inclusion bodies.

3.8. Refolding and haem reconstitution of SerC

Denatured protein was refolded by the rapid dilution technique, or by dialysis (section 2.35). The rapid dilution technique involves adding a small volume, in this case 1 ml, of denatured protein dropwise to a large volume of refolding buffer (100 ml), which does not contain the denaturant. In this case, the refolding buffer was based upon one used by Karlsson *et al*., (2005) to refold the ClrC subunit of the chlorate reductase from *I. dechloratans*. The refolding buffer contains 100 mM NaCl to help stabilise the refolding proteins, and 0.4 M arginine which helps to avoid aggregation of proteins during refolding (Arakawa *et al.,* 2007), as well as a 2-fold molar excess of hemin chloride to the concentration of protein. In step-wise dialysis, the denatured protein was sealed inside dialysis tubing and placed into 1 L of refolding buffer containing 6 M urea, then stirred at 4ºC for three hours. This was repeated two further times, reducing the urea concentration in the buffer by 2 M each time. The final refolding step into 0 M urea was allowed to dialyse overnight. Both methods were carried out with and without hemin chloride in the buffer.

Unfortunately, neither of the methods of refolding yielded any soluble protein, all SerC precipitated out during refolding. As we observed earlier, the periplasmic leader sequence of SerC might not be recognised by the *E. coli* Sec system, therefore the protein is not exported to the periplasm, and the signal sequence is uncleaved. This could well be interfering with the folding of the protein *in vivo*, and in our refolding trials, and preventing reconstitution of the protein.

3.9. Discussion

The determination of the redox potential of SerC has allowed us to add to our knowledge of the redox centres in SerABC, and is the first periplasmic reductase of the Type II molybdo-enzymes to have the potential of its *b*-haem determined. Figure 3.10 shows the known midpoint potentials of redox centres within Nar, Ser, Ebd and Ddh, for comparison, from the redox potential of the substrate to the average potential of quinols in the Q-pool. Nar is perhaps the best characterised, as the midpoint potentials of all redox centres are known, and it is the only member of the family in which the unusual FS0 cluster has been characterised. SerABC is the least studied, although the recent publication of the redox potentials of the FS1-4 clusters of SerB (Dridge *et al.*, 2007) and now the *b*-haem of SerC can be added to the picture. The value of +234 mV

determined in this work is similar to those determined for EbdC and DdhC, although it is the lowest of the three. NarI also contains *b*-haems, but is membrane bound and the haems are lower potential (120 and 20 mV). A difference between NarI and the *b*-haems of SerC, EbdC and DdhC is the co-ordination of the haems. In NarI, both haems have *bis*-histidinyl co-ordination, whereas the periplasmic haems are co-ordinated by methionine and lysine residues, and this could contribute to the differences in potential. The sulfur of methionine residues is a good electron acceptor, and could contribute to stablilising the reduced state of the haem, therefore raising the midpoint potential. The high potential of SerC is unusual however, as both Ebd and Ddh are dehydrogenase enzymes which work in the opposite direction to Ser, so the presence of a high potential haem in the C subunit can draw electrons from the active site for transfer to downstream electron acceptors. Little is known about the evolution of the type II DMSO reductase family, but it is possible that the reductase enzyme evolved from a dehydrogenase enzyme, using substrates such as selenate and chlorate as electron acceptors because a high potential substrate was necessary to overcome the otherwise unfavourable high potential of the C subunit. It is also relatively unusual to find a *b*-type haem located in the periplasm, few are known except SerC homologues and cytochrome b_{562} from *E. coli* which is of unknown function. Assembly of *b*-type cytochromes is poorly understood compared to *c*-type cytochromes, and the benefit of having a *b*-haem instead of the more common *c*-type cytochrome in the periplasm is not clear. One of the type II molybdo-enzymes possesses a *c*-type cytochrome as a γ subunit, perchlorate reductase from *D. agitata* has a tetra-haem cytochrome *c* subunit in place of the *b*-haem of SerC/EbdC/ClrC, but the enzyme was missing this subunit when purified (Kengen *et al.*, 1999), unlike other enzymes in the family, suggesting it might act as an electron shuttle rather than part of the heterotrimeric complex.

As the potential of SerC is relatively high, it could accept electrons from a number of sources, such as a membrane bound donor or a periplasmic *c*-type cytochrome. The identification in this study of a protein from *Sulfurihydrogenibium* sp. YO3AOP1 which shows homology to SerC but has an additional predicted *c*-type cytochrome domain suggests that a *c*-type cytochrome could be the electron donor to SerC. This protein and the homologue identified from *Hydrogenivirga* sp. 128-5-R1-1 could bind both *c* and *b*-type haem, which is a unique property – no other polypeptides have yet been identified with this characteristic. It is possible however, that they represent a form of the γ subunit of type II molybdo-enzymes which have homology to the *b*-haem binding

subunits, but have evolved to bind a *c*-type haem instead, perhaps to provide a more stable protein. Both *Sulfurihydrogenibium* and *Hydrogenivirga* sp. are known to be thermophilic organisms (Nakagawa *et al.*, 2004, Takai *et al.*, 2003) so perhaps utilisation of a *c*-type cytochrome would confer higher thermal stability upon the enzyme. It would be interesting therefore, to investigate the haem binding of these novel proteins and discover if they do indeed bind both *b* and *c*-type haem. The purification of SerABC revealed a *c*-type cytochrome which co-purifies with the selenate reductase, possibly suggesting an interaction between the two. This cytochrome could be a candidate electron donor to SerC, and will be considered further in chapter 4.

In order to obtain SerC independently of the A and B subunits to study its interactions with upstream electron donors, the *serC* gene was cloned and transformed into *E. coli* BL21 (DE3). Unfortunately, attempts to express SerC in *E. coli* were unsuccessful, as the protein in inclusion bodies could not be refolded. This is thought to be due to the Sec leader sequence not being recognised by the *E. coli* Sec machinery, and therefore interfering with the folding of the protein. Refolding and reconstitution of the similar ClrC protein from *I. dechloratans* was successful when expressed with the signal sequence and also a GST (glutathione S-transferase) tag (Karlsson & Nilsson, 2005). The expression resulted in inclusion bodies, suggesting that the signal sequence was not correctly recognised, but the GST fusion may have assisted in refolding the protein as it is thought to aid stability and solubility of refolded proteins (Kapust & Waugh, 1999). The authors do not state however, whether the N-terminal signal sequence is cleaved in the reconstituted protein. The addition of a fusion protein such as GST or maltose binding protein (MBP) could be used to aid refolding of SerC in future studies. As reconstituted SerC could not be obtained, the whole SerABC complex will be used to examine interactions with potential electron donors.

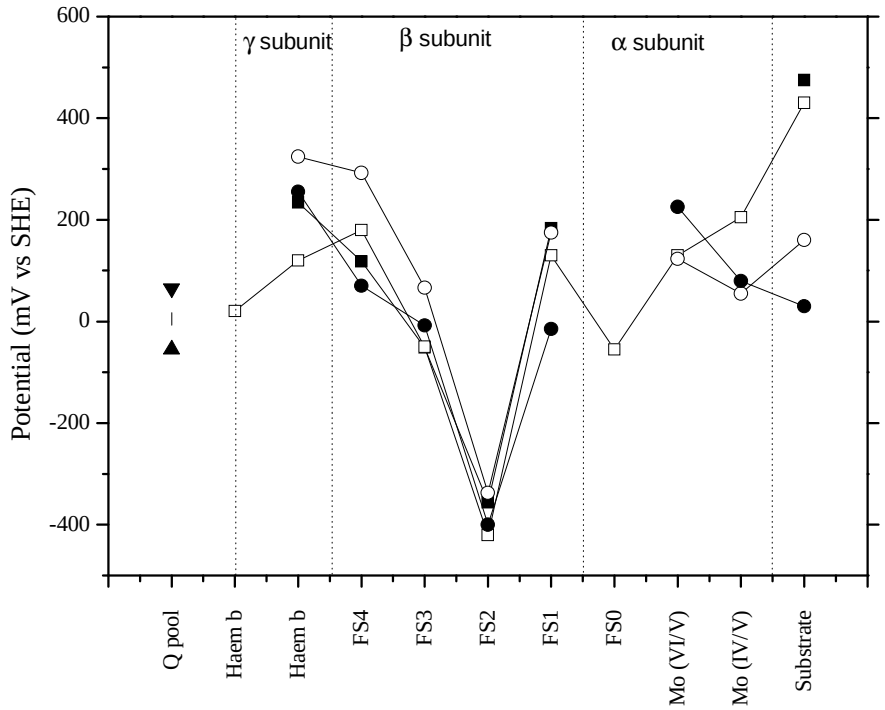

Figure 3.10: Midpoint potentials of redox clusters in selected type II DMSO reductase family enzymes.

■ = SerABC, □ = NarGHI ● = EbdABC, ○ = DdhABC.

4. Identifying a soluble electron donor to SerABC

4.1. Introduction

The route by which electrons are transferred to SerABC is vital to understanding the bioenergetics of selenate respiration, and how selenate reduction can generate a proton-motive force (pmf) that is sufficient to support growth. The characterisation of the selenate reductase enzyme from *T. selenatis* has not yet addressed the mechanism by which electrons are transferred from the cytoplasmic membrane of the cell to periplasmic SerABC. As SerABC appears to be soluble and not associated with the inner or outer membrane, it is likely that another protein acts as a shuttle to take electrons from the membrane and deliver them to the *b*-haem of SerC, allowing their further passage, via the iron-sulfur clusters of SerAB, to the molybdopterin co-factor for reduction of selenate to selenite. Among the related DMSO reductase family of molybdo-enzymes, there are a number of different routes of electron transfer to terminal reductases, although the majority catalyse reactions with a lower redox potential than the selenate/selenite couple (+475 mV), for example, the DMSO/DMS couple catalysed by DMSO reductase is +160 mV and TMAO/TMA is +130 mV (McCrindle *et al.*, 2005). The high potential of the selenate/selenite couple has been suggested to enable the use of high potential *c*-type cytochromes as intermediate electron carriers (McEwan *et al.*, 2002), which is not a pathway known for any of the other members of the DMSO reductase family, so showing electron donation from a soluble cytochrome *c* to SerABC would represent a novel electron transport chain within this family.

The aim of this section, therefore, is to identify soluble *c*-type cytochromes expressed during selenate respiration, and test for their ability to donate electrons to SerABC for selenate reduction.

4.2. Profiling cytochrome expression during selenate respiration

In order to identify candidates for electron transfer to SerABC, a profile of the cytochromes expressed during selenate respiration was undertaken. Periplasmic and membrane fractions were prepared from *T. selenatis* cultures grown under selenate or nitrate respiring anaerobic conditions, as detailed in sections 2.2 and 2.3. These samples were run on SDS-PAGE gels and subsequently haem stained to identify *c*-type cytochromes (Figure 4.1). In this chapter, we will consider the periplasmic cytochromes; the possibility of a membrane bound electron donor is discussed further in chapter 5. In total seven periplasmic and membrane bound cytochromes were identified which are expressed during selenate and nitrate respiration, but the ones of most interest to this study are those which seem to be upregulated in selenate growth conditions, and therefore are more likely to be involved in selenate respiration. The periplasmic cytochromes of interest were identified as proteins with approximate molecular weights of 25, 12 and 6 kDa, although the broad band around 12 kDa appears to be two cytochromes which are very close in size. Cytochromes were named according to their size, so that the highest molecular weight protein was called cytochrome *c*1, and the smallest cyt*c*7. According to this designation, the proteins of interest are cyt*c*4, cyt*c*6 and cyt*c*7. Cyt*c*4 and cyt*c*7 seem to be the most highly upregulated of these, indeed cyt*c*7 does not appear to be expressed under nitrate respiring conditions. Interestingly, cyt*c*4 appears in the membrane fraction as well as the periplasmic fraction, suggesting it may be associated with the membrane. These two cytochromes were therefore considered for further study.

Cyt*c*1 (approximately 60 kDa) is the single cytochrome identified which is upregulated during nitrate respiration compared to selenate. Part of a gene coding for a cd_1 nitrite reductase has previously been amplified from *T. selenatis* (Song & Ward, 2003), and nitrite reductase activity has been detected in the periplasm (Demolldecker & Macy, 1993). Cd_1 type nitrite reductases contain a *c* and an unusual d_1-type haem, and so would be detectable by haem staining. The size of nitrite reductases of this type from other organisms is consistent with the size of cyt*c*1, so it is possible that cyt*c*1 is the nitrite reductase enzyme.

4.3. Purification of cytochrome *c*7

As a candidate for electron transfer during selenate respiration, cyt*c*7 was purified from the soluble fraction of selenate respiring *T. selenatis* by gel filtration chromatography using a Superdex 200 16/60 column, equilibrated with 20 mM Tris-HCl pH 8.0. The eluted protein was collected in 1.5 ml fractions and monitored for protein by absorbance at 280 nm (Figure 4.2a). A FLUOstar Optima plate reader (BMG Labtech) was then used to measure the absorbance at 410 nm of each fraction in a 96 well microtitre plate (Greiner Bio One) to look for the presence of cytochromes (Figure 4.2b). Fractions from across the elution profile were analysed by SDS-PAGE (Figure 4.3). Pure cyt*c*7 was observed in the fraction corresponding to an elution volume of 114.5 ml, and the adjacent fractions (111.5-116 ml) were pooled and concentrated. It was also noted that another cytochrome was visible on the haem stained SDS-PAGE gel at approximately 40 kDa which was not visible on the original periplasm or membrane haem stain, presumably because it was not present in sufficient concentration to be viewed and therefore is not an immediate candidate for a role in selenate respiration.

4.4. Spectroscopic characterisation of cytochrome *c*7

The purified cytochrome exhibited spectral features typical of *c*-type cytochromes (see figure 4.4a). The reduced spectrum showed absorbance maxima at 415, 522 and 551 nm. Oxidised cyt*c*7 shows a shift in the Soret band to 409 nm and a broad feature around 525 nm. A charge transfer band at 695 nm was not evident in the oxidised spectrum, but low yields of protein meant that obtaining a sufficiently high concentration to visualise this weak feature was not possible.

4.5. Electron donation to SerABC by cytochrome *c*7

In order to test whether cyt*c*7 was able to donate electrons to SerABC for reduction of selenate, a spectroscopic assay was used to monitor the redox state of cyt*c*7 via its UV-visible spectrum. Cyt*c*7 was reduced by titration with a weak solution of sodium dithionite, and mixed with selenate reductase and selenate in an anaerobic assay as described in section 2.10. Cyt*c*7 was used at around a 10 fold excess compared to SerABC, to minimise interference of the *b* haem spectrum of SerC with that of cyt*c*7. No re-oxidation of the haem was observed, suggesting that cyt*c*7 is not able to act as electron donor to SerABC *in vitro*. It was considered that cyt*c*7 might act as a selenite reductase, reducing selenite to elemental selenium, so the same assay was carried out with reduced cyt*c*7 and selenite alone, but again no re-oxidation was observed (data not shown).

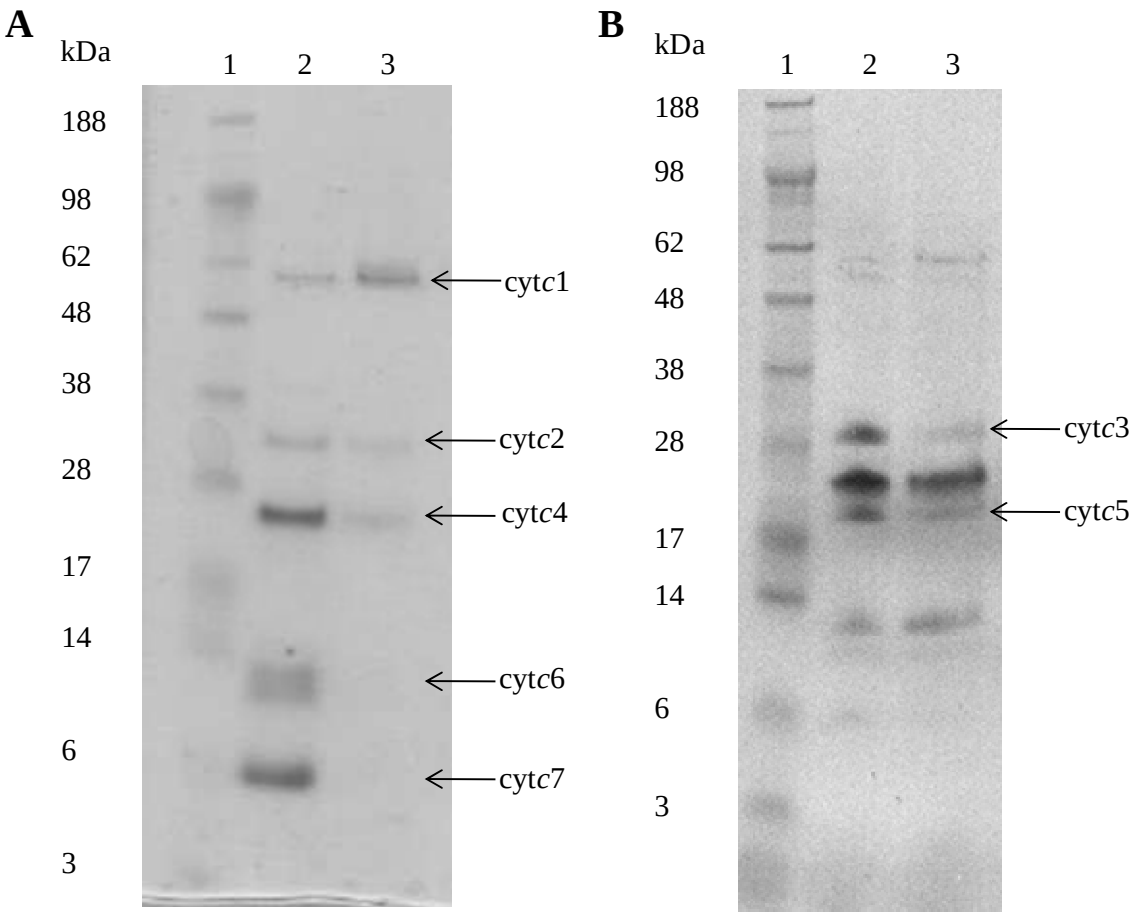

Figure 4.1: Haem stained periplasmic and membrane fractions from *T. selenatis*. SDS-PAGE gels stained for *c*-type cytochromes, showing periplasmic and membrane cytochromes expressed during selenate and nitrate respiration. A: periplasmic fractions, B: membrane fractions. Lane 1 – Invitrogen SeeBlue Plus2 Prestained Standard. Lane 2 –selenate grown cells. Lane 3 – nitrate grown cells. 7 µg of protein was loaded on each lane.

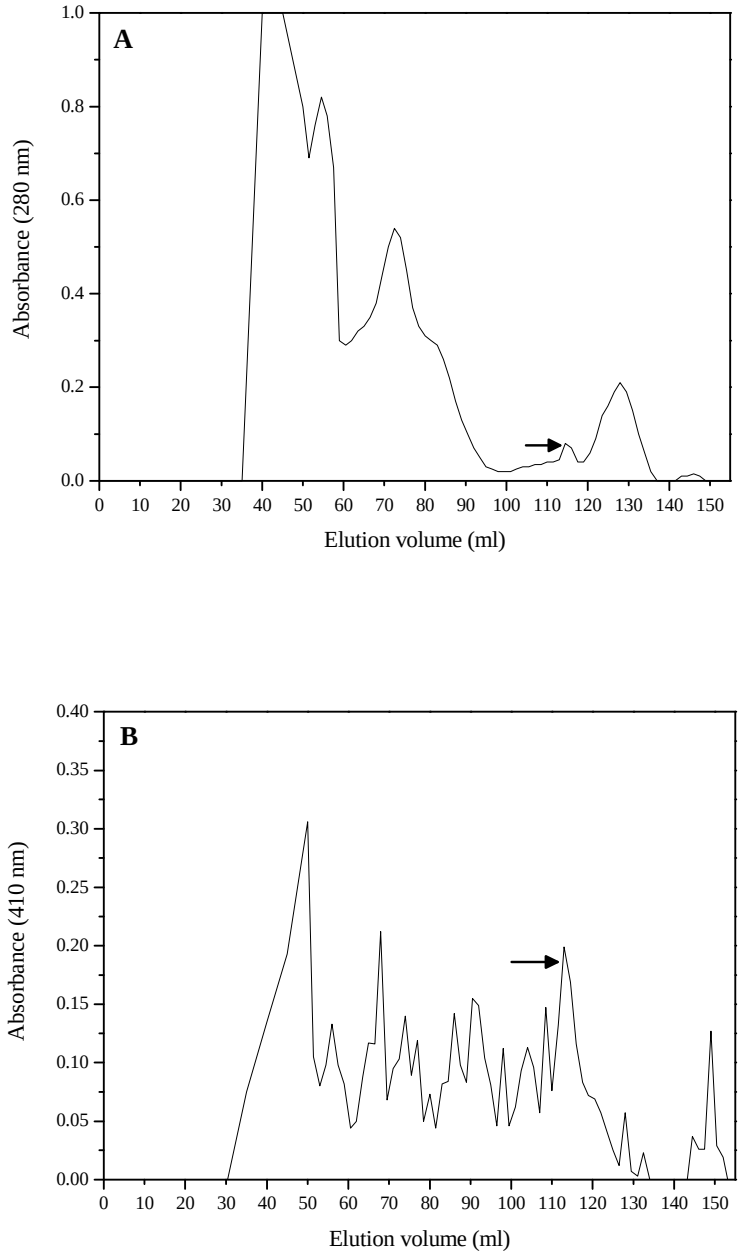

Figure 4.2: Purification of cytochrome *c*7 from *T. selenatis* by gel filtration chromatography.

The column used was Superdex 200 16/60, equilibrated with 20 mM Tris-HCl, pH 8.0. A: absorbance of eluted fractions at 280 nm, B: absorbance at 410 nm. Peaks containing cyt*c*7 are indicated by an arrow.

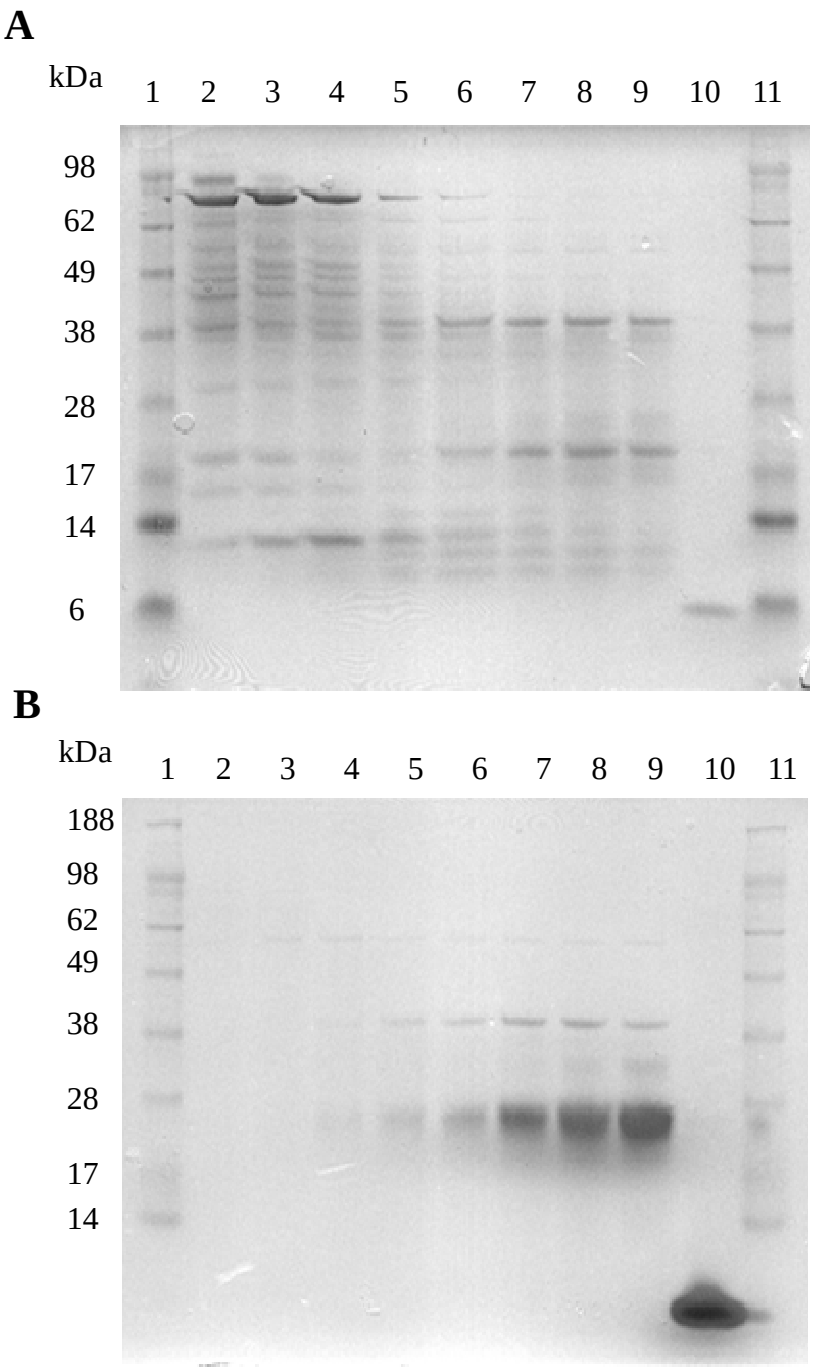

Figure 4.3: SDS-PAGE analysis of the purification of cytochrome *c*7 from *T. selenatis*. The same fractions were run on each gel; gel A is stained for total protein, gel B is haem stained. Lane 1 - Invitrogen SeeBlue Plus2 Prestained Standard. Lane 2 – fraction corresponding to an elution volume of 65 ml. Lane 3 – 68 ml. Lane 4 – 71 ml. Lanes 5-9 – 1.5 ml fractions between 74-80 ml. Lane 10 – 114.5 ml. Lane 11 - Invitrogen SeeBlue Plus2 Prestained Standard. Cyt*c*7 can be observed in lane 10.

A

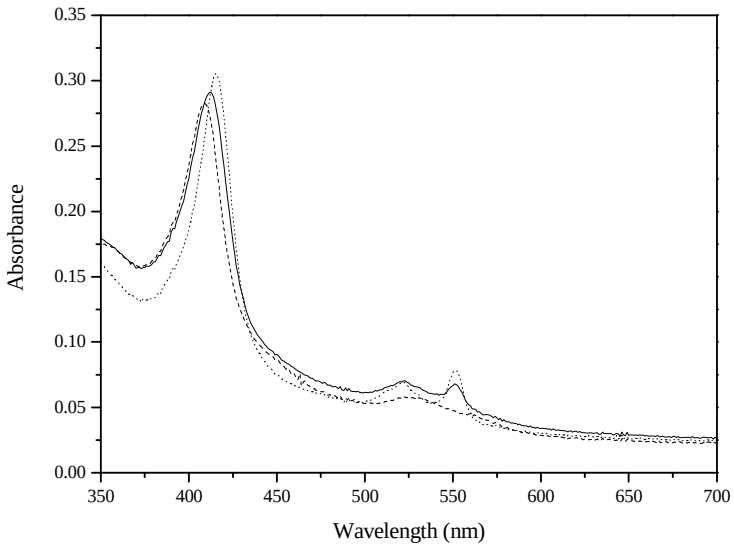

B

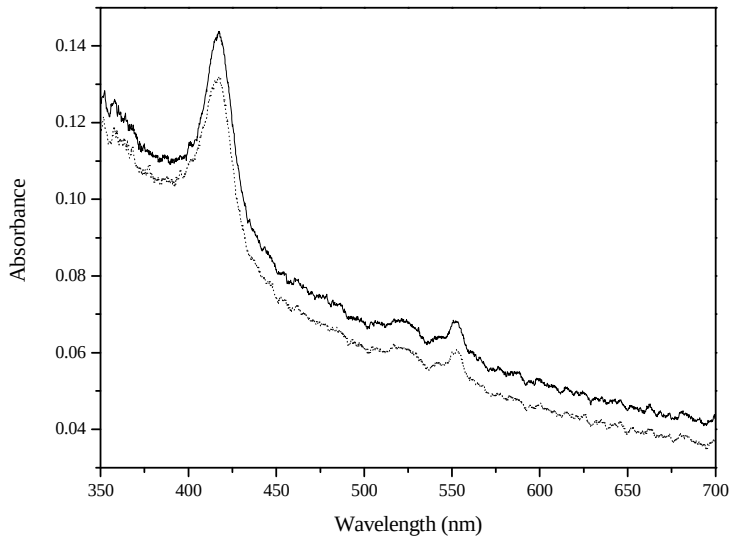

Figure 4.4: UV-visible absorbance spectroscopy of cytochrome *c*7.

A: UV-visible absorbance spectra of 3 µM cyt*c*7 as purified (solid line), reduced with sodium dithionite (dotted line) and oxidised with potassium ferricyanide (dashed line).

B: Cyt*c*7 (1.5 µM) reduced with dithionite (solid line) was mixed with 0.2 µM SerABC and 20 mM selenate and re-oxidation (dotted line) was monitored by wavelength scanning UV-visible spectroscopy.

4.6. Identification of cytochrome *c*4 as a candidate electron donor

During selenate reductase purification as detailed in chapter 3, it was noted that a cytochrome of approximately 25 kDa co-purifies with the selenate reductase enzyme until the gel filtration chromatography step. This cytochrome (cyt*c*4) was also identified as one of those upregulated during selenate respiration conditions, and therefore was of interest for further characterisation.

As the initial purification strategy for cyt*c*4 was based on its co-purification with SerABC, it was observed that some cyt*c*4 was lost during the early stages, including that of periplasmic fractionation. SDS-PAGE gels of haem stained membranes also showed a population of cyt*c*4 which seemed to be associated with the membrane fraction (figure 4.1). As cyt*c*4 is also seen in the periplasmic fraction it is likely that the protein is associated with the membrane in some conditions, rather than strongly bound to it. A new purification strategy was then developed for cyt*c*4, starting from whole soluble cell fraction, rather than periplasmic, as it was hoped that the sonication step in preparing soluble fraction would result in more of the cyt*c*4 disassociating from the membrane. This optimised purification strategy is detailed below.

4.7. Optimised purification of cytochrome *c*4

Crude soluble fraction was applied to a 70 ml Fast-Flow Q Sepharose anion exchange column at pH 8.5 (30 mM Tris-HCl), and eluted with a linear gradient of 0-300 mM NaCl (figure 4.5). A broad pink band eluted at approximately 150 mM NaCl, and SDS-PAGE analysis confirmed fractions between 130 and 175 ml to be cyt*c*4 (see figure 4.5). These fractions were pooled, concentrated to 6 ml, and aliquots of 2 ml were then run on a Sephadex 200 16/60 gel filtration column equilibrated with 30 mM Tris-HCl pH 8.5. Fractions containing cyt*c*4 were identified using SDS-PAGE as before (figure 4.6), and pooled. The pooled protein was then further purified using a 1 ml MonoQ column, a strong anion exchange resin. The column was equilibrated with 30 mM Tris-HCl, pH 8.5, and bound proteins eluted with a linear gradient of the same buffer, containing 1 M NaCl (figure 4.7a). Again, a bright pink band was observed eluting from the column, at approximately 10-15% B (100-150 mM NaCl). The eluted fractions containing cyt*c*4 still contained impurities as determined by SDS-PAGE (figure 4.7b), so fractions from 19-23 ml were pooled and retained for further purification. As a final purification step, the pooled protein was dialysed overnight into 1 M ammonium sulfate

in 30 mM Tris-HCl, pH 8.5 and then loaded onto a 20 ml Phenyl Sepharose column (GEHealthcare). Proteins were eluted with a 140 ml linear gradient of 1-0 M ammonium sulfate (figure 4.8a), and a pink band was eluted at 80-90%, equivalent to 200-100 mM ammonium sulfate. SDS-PAGE analysis of these peak fractions showed the cyt*c*4 to be pure (figure 4.8b). A summary of the purification steps is shown in table 4.1.

4.8. Determination of the pI of cytochrome *c*4 by isoelectric focusing

In order to determine the pI of cyt*c*4 to develop the optimised purification protocol described above, a small amount of protein purified during the SerABC purification was subjected to isoelectric focusing. Initial experiments on broad pI range gels indicated that cyt*c*4 had a low pI, but were not clearly resolved so an exact pI could not be established. Further experiments using low pI range gels (4.0-6.5) were more successful and a pI of 4.6 was determined by comparison to markers of known pI (figure 4.9).

4.9. Spectroscopic characterisation of cytochrome *c*4

UV-visible spectroscopy of purified cyt*c*4 (see figure 4.10) shows an absorbance spectrum typical of a low-spin cytochrome *c*. Cyt*c*4 is purified in a partially reduced state, as with cyt*c*7, but does not readily become oxidised, even after lengthy exposure to air. Protein reduced with dithionite shows a Soret band at 414 nm, an α-band at 550 nm and a β-band at 519 nm. The α-band shows asymmetry, with a shoulder at 545 nm suggesting a composite band, possibly due to the presence of more than one haem in the protein. Cyt*c*4 oxidised with ferricyanide has a Soret band at 409 nm and a broad feature at 528 nm. A charge-transfer band at 695 nm indicative of His/Met ligation to the haem was not observed (not shown).

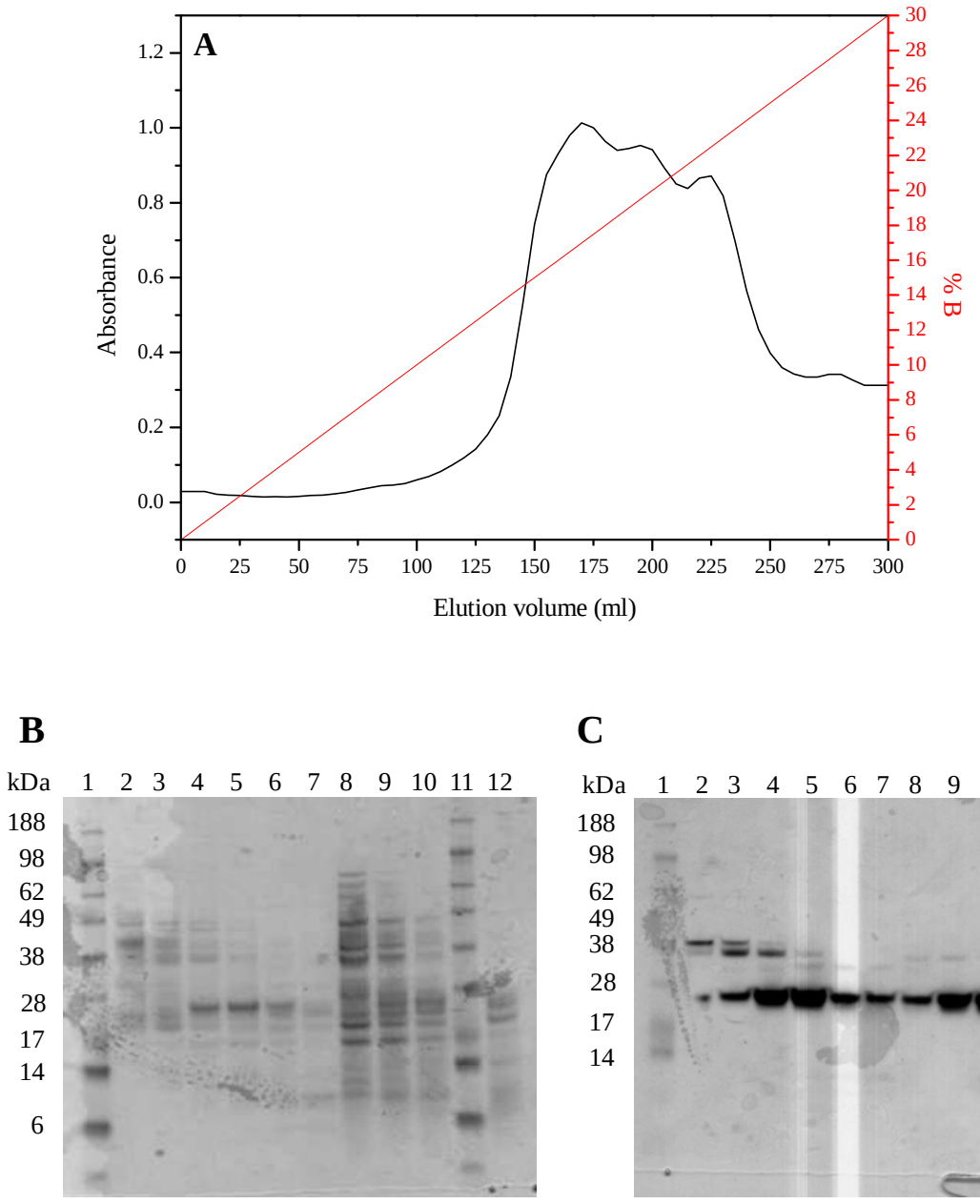

Figure 4.5: Anion exchange chromatography of cytochrome *c*4.

A: Absorbance of eluted fractions at 280 nm (black) and linear gradient of 1 M NaCl (red) indicated on the axis as % of 1 M NaCl. B: SDS-PAGE gels of eluted fractions. The same fractions were run on each gel. Left hand gel is stained for total protein, right gel is haem stained. Lanes 1 and 11 – Invitrogen SeeBlue Plus2 Prestained Standard. Lanes 2-10 and 12 – 5 ml fractions between elution volumes 125-175 ml.

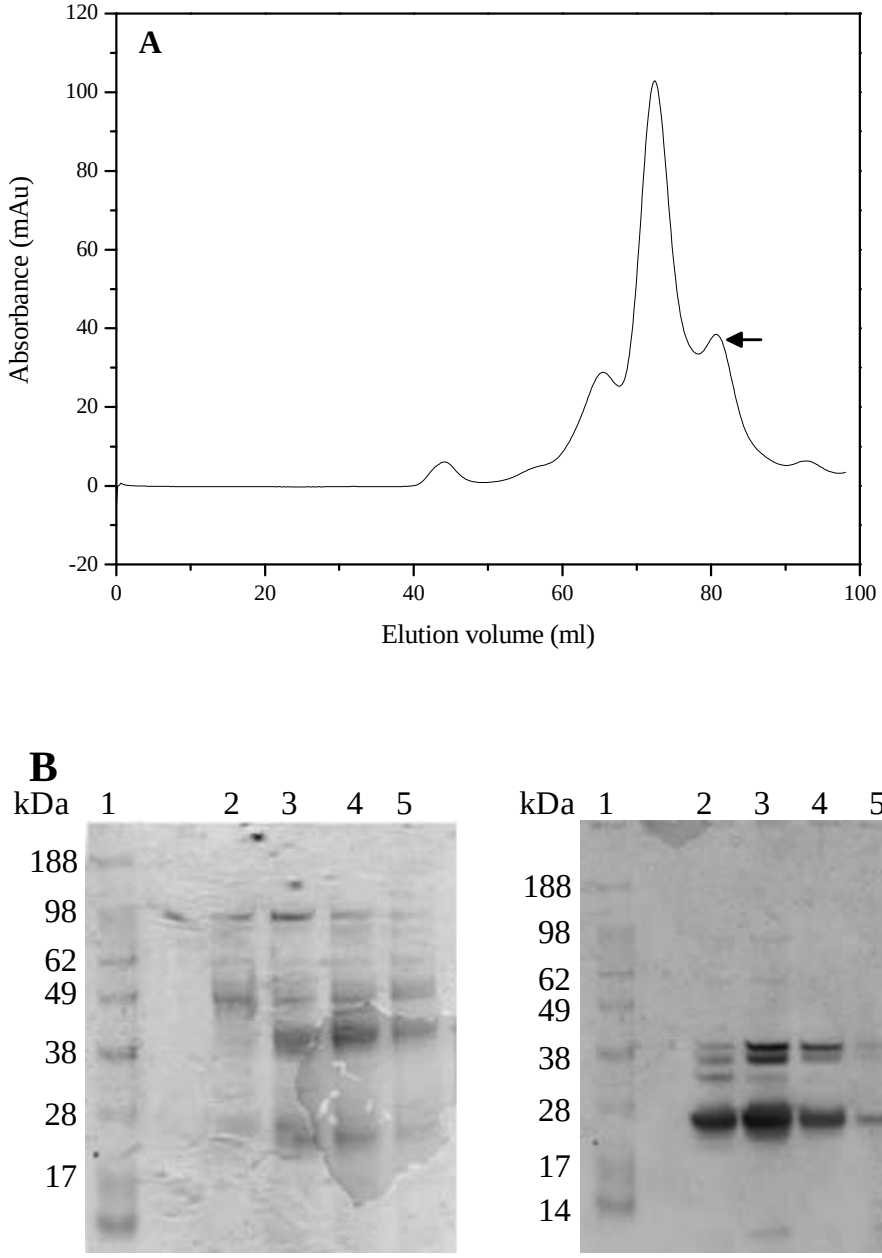

Figure 4.6: Gel filtration chromatography of cytochrome *c*4.

A: absorbance at 280 nm of eluted fractions from Superdex 200 16/60 column, in 20 mM Tris pH 8.5. The arrow indicated the peak containing cyt*c*4. B: SDS-PAGE gels of eluted fractions. The same fractions are run on both gels. Left gel is stained for total protein, right gel is haem stained. Lane 1 - Invitrogen SeeBlue Plus2 Prestained Standard. Lanes 2-5 - 3ml fractions of elution volumes between 77 and 89 ml.

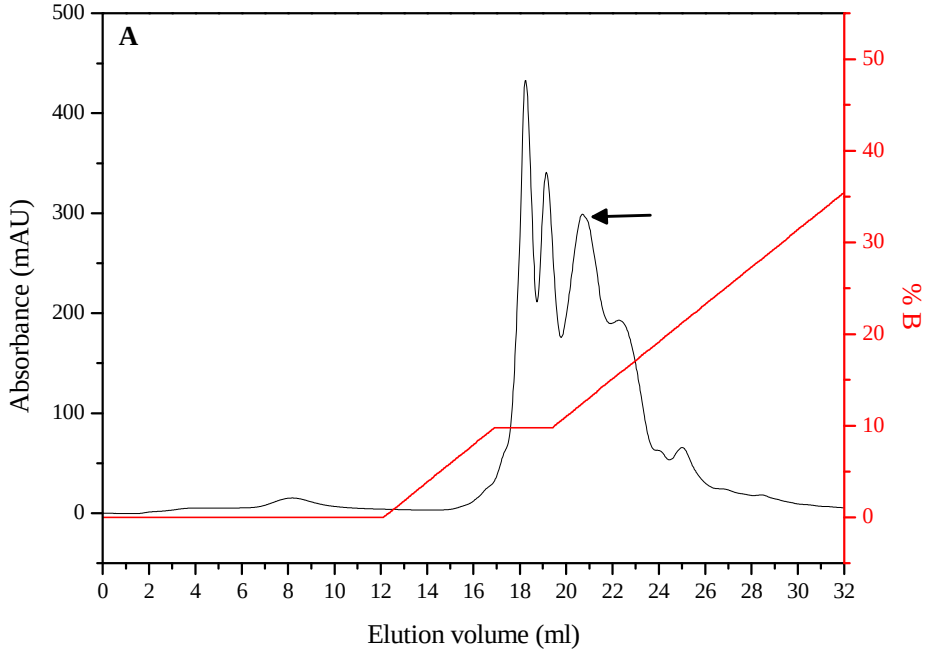

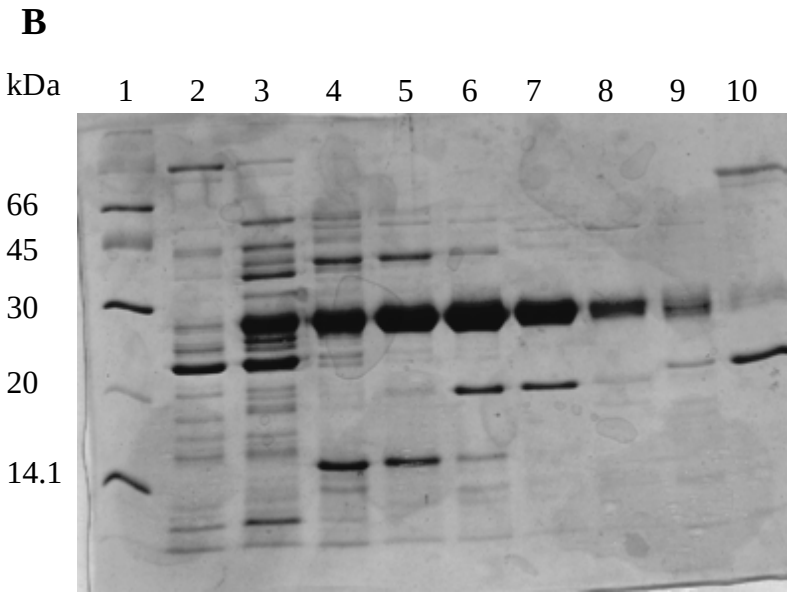

Figure 4.7: MonoQ chromatography of cytochrome *c*4.

A: Absorbance at 280 nm for eluted fractions (black) and increasing gradient of 1 M NaCl indicated as a percentage (red). The peak containing cyt*c*4 is indicated by an arrow. B: SDS-PAGE gel of fractions from MonoQ column stained for protein. Lane 1 – Low molecular weight protein marker (GEHealthcare). Lanes 2-10 – 1 ml fractions between elution volumes 17-25 ml.

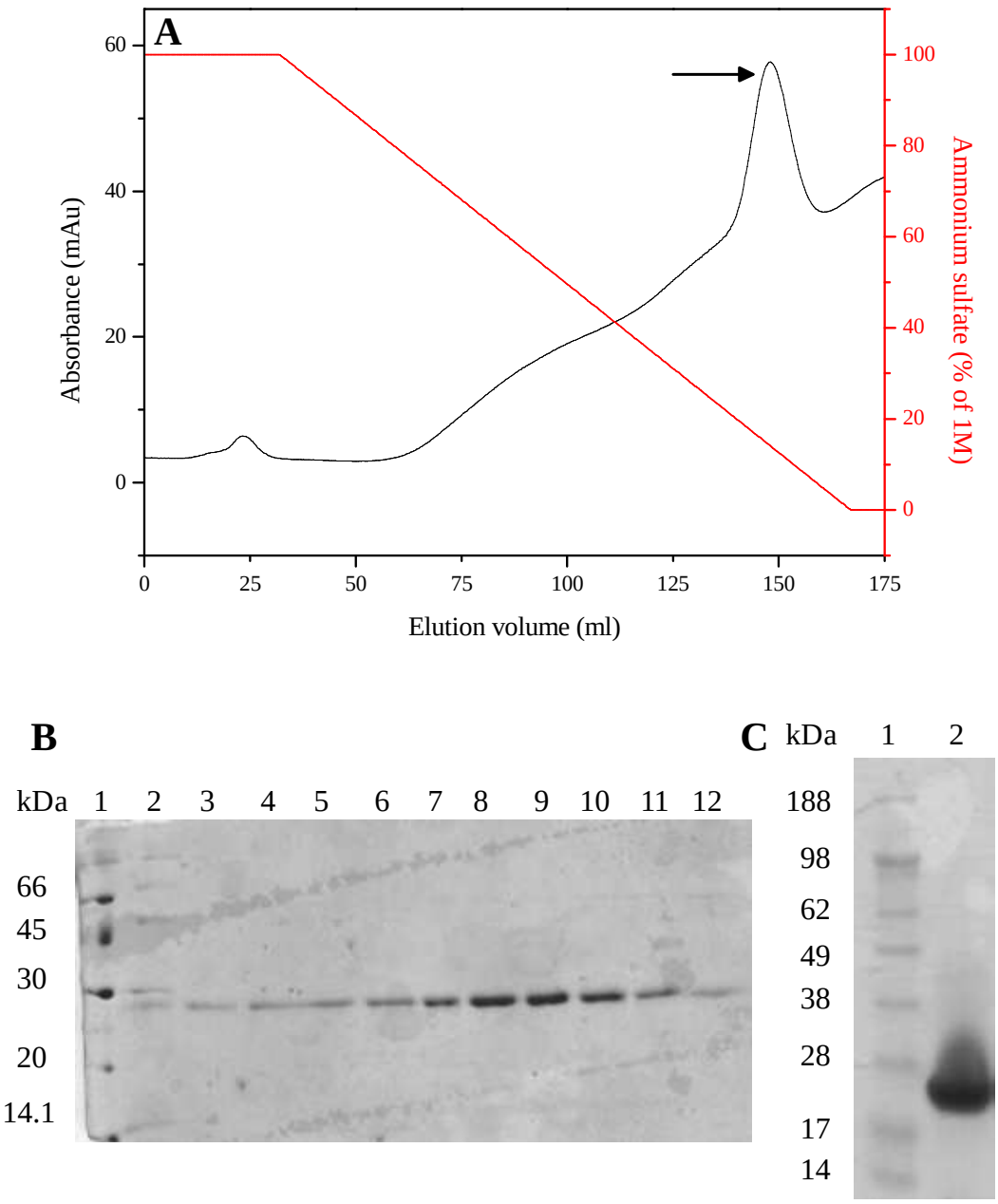

Figure 4.8: Phenyl Sepharose chromatography of cytochrome *c*4.

A: Absorbance at 280 nm for eluted fractions (black) and increasing gradient of buffer without 1 M ammonium sulfate (red). The peak containing cyt*c*4 is indicated by an arrow. B: SDS-PAGE gel of eluted fractions from Phenyl Sepharose column, stained for total protein. Lane 1 – Low molecular weight protein marker (GEHealthcare). Lanes 2-12 – 3 ml fractions between elution volumes 130-163 ml. C: SDS-PAGE gel stained for haem. Lane 1 – Invitrogen SeeBlue prestained standard, lane 2 – pooled and concentrated fractions.

Table 4.1: Summary of the purification of cytochrome *c*4 from *T. selenatis*.

Purification step	Total volume (ml)	$A_{280\ nm}$	$A_{410\ nm}$	Purity index A_{410}/A_{280}
Soluble fraction	200	2.416	1.509	0.624
FFQ	32	1.578	0.830	0.526
Gel filtration	25	0.335	0.694	2.70
MonoQ	5 (then diluted 1/100)	0.025	0.091	3.64
Phenyl Sepharose	10	0.131	0.717	5.47

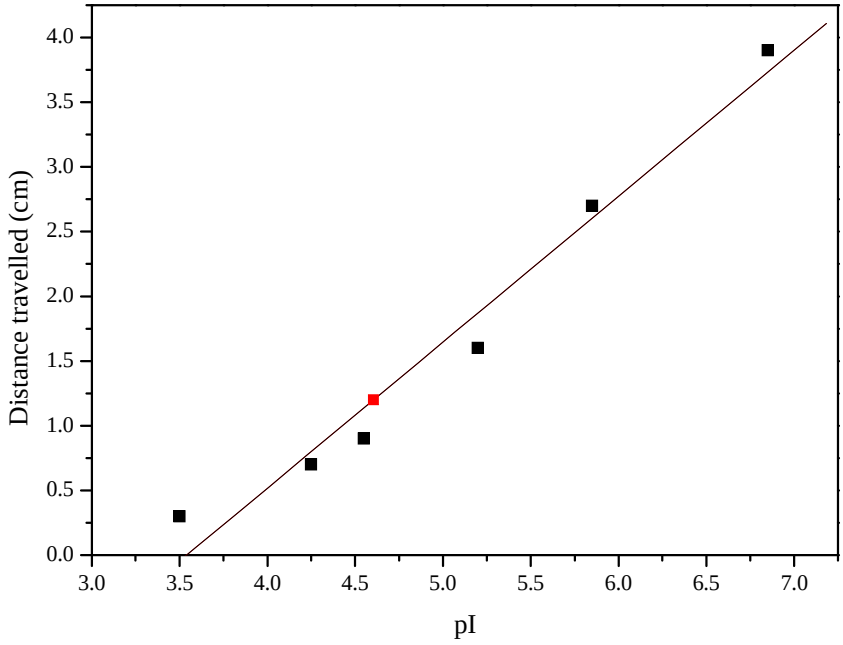

Figure 4.9: Determination of the pI of cytochrome *c*4 by IEF.

Distance migrated from the anode side of the IEF gel by markers of known pI (black) and a line of best fit used to estimate the pI of cyt*c*4 (red)

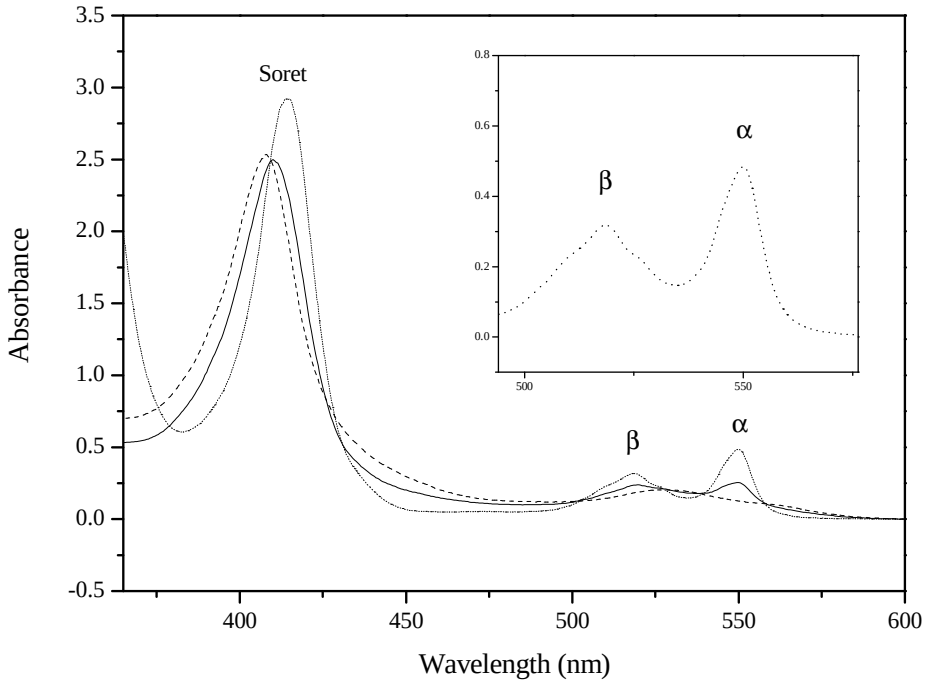

Figure 4.10: UV-visible absorption spectroscopy of cytochrome *c*4.

Spectra of 25 μM cyt*c*4 as purified (solid line), reduced with sodium dithionite (dotted line) and oxidised with potassium ferricyanide (dashed line). Inset is magnified view of α and β absorbance regions of the spectra of reduced cyt*c*4.

4.10. Electron donation to SerABC by cytochrome *c*4

As for cyt*c*7, cyt*c*4 was tested for its ability to donate electrons to SerABC in an anaerobic assay. In this case, after incubation with enzyme and substrate, the visible absorbance spectrum is shifted after approximately 15-20 minutes (figure 4.11). The Soret band shifts from 414 nm to 410, and decreases in intensity, and the α/β peaks broaden and decrease in intensity, indicative of re-oxidation of the haem. Using the turnover rate for SerABC calculated by Dridge, 2007 (0.4 s^{-1}), with cyt*c*4 at a 10-fold excess to SerABC, you could expect to oxidise the cyt*c*4 in approximately 25 seconds. The observed time for oxidation was much greater than this calculated time, however, and this could be due to the fact that the turnover rate used was determined using data from methyl viologen assays. Methyl viologen donates electrons directly to the molybdenum for catalysis, whereas in this experiment electrons were passed through the other redox centres of SerABC prior to reduction of selenate, and this is likely to be slower than the methyl viologen rate. Indeed, Craske and Ferguson (1986) showed that Nar from *P. denitrificans* has a 50-fold higher V_{max} with methyl viologen than with the ubiquinol analogue duroquinol. A 50-fold decrease in the rate of selenate reductase would result in an oxidation time of slightly over 20 minutes, which is in line with the observed data. Cyt*c*4 incubated with SerABC, selenate or selenite alone did not exhibit any shifts in absorbance (data not shown), suggesting that the cytochrome is capable of donating electrons to SerABC for the reduction of selenate to selenite *in vitro*, and therefore could be an *in vivo* electron donor to SerABC.

4.11. Determination of the redox potential of cytochrome *c*4

The redox potential of the haem of cyt*c*4 was measured spectrophotometrically according to the method of Dutton (1978), as described in section 2.13, by monitoring the absorbance of the α-band at 551 nm (adjusted by reference to an isosbestic point at 560 nm) during reduction or oxidation of the haem. The fraction of protein reduced at each measured potential was calculated, then plotted as a function of redox potential vs. the standard hydrogen electrode (SHE) (see figure 4.12). Nernst curves for n=1 and n=2 (where n is number of electrons transferred) were fitted using TableCurve 2D (Systat Software Inc.), and are also shown in figure 4.12. Interestingly, the data for cyt*c*4 fits more closely to an n=2 curve, suggesting the cytochrome has two haems. A mid-point potential of +282 ±4 mV for the cytochrome was calculated, but we were unable to resolve separate potentials. This redox potential is slightly higher than that determined

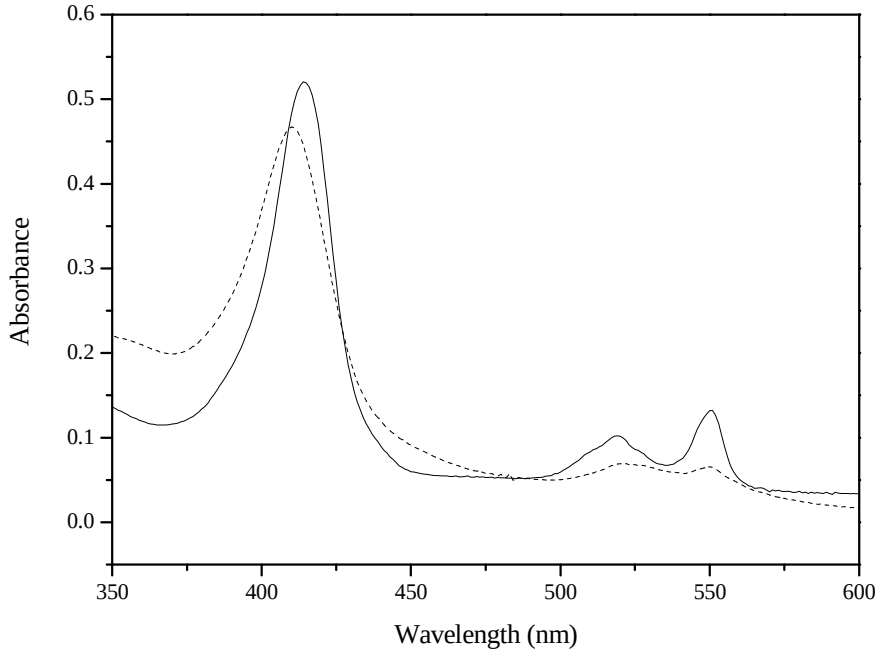

Figure 4.11: Spectroscopic assay of electron donation from cytochrome *c*4 to SerABC. Cyt*c*4 (5 μM) reduced with dithionite (solid line) was mixed with 0.5 μM SerABC and 20 mM selenate and re-oxidation after 20 minutes was monitored by wavelength scanning UV-visible spectroscopy (dashed line).

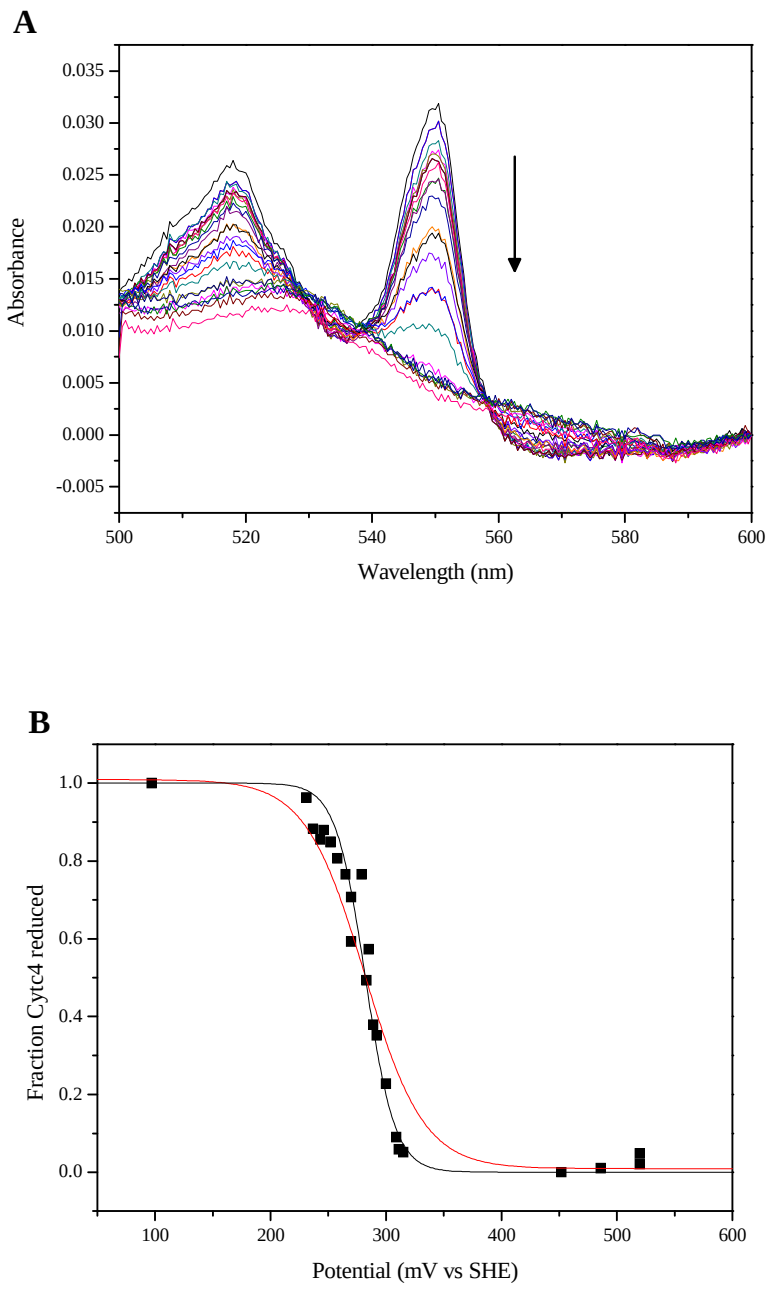

Figure 4.12: Optical redox titration of cytochrome *c*4.

A: α and β region of cyt*c*4 spectra during titrations. Black arrow indicates increasing redox potential. B: Fraction of cytochrome reduced as calculated with reference to absorbance at 551 nm, as a function of redox potential. Nernst curves for n=1 electrons (red) and n=2 electrons (black) are also shown. Titrations were recorded using protein at 1 µM in 30 mM Tris pH 7.5, at 21ºC.

for the *b*-haem of SerC (+ 234 mV) in section 3.4, which cyt*c*4 is a possible electron donor to, but still lower than the selenate to selenite couple (+475 mV), which would act as a powerful draw to pull the electrons through the redox centres of SerABC.

4.12. Protein sequence determination and analysis

In order to determine an exact mass for cyt*c*4, Matrix-Assisted Laser Desorption Ionization Time-of-Flight (MALDI-TOF) analysis was carried out and gave a molecular weight of 23,558 Da, not including haem groups. This fits with the observed size of ~ 25 kDa seen on SDS-PAGE gels, including approximately 600 Da per haem group. Cyt*c*4 was run on an SDS gel and blotted onto a polyvinylidene difluoride membrane (PVDF – Amersham HyBond-P). The blotted band was excised and subjected to N-terminal sequencing up to the 10th amino acid (aa) (both MALDI-TOF analysis and N-terminal sequencing were carried out by the Pinnacle Proteomics department at the University of Newcastle), producing the sequence GPPACKKEGI. Previous work by Dr J. Santini, UCL (personal communication) added a further 20 aa of sequence (VWNAQEGEKIEALQKKGDVT). These combined sequences were inputted into the sequence searching tool BLAST at NCBI. Only one match was found in the BLAST database – a class I *c*-type cytochrome from *Dechloromonas aromatica*. This protein is a di-haem cytochrome with a predicted mature molecular weight of approximately 24.5 kDa (excluding haem), very similar to that of cyt*c*4 from *T. selenatis*. This alignment is further evidence in favour of the hypothesis that cyt*c*4 is a di-haem cytochrome. The sequence of the *D. aromatica* cytochrome was then submitted to BLAST to see if a longer sequence resulted in more matches. This produced a large number of cytochromes with identity to the *D. aromatica* protein, most of which are classified as cytochromes c_4, a group of di-haem cytochromes *c* characterised by high redox potentials, a low intensity asymmetrical α band around 550 nm and a low α/β peak ratio (Pettigrew & Brown, 1988, Pettigrew & Moore, 1987). It should be noted that the name of this group of cytochromes has no relation to the name cyt*c*4 given to this protein due to its size as discussed in section 4.2. For clarity, the *T. selenatis* protein is referred to with a large 4, as in cyt*c*4, while the dihaem family of cytochromes c_4 are distinguished by using a subscript number 4. A number of members of this group have been characterised, including members from *Acidithiobacillus ferrooxidans* (Cavazza *et al.*, 1996, Giudici-Orticoni *et al.*, 2000), *Pseudomonas stutzeri* (Christensen, 1994), *Thiocapsa roseopersicina* (Branca *et al.*, 2007b) and *Azotobacter vinelandii* (Swank & Burris, 1969). Cytochromes c_4 have been proposed to be electron donors to cytochrome

oxidases, due to the presence of a cytochrome c_4 in the aerobe *A. vinelandii* (Swank & Burris, 1969) but the discovery of a cytochrome c_4 in *T. roseopersicina*, a facultative anaerobic photosynthetic bacterium, suggests that their roles may be much more varied (Branca *et al*., 2007b, Branca *et al.*, 2007a).

In order to clarify whether cyt*c*4 from *T. selenatis* is a member of this group, more sequence information was needed. A sample of cyt*c*4 was sent to the University of York proteomics facility, where it underwent tryptic digestion, mass spectroscopy and LC-MS/MS to obtain peptide fragments and their sequences. This procedure resulted in three further peptides which showed similarity to the *D. aromatica* sequence, bringing the total sequence for the *T. selenatis* cyt*c*4 to 60 aa, 51 of which were the same as the *D. aromatica* protein (85% identity) (figure 4.13, see figure legend for sequences of peptides). Cyt*c*4 and the *D. aromatica* cytochrome align most closely to cytochromes from *Magnetospirillum* species, but these proteins have not yet been characterised. An alignment of further cytochrome c_4 sequences, as obtained from the BLAST search using *D. aromatica* as the query sequence, is shown below (figure 4.14).

Structural data is available for 2 cytochromes c_4, from *P. stutzeri* (Kadziola & Larsen, 1997) and *A. ferrooxidans* (Abergel *et al*., 2003). The two haems in each case both have His-Met axial ligation, and the methionine residues identified as ligands are conserved throughout the cytochrome c_4 group. Additionally, a number of residues identified to be involved in haem stabilisation (Abergel *et al.*, 2003) are also conserved. These are highlighted in figure 4.15.

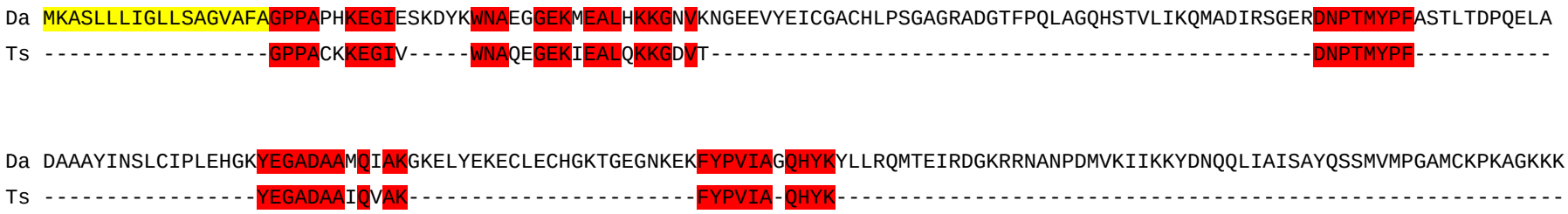

Figure 4.13: Sequence alignment between *T. selenatis* cytochrome *c*4 and *D. aromatica c*-type cytochrome, class I.

Residues highlighted in red are conserved between the two sequences; residues highlighted in yellow are the predicted signal sequence for the *D. aromatica* cytochrome which would be cleaved to produce the mature protein. Sequence obtained from the following sources: N-terminal sequencing – GPPACKKEGI, personal communication from Dr J. Santini – VWNAQEGEKIEALQKKGDVT, peptides from LC-MS/MS – DNPTMYPF, YEGADAAIQVAK, FYPVIAQHYK.

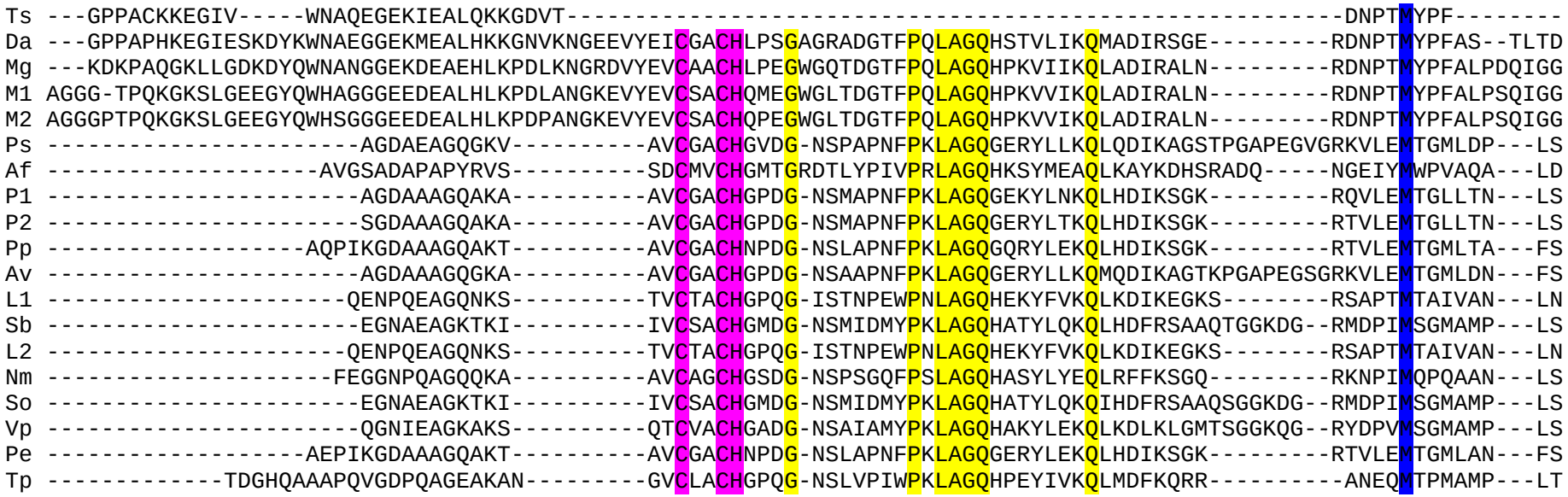
Ts ---GPPACKKEGIV-----WNAQEGEKIEALQKKGDVT----------DNPTMYPF--------
Da ---GPPAPHKEGIESKDYKWNAEGGEKMEALHKKGNVKNGEEVYEICGACHLPSGAGRADGTFPQLAGQHSTVLIKQMADIRSGE---------RDNPTMYPFAS--TLTD
Mg ---KDKPAQGKLLGDKDYQWNANGGEKDEAEHLKPDLKNGRDVYEVCAACHLPEGWGQTDGTFPQLAGQHPKVIIKQLADIRALN---------RDNPTMYPFALPDQIGG
M1 AGGG-TPQKGKSLGEEGYQWHAGGGEEDEALHLKPDLANGKEVYEVCSACHQMEGWGLTDGTFPQLAGQHPKVVIKQLADIRALN---------RDNPTMYPFALPSQIGG
M2 AGGGPTPQKGKSLGEEGYQWHSGGGEEDEALHLKPDPANGKEVYEVCSACHQPEGWGLTDGTFPQLAGQHPKVVIKQLADIRALN---------RDNPTMYPFALPSQIGG
Ps ----------------------AGDAEAGQGKV----------AVCGACHGVDG-NSPAPNFPKLAGQGERYLLKQLQDIKAGSTPGAPEGVGRKVLEMTGMLDP---LS
Af --------------------AVGSADAPAPYRVS----------SDCMVCHGMTGRDTLYPIVPRLAGQHKSYMEAQLKAYKDHSRADQ-----NGEIYWPVAQA---LD
P1 ----------------------AGDAAAGQAKA----------AVCGACHGPDG-NSMAPNFPKLAGQGEKYLNKQLHDIKSGK---------RQVLEMTGLLTN---LS
P2 ----------------------SGDAAAGQAKA----------AVCGACHGPDG-NSMAPNFPKLAGQGERYLTKQLHDIKSGK---------RTVLEMTGLLTN---LS
Pp -------------------AQPIKGDAAAGQAKT----------AVCGACHNPDG-NSLAPNFPKLAGQGQRYLEKQLHDIKSGK---------RTVLEMTGMLTA---FS
Av ----------------------AGDAAAGQGKA----------AVCGACHGPDG-NSAAPNFPKLAGQGERYLLKQMQDIKAGTKPGAPEGSGRKVLEMTGMLDN---FS
L1 ----------------------QENPQEAGQNKS----------TVCTACHGPQG-ISTNPEWPNLAGQHEKYFVKQLKDIKEGKS--------RSAPTMTAIVAN---LN
Sb ----------------------EGNAEAGKTKI----------IVCSACHGMDG-NSMIDMYPKLAGQHATYLQKQLHDFRSAAQTGGKDG--RMDPIMSGMAMP---LS
L2 ----------------------QENPQEAGQNKS----------TVCTACHGPQG-ISTNPEWPNLAGQHEKYFVKQLKDIKEGKS--------RSAPTMTAIVAN---LN
Nm --------------------FEGGNPQAGQQKA----------AVCAGCHGSDG-NSPSGQFPSLAGQHASYLYEQLRFFKSGQ---------RKNPIMQPQAAN---LS
So ----------------------EGNAEAGKTKI----------IVCSACHGMDG-NSMIDMYPKLAGQHATYLQKQIHDFRSAAQSGGKDG--RMDPIMSGMAMP---LS
Vp ----------------------QGNIEAGKAKS----------QTCVACHGADG-NSAIAMYPKLAGQHAKYLEKQLKDLKLGMTSGGKQG--RYDPVMSGMAMP---LS
Pe -------------------AEPIKGDAAAGQAKT----------AVCGACHNPDG-NSLAPNFPKLAGQGERYLEKQLHDIKSGK---------RTVLEMTGMLAN---FS
Tp ------------TDGHQAAAPQVGDPQAGEAKAN---------GVCLACHGPQG-NSLVPIWPKLAGQHPEYIVKQLMDFKQRR---------ANEQMTPMAMP---LT

Figure 4.14: Sequence alignments of cytochromes c_4 and available sequence data for cyt*c*4 from *T. selenatis*.

Bacterial strains from which sequence data is taken are abbreviated as follows; Ts – *T. selenatis*, Da – *D. aromatica* RCB, Mg – *M. gryphiswaldense* MSR-1. M1 – *M. magneticum* AMB-1, M2 – *M. magnetotacticum* MS-1, Ps – *P. stutzeri*, Af – *A. ferrooxidans*, P1 – *P. fluorescen*s Pf-5, P2 - *P. fluorescens* PfO-1, Pp – *P. putida* GB-1, Av – *A. vinelandii*, L1 – *L. pneumophila* str. Paris, Sb – *S. baltica* OS195, L2 – *L. pneumophila* str. Lens, Nm – *N. mobilis* NB-231, So – *S. oneidensis* MR-1, Vp – *V. parahaemolyticus* AQ3810, Pe – *P. entomophila* L48 and Tr – *T. roseopersicina*. Cytochrome *c* binding motifs (CXXCH) are highlighted in pink, conserved axial methionine residues (M) are highlighted in blue, and other conserved residues are highlighted yellow.

4.13. Tryptic digest of cytochrome *c*4

In order to clarify whether cyt*c*4 is a di-haem cytochrome, native protein was digested with trypsin as described in section 2.21. The resulting fragments were analysed by SDS-PAGE, both Coomassie and haem stained, and compared to undigested cyt*c*4 (figure 4.15. There are 3 bands resulting from the tryptic digest visible on the gels (along with a small band of undigested cyt*c*4), with approximate masses of 20, 12 and 4 kDa. All three bands are visible on both Coomassie and haem stained gels indicating that all fragments have at least one haem covalently bound. The sequence data available for cyt*c*4 as described above shows that the *T. selenatis* cytochrome has a high degree of similarity to that from *D. aromatica*, so the complete sequence for the *D. aromatica* cytochrome was used to try and deduce possible tryptic digest sites.

There are two structures of cytochromes c_4 determined by X-ray crystallography available, from *P. stutzeri* and *A. ferrooxidans*, and initially the two structures were superimposed using SSM in Coot (Krissinel & Henrick, 2004, Emsley & Cowtan, 2004) to assess structural conservation (see figure 4.16a and b). The secondary structure of the proteins aligned over 158 residues, with a sequence identity of 32.9% and an rmsd (root mean square displacement) of 1.35 Å, so they can be considered structurally homologous. The *D. aromatica* sequence shows a higher identity to that of *P. stutzeri* (31%) than to that of *A. ferrooxidans*, so sites at which trypsin cuts (adjacent to arginine and lysine residues) in the *D. aromatica* sequence were highlighted on the approximate corresponding residue of the *P. stutzeri* structure, and those judged most likely to be accessible to the protease, i.e. those in loops, were marked on the structure (see figure 4.16c and d). When the sizes of fragments resulting from these cuts were calculated, several in the range of 18-22 kDa would be formed, with one or two haems attached. This could account for the broad band at approximately 20 kDa seen on the gel (figure 4.15). The proximity of the first CXXCH motif to the N-terminus of the protein also means that small (5-7 kDa) fragments binding haem would be produced, although are likely to appear smaller than this as the *D. aromatica* cytochrome c_4 has a long N-terminal loop which contains a number of lysine residues that could be targeted by trypsin and so could be digested into fragments too small to visualise on an SDS-PAGE gel, therefore producing smaller fragments than predicted, such as the ~4 kDa band visible on the gels. A trypsin site is also present in the loop connecting the two domains of the protein which would result in fragments of approximately equal size (12.8 and

11.6 kDa) each binding a haem residue, possibly corresponding to the ~12 kDa band on the gel. This modelling assists in confirming cyt*c*4 as a di-haem cytochrome.

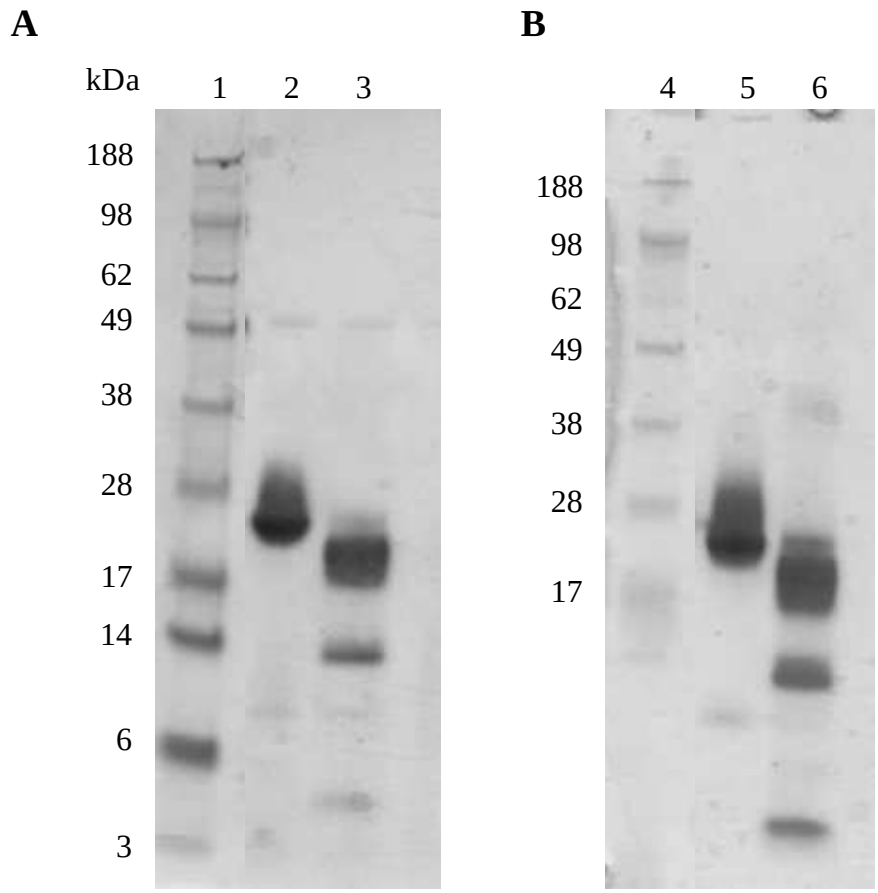

Figure 4.15: Tryptic digest of cytochrome *c*4.

SDS-PAGE analysis of native cyt*c*4 digested with trypsin for 1 hour at 37°C. Gel A is stained for total protein, gel B is haem stained. Lanes 1 and 4 – Invitrogen SeeBlue Plus2 Prestained Standard. Lanes 2 and 5 – undigested cyt*c*4. Lanes 3 and 6 – cyt*c*4 after digestion with trypsin.

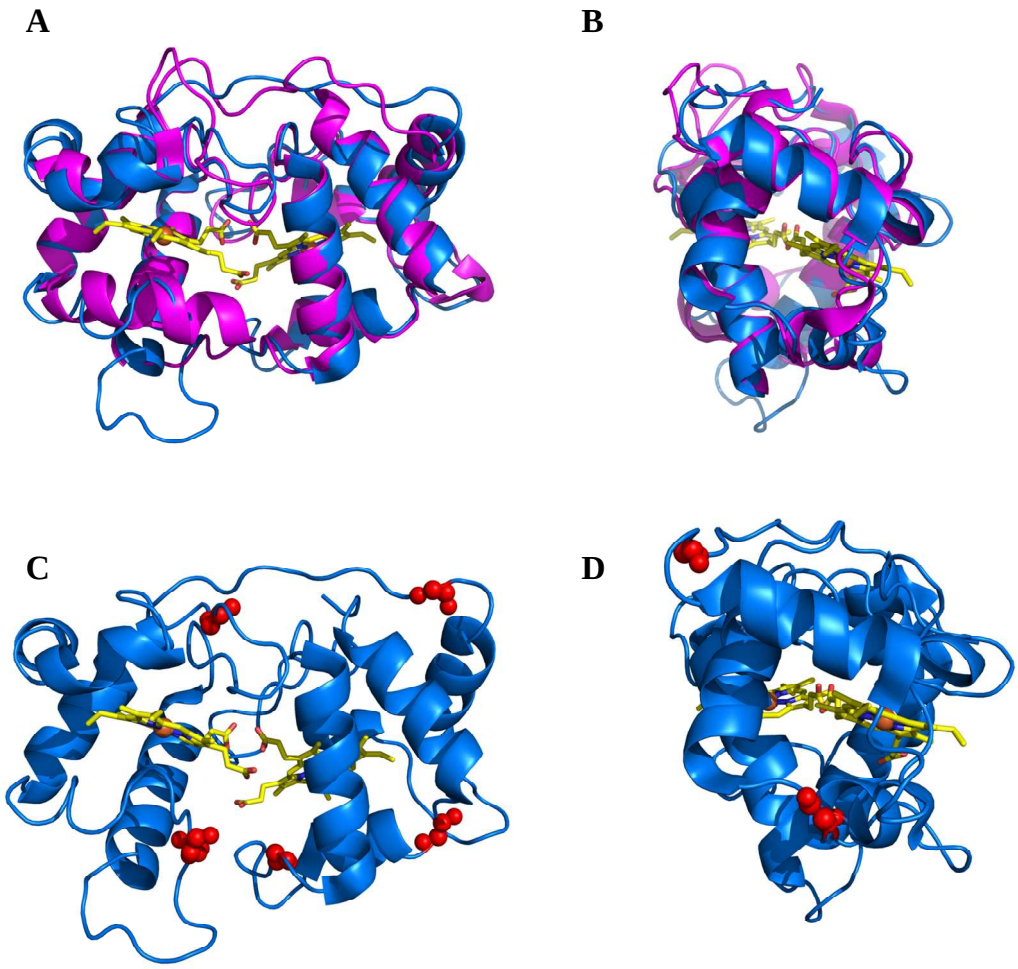

Figure 4.16: Structural models of cytochromes c_4.

A and B: Structural superposition of the cytochromes c_4 from *P. stutzeri* (blue, PDB code 1ETP) and *A. ferrooxidans* (pink, 1H1O). Haem groups are shown in yellow.

C and D: *P. stutzeri* cytochrome c_4 structure (blue) with predicted tryptic digest sites from *D. aromatica* cytochrome c_4 in red. Haem groups are shown in yellow. Images were prepared using PyMOL (DeLano, 2002).

4.14. EPR spectroscopy of cytochrome *c*4

The EPR spectrum of oxidised cyt*c*4 from *T. selenatis* is shown in Figure 4.17. The continuous wave perpendicular mode X-band spectrum is dominated by two rhombic type signals with g-values assigned as g_1~3.64, g_2~2.29, g_3~unresolved; and $g_{1'}$~2.83, $g_{2'}$~2.10, $g_{3'}$~unresolved. The g_3 feature in each case would normally be observed in the g~1.2 - 1.5 region but is often too broad to be detected. The additional signal at g~6.16 is typical of the $g_{1,2}$ feature of a high-spin (S=5/2) haem Fe(III), probably arising from a minor percentage (<2%) of damaged haem that has lost either a distal or axial ligand. The derivative shaped feature at g~4.3 is typical of the signal observed from contamination by adventitious (non-haem) high-spin Fe(III), normally surface bound to the protein and present due to Fe salts in the purification buffer. The two rhombic haem signals are interesting and worthy of further comment. The spectral line shapes and g-values confirm that both haems are low spin (S=1/2) when recorded at a temperature of 20 K. The observed g-values for the g_1 and $g_{1'}$ features lie in the region between g3.7 - 2.7 and are consistent with resonances that arise from *c*-type cytochromes (Hartshorne *et al.*, 2007). One of the haem groups displays g-values at $g_{1'}$~2.83 and g_2~2.10. The $g_{1'}$ feature at 2.83 is lower than that observed for other members of the cytochrome c_4 family, (typically around g_1~3.22 as shown for c_4 from *Azotobacter vinelandii* (Gadsby *et al.*, 1989)) and is more similar to the g_1 feature typically observed in *c*-type cytochromes in which the haem Fe is co-ordinated by two histidine ligands. However, since the electron-donating properties of the *bis*-histidine imidazole-ring nitrogen ligands help to stabilize the oxidised Fe(III) state over the reduced Fe(II) state, *c*-type cytochromes with *bis*-histidine co-ordination show more negative haem redox potentials. Consequently, since both haems of cyt*c*4 from *T. selenatis* have redox potentials at about +280 mV, it is considered more likely that this haem has methionine/histidine co-ordination, possibly with distorted geometry in relation to the relative positions of the axial and distal ligands. The second haem shows a signal with weaker intensity and displays a broad feature at g_1~3.64 and a derivative g_2 feature at ~2.29. These spectral features are similar to those observed for the second haem in c_4 from *A. vinelandii* (Gadsby *et al*., 1989). Assignment of the haem axial ligand in the case for c_4 from *A. vinelandii* was determined further by MCD spectroscopy and again confirmed the presence of a methionine/histidine co-ordination.

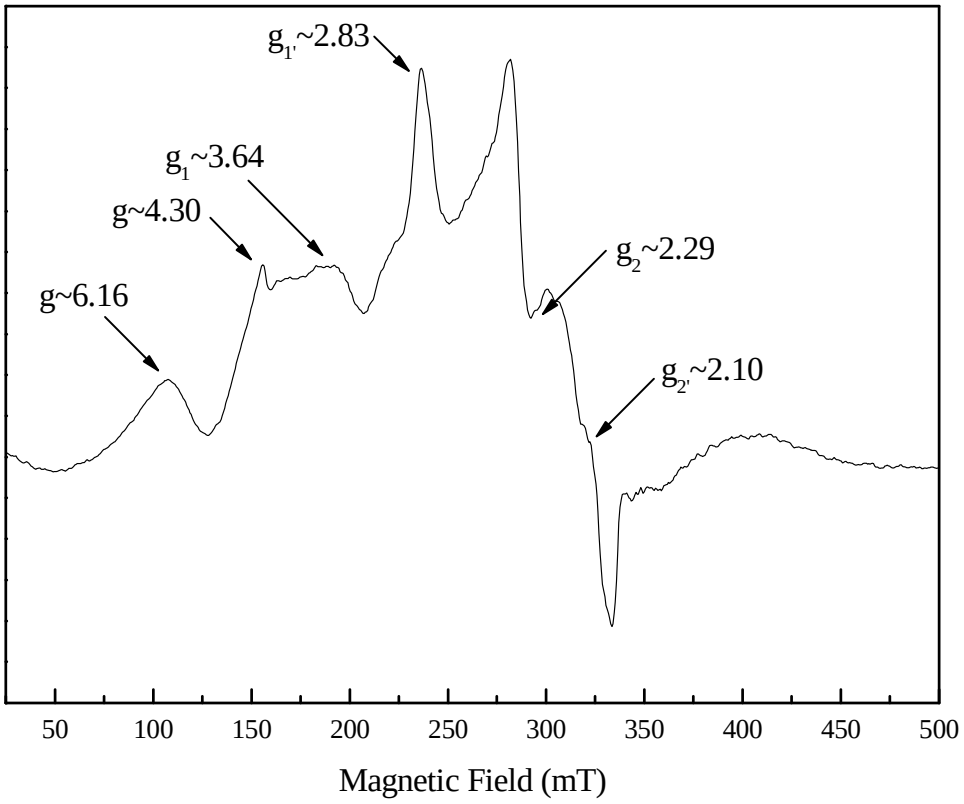

Figure 4.17: EPR spectrum of oxidised cytochrome *c*4 from *T. selenatis*.
Conditions of measurement: Temperature 20 K, power 2 mW, microwave frequency 9.39 GHz, modulation amplitude 10 G. Cyt*c*4 was at 15 µM, in 50 mM PIPES, pH 6.0.

Given the similarity of the EPR spectrum of one of the haems in *c*4 to that in c_4 from *A. vinelandii*, and the fact that both haems in cyt *c*4 show high redox potential (+280mV), it seems reasonable to suggest that Fe(III) in both the haem groups is ligated by methionine/histidine residues. Upon reduction by the addition of sodium dithionite all EPR signals in *c*4 were lost consistent with reduction of Fe(III) to EPR silent Fe(II).

4.15. Crystallisation trials

Crystallization trials were set up to attempt to generate diffracting crystals of cyt*c*4 for X-ray structure determination. Cyt*c*4 was concentrated to approximately 10 mg ml^{-1} and crystallisation trials were set up as described in section 2.22. Microdrop crystallisation and subsequent optimisation of the screening conditions yielded small pink-coloured crystals (see figure 4.18 for an example). Unfortunately none of the crystals obtained produced diffraction patterns. Production of better quality crystals was limited by the large amount of bacterial culture required to purify sufficient cyt*c*4 for crystallisation. In order to produce enough protein for further crystallisation, it will be more efficient to clone and overexpress the cyt*c*4 gene.

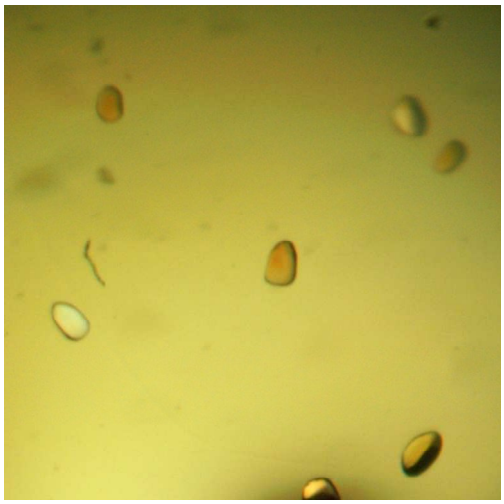

Figure 4.18: Cytochrome *c*4 crystals.
Crystals resulting from screening condition 0.2 M calcium acetate, 0.1 M sodium cacodylate pH 6.5 and 40% v/v PEG 300.

4.16. Investigation of interaction between cytochrome *c*4 and SerABC

As cyt*c*4 is a potential *in vitro* electron donor to SerABC, the physical interaction between the cytochrome and enzyme merits further investigation. Electron transfer between proteins is typically extremely rapid in order to support growth, as in the case of selenate respiration. If cyt*c*4 does act as a shuttle between a membrane bound protein and the water-soluble selenate reductase one could imagine the interaction between them to be short-lived. However, it has been shown during this study that cyt*c*4 co-purifies with SerABC through several steps, which could imply a stronger interaction. Additionally, it has also been shown that cyt*c*4 is present in both the membrane and periplasmic fractions of selenate grown cells, similarly to other members of the cytochrome c_4 group which have been shown to be present in the periplasm, and attached to the inner membrane (Pettigrew & Brown, 1988). It could be that cyt*c*4 has a weak association with the membrane to bring it into contact with, for example a quinol-cytochrome *c* oxidoreductase (QCR) from which it could receive electrons and then pass to SerABC, either by recruiting SerABC, or dissociating from the membrane and shuttling electrons to SerABC.

In order to investigate whether there was a measurable interaction between SerABC and cyt*c*4 two approaches were used; analysis by native-PAGE and Surface Plasmon Resonance (SPR). A strong interaction should be distinguishable by native-PAGE analysis, so purified SerABC was mixed with increasing amounts of cyt*c*4 and run on a native-PAGE gel, which was subsequently stained for total protein and haem. SerABC can be seen in the wells at the top of the gel, so it is not possible to look for a shift in the SerABC band if it binds cyt*c*4. Instead, the gel was haem stained to see if interaction with SerABC was causing any cyt*c*4 to be retarded at the top of the gel with the SerABC. Figure 4.19c shows that this is not the case – the only haem staining bands are cyt*c*4 alone.

SPR is capable of detecting much weaker interactions than native-PAGE, so this was used to investigate further the possibility of an interaction between SerABC and cyt*c*4. In SPR, polarised light strikes a thin layer of gold at the interface between two media of differing refractive index (the glass surface of the sensor, and the buffer above the gold layer), and is reflected at a certain angle. When small molecules such as proteins are bound to the sensor, the refractive index at the interface changes, which alters the angle

of the reflected polarised light in proportion to the mass of the bound molecules. This allows quantification of binding between molecules such as proteins, and calculation of association/dissociation constants.

Initially, SerABC equivalent to 5000 Response Units (RU) was bound to one flow-cell of a CM5 sensor chip as detailed in section 2.20 (see figure 4.20a), and 30 µl of ~200 nM cyt*c*4 in HBS was injected over the flow-cells. No difference between binding to the reference flow-cell and that with SerABC bound was immediately apparent, but upon closer inspection a slight difference in the dissociation of cyt*c*4 between the test and reference flow cells was observed (figure 4.20b). This slight difference can be attributed to non-specific interactions between the proteins and is not indicative of a genuine interaction. When cyt*c*4 was bound to the chip and SerABC used as analyte, no interaction could be observed as SerABC appeared to aggregate and bind to the test and reference flow-cells equally, and could not be removed easily (data not shown). No measurable interaction between SerABC and cyt*c*4 can be detected either by native-PAGE or SPR, and therefore we can assume any binding between the two is of a weak and transitory nature.

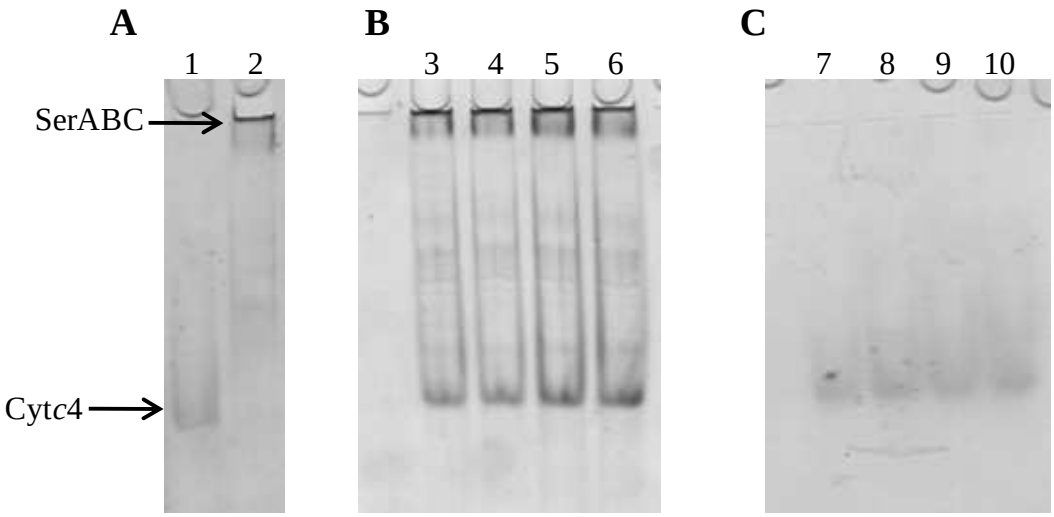

Figure 4.19: Native PAGE analysis of interaction between cytochrome *c*4 and SerABC. Gels A and B: Stained for total protein. Lane 1 - 5 µg cyt*c*4. Lane 2 - 5 µg SerABC. Lanes 3-6, 5 µg of SerABC and 6, 8, 10 and 12 µg of cyt*c*4 respectively. C: Stained for haem. Lanes 7-9, 5 µg of SerABC and 6, 8, 10 and 12 µg of cyt*c*4 respectively.

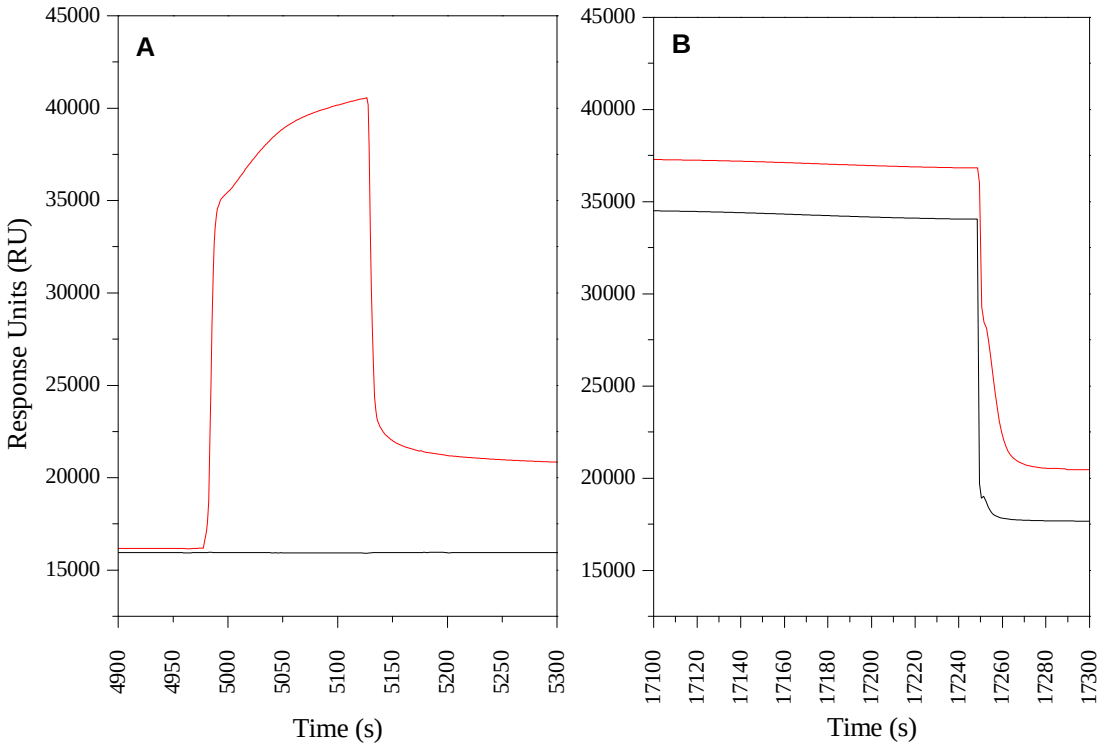

Figure 4.20: Analysis of the interaction between cytochrome *c*4 and SerABC by SPR. A: Binding of 1 µM SerABC in HEPES buffered saline to the activated test flow-cell (red) in comparison to the reference flow-cell (black). B: Dissociation of cyt*c*4 from the test (red) and reference (black) flow-cells. Cyt*c*4 was at a concentration of 200 nM in HBS.

4.17. Identification of the *cytc4* gene

To confirm the role of cyt*c*4 in selenate respiration, it was necessary to attempt to construct a mutant stain of *T. selenatis* in which the cyt*c*4 gene was inactivated. To accomplish this, the DNA sequence of the *cytc4* gene is required, so degenerate primers were used to try and amplify the gene. The obtained DNA sequence information could also be used to clone and express cyt*c*4 to provide more protein for crystallisation trials. Two sets of PCR primers were designed to amplify the gene coding for cyt*c*4 from *T. selenatis*, the sequences of which can be found in table 2.3. The forward primer was based on the N-terminal amino acid sequence, and the corresponding DNA sequence of the *D. aromatica* cytochrome, while the reverse primers were designed towards peptide sequences obtained from LC-MS/MS. PCR under varying conditions yielded a number of DNA fragments which were purified and cloned into the blunt-ended cloning vector pGEM-T, then sent for DNA sequencing. Unfortunately, none of the sequenced fragments had any homology to cytochrome *c* genes, and seemed to be the result of non-specific amplification.

4.18. Discussion

This work set out to identify possible soluble electron donors to the periplasmic selenate reductase enzyme. Two cytochromes *c* were purified from selenate respiring cultures of *T. selenatis*. Cyt*c*7 is upregulated in selenate respiration, has an apparent molecular mass of approximately 6 kDa, and a UV-visible spectrum typical of a low-spin cytochrome *c*. It was found that cyt*c*7 was unable to donate electrons to SerABC in a spectroscopic assay, and incubation of the reduced protein with selenate or selenite alone did not result in oxidation of the haem. The upregulation of cyt*c*7 during selenate respiration is interesting, but its physiological role is undefined with regard to the selenate respiratory pathway. As it is not able to act as electron donor to SerABC, it was not considered further in this work, but it could possibly function in the selenite respiratory pathway, perhaps as an electron donor to a selenite reductase.

The second cytochrome studied was cyt*c*4, which has a molecular mass of 23.5 kDa, and was assigned on the basis of sequence evidence to a class of cytochromes c_4, a group of di-haem cytochromes found in numerous bacterial species. In contrast to cyt*c*7, cyt*c*4 was able to donate electrons to SerABC, suggesting it could be a physiological electron donor to selenate reductase. The group of cytochromes c_4 has been well studied

in terms of their biophysical characteristics, yet very little is known about their function. Only two members of the family have an assigned role. One is from *A. ferrooxidans*, where of the four cytochromes c_4 identified in the genome, two have been purified, and one (CYC_{41}) is implicated in the transfer of electrons between rusticyanin and an aa_3 cytochrome oxidase in the iron oxidation pathway (Malarte *et al.*, 2005). The other is from the aerobe *A. vinelandii* and is thought to transfer electrons between a QCR and a cbb_3 terminal oxidase (Bertsova & Bogachev, 2002). The cytochrome c_4 from *T. roseopersicina* is highly expressed during anaerobic, photosynthesising conditions and a role has been proposed for cytochrome c_4 linking the QCR (quinol-cytochrome *c* oxidoreductase) and the photosynthetic reaction centre P870 (Branca et al., 2007b, Tomcova *et al.*, 2006), but no evidence to support this theory has yet been published.

In terms of the biophysical characteristics determined within this study, cyt*c*4 also fits in well with the distinctive features associated with the cytochrome c_4 group. They are distinguishable by their high redox potentials (usually > +200 mV) (Leitch *et al.*, 1985) which correlates well with the potential of +284 ±4 mV determined for cyt*c*4. The cytochromes c_4 also have a characteristic UV-visible spectrum; the α–band is asymmetric, reflecting different spectroscopic contributions from the two haems and there is a comparatively low α:β peak ratio (Pettigrew & Brown, 1988). These features are evident in the spectrum of cyt*c*4, which has a shoulder at around 545 nm, and an α:β ratio of ~1.5, compared to 1.87 for horse heart cytochrome *c* (Pettigrew & Moore, 1987). The structural data for the cytochromes c_4 shows that both haems have histidine and methionine axial ligands (Abergel et al., 2003, Kadziola & Larsen, 1997), and these residues are conserved throughout the family, as can be seen in the sequence alignment in figure 4.16. The amino acid sequence obtained for *T. selenatis* cyt*c*4 shows that at least one of the methionine residues is present, but the characteristic UV-visible spectral feature at 695 nm indicating His-Met ligation is not obvious. This feature is only visible at high concentrations however, so it could be that the concentration in the cuvette was not sufficient to allow this peak to be visualised. The EPR spectroscopic data did suggest His-Met ligation of at least one of the haems, although the g-values of the other haem were closer to those expected for a His-His ligated haem. It can be observed from the sequence alignment that at least one methionine is conserved in the available cyt*c*4 sequence, but further amino acid sequence would be necessary to confirm the presence of a second. As noted earlier however, the high potential of both the haems make it more likely that both are His-Met ligated, as His ligands act to withdraw electrons and

stabilise the oxidised form of the haem, resulting in a lower midpoint potential. Cyt*c*4 was put into crystallisation trials in order to try and obtain an X-ray diffraction structure of the protein, which would clarify assignment of the ligands, but the crystals produced did not diffract when tested.

The spectroscopic characterisation and sequence alignments place cyt*c*4 within the cytochrome c_4 group, so one can assume that it is a di-haem cytochrome, although the sequence data does not cover either of the CXXCH binding motifs. This di-haem classification was confirmed by tryptic digestion of the folded protein and mapping of trypsin cut sites onto the existing structure of *P. stutzeri* cytochrome c_4 as described in section 4.14. These structures show proteins composed of 2 domains, thought to arise from gene duplication of a mono-haem cytochrome (Brown *et al.*, 1999), connected by a linker. Interestingly, it has been proposed that mitochondrial cytochrome c_1, part of the QCR complex, is a descendant of the proteobacterial cytochromes c_4 and in fact arises from a structural collapse of a cytochrome c_4 after loss of haem binding ability in the C-terminal domain (Baymann *et al.*, 2004). There are several examples of proteobacterial QCR operons containing a cytochrome c_1 gene which encodes for a di-haem protein seemingly related to the cytochromes c_4 (Schutz *et al.*, 2000), thus it appears that cytochromes c_4 are an evolutionarily ancient family.

Although no measurable interaction between cyt*c*4 and SerABC could be detected here, it is likely that no strong interaction is needed, as long as the haems of cyt*c*4 and SerC can be brought close enough for electron transfer to take place, typically stated as ~14 Å (Page *et al.*, 1999). The high potential of the selenate/selenite couple and that of SerC itself will act as a draw for electrons.

The involvement of cyt*c*4 in the selenate respiratory chain as shown here is a new role for a member of the cytochrome c_4 family, which have previously been thought to act as electron donors to oxidases due to their high redox potentials. The potential of the selenate/selenite couple (+475 mV) also allows the use of a high potential cytochrome as an intermediate electron shuttle, as predicted by McEwan *et al*., (2002) and cyt*c*4 can fulfil this role. *T. selenatis* cyt*c*4 shows highest identity to that from the related bacterium *D. aromatica*, both are members of the β-proteobacterial class, and as discussed previously, *D. aromatica* expresses a perchlorate reductase enzyme (PcrABC) which shows certain similarities to SerABC. It is a member of the DMSO reductase

family of molybdo-enzymes, and the A and B subunits are homologous to those of the selenate reductase, but the C subunit is very different, instead of binding a *b*-type haem as SerC is predicted to do, PcrC contains 4 CXXCH motifs indicating it is a tetra-haem *c* type cytochrome, predicted to accept electrons from a membrane bound quinol dehydrogenase of the NapC/NirT type (Bender *et al.*, 2005). This arrangement could be possible for the selenate reductase pathway, if cyt*c*4 transfers electrons between a quinol dehydrogenase and SerC. Although PcrC is a tetra-haem cytochrome and cyt*c*4 a di-haem, the homologous tetra-haem c_{554} from *Nitrosomonas europaea* has been shown to be a two electron carrier (Iverson *et al.*, 1998), so both PcrC and cyt*c*4 could transfer the same number of electrons. Alternatively, a different membrane bound complex such as the QCR could transfer electrons to cyt*c*4, although it is not known whether *T. selenatis* expresses a QCR. The involvement of membrane bound cytochromes in selenate respiration will be considered further in chapter 5.

5. The role of membrane bound cytochromes in selenate respiration

5.1. Introduction

Within the DMSO reductase group of molybdo-enzymes, a number of pathways of electron transport have been established, and a variety of membrane-bound proteins have been implicated. These membrane-bound cytochromes are responsible for extracting electrons from the quinol pool so that they can be transferred to the associated downstream terminal reductases and it is not yet clear which type is involved in selenate respiration in *T. selenatis*. The existing literature provides several routes by which electrons are transferred and these are summarised in figure 5.1. Briefly, the membrane bound nitrate reductase NarGH receives its electrons from its dedicated NarI membrane integral subunit, which contains two *b*-haems; the DMSO reductase from *E. coli* (DmsABC) has a similar organisation of subunits (McCrindle *et al.*, 2005), but faces the periplasm. Some membrane bound nitrate reductases also face the periplasm, and these have been termed pNar enzymes (Martinez-Espinosa *et al.*, 2007), found in some bacteria and archaea, although the NarI subunit is not present, and the alternative membrane bound electron donor to pNarGH has not been definitively characterised. The *E. coli* TMAO reductase TorA, *Rhodobacter* sp. DMSO reductase DorA (McCrindle *et al.*, 2005), and the periplasmic nitrate reductase NapAB (Potter *et al.*, 2001) accept electrons from dedicated tetra or penta-haem quinol dehydrogenases in the membrane (TorC/DorC/NapC). In the case of Nap, there is also an alternative pathway; the *nap* gene cluster in *E. coli* for example, also contains *napG* and *napH*, which code for iron-sulfur proteins responsible for electron transfer from ubiquinol to NapC (Brondijk *et al.*, 2004). It could be the case that *T. selenatis* does not adhere to any of these pathways; McEwan *et al*., (2002) postulated that the selenate reductase of *T. selenatis* could receive electrons from quinol: cytochrome *c* oxidoreductase (QCR) via a high-potential *c*-type cytochrome, due to the high potential of the selenate/selenite couple. This has not been seen in any of the DMSO reductase family, but is a common pathway for enzymes such as the periplasmic cd_1 nitrite reductase from *P. pantotrophus* (Moir *et al*., 1993).
The high-potential cytochrome (cyt*c*4) isolated in chapter 4, which can donate electrons to SerABC is evidence in favour of McEwan's hypothesis, but the involvement of a QCR in selenate respiration in *T. selenatis* has not yet been investigated, and was a major component of this work.

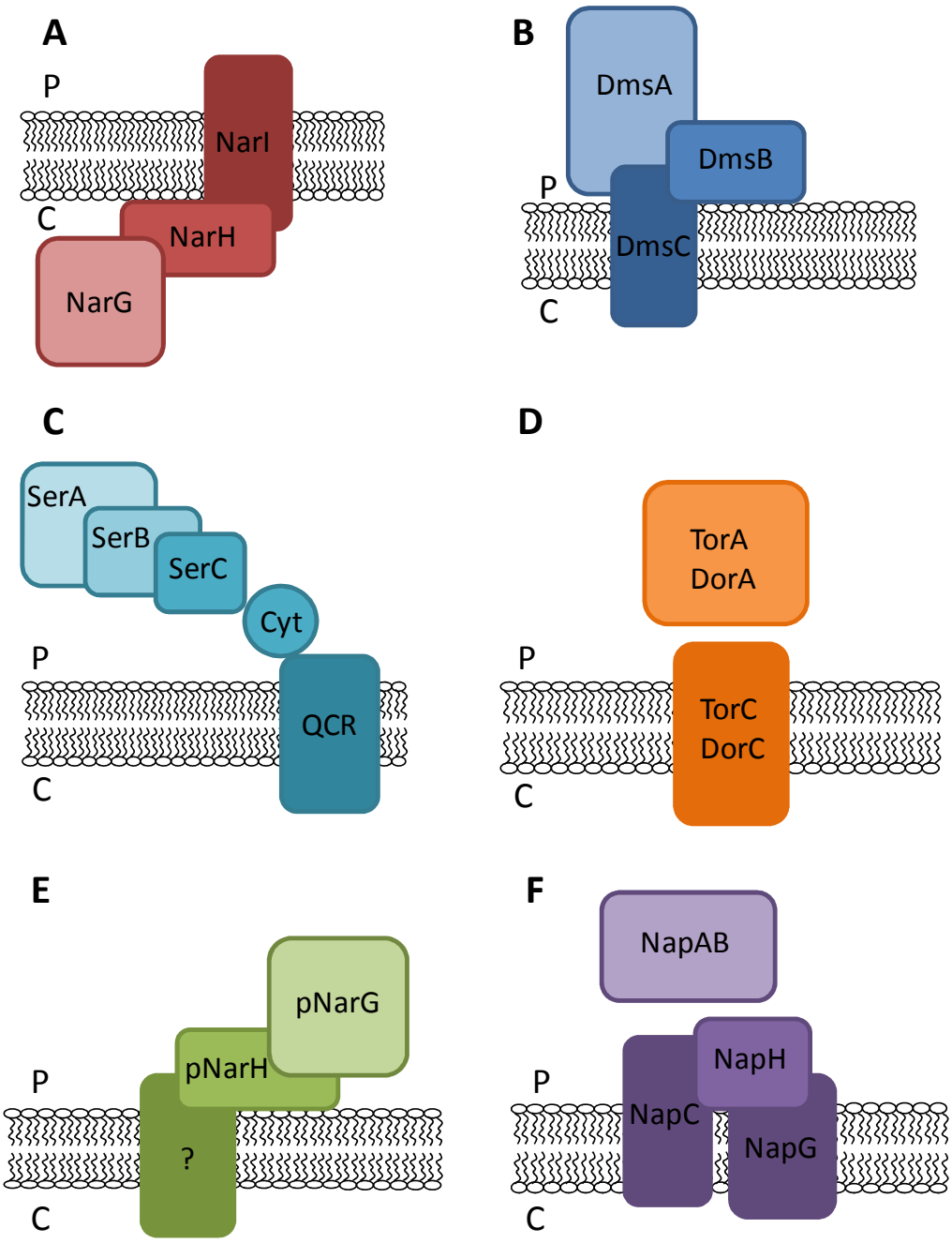

Figure 5.1: Representation of electron transfer chains to molybdo-enzymes of the DMSO reductase family.

A – NarGHI, cytoplasmic facing membrane bound nitrate reductase from *Paracoccus* sp., B – DmsABC, periplasmic facing DMSO reductase from *E. coli*, C – SerABC periplasmic selenate reductase, possible electron transport chain from a QCR in the membrane via a soluble *c*-type cytochrome, D – TorCA/DorCA, periplasmic enzyme and membrane bound multihaem quinol dehydrogenase exemplified by DMSO/TMAO reductase from *Rhodobacter* sp. and *E. coli* respectively. E – pNarGH, periplasmic facing membrane bound nitrate reductase from archaea such as *Haloarcula marismortui*. F – NapABCGH, periplasmic nitrate reductase from *E. coli*.

5.2. Identification of a quinol: cytochrome *c* oxidoreductase in *T. selenatis*

Soluble cytochromes acting as electron carriers such as those identified in chapter 4 need to accept electrons from an upstream donor. Commonly, this comes in the form of a QCR, however it is not known whether *T. selenatis* possesses a QCR. Related bacteria such as *Paracoccus* species do, but other Gram negative bacteria such as *E. coli* do not express one (Richardson, 2000). To establish whether *T. selenatis* expresses a QCR it was necessary to determine whether the genes encoding for a QCR were present. Primers for PCR amplification were designed based on conserved regions of genes coding for QCRs from other organisms. The most conserved region was that encoding the *b* haem subunit, therefore the primers were designed around this section, based on the sequence of *P. denitrificans* (for primer sequences see table 2.3 and figure 5.2). The expected size of the PCR product (assuming similarity to *P. denitrificans*) was 690 bp, and PCR using these primers produced a DNA fragment of approximately this size (see figure 5.3). The DNA bands visible on the gel were excised, purified from the gel slice and ligated into pGEM-T Cloning Vector, then transformed into *E. coli* JM109. Transformants containing the PCR product were selected by blue/white screening. Inactivation of the β-galactosidase *lac*Z gene in pGEM-T due to insertion of the cloned fragment can be detected by testing for the ability of the transformants to hydrolyse the substrate X-Gal and produce a blue precipitate. Transformants containing the cloned fragment appear white and those where the *lac*Z gene has not been inactivated are blue.

Plasmids from successful transformants were purified, and sent to MWG-Biotech for sequencing of the insert. Around 670 bp of sequence were returned, and searching for similar sequences using the BLAST tool at NCBI confirmed that the PCR product was highly similar to part of the gene for the *b*-haem subunit of a QCR. The *T. selenatis* gene sequence was translated and homologous sequences found again using the BLAST searching tool. The sequence of the QCR from *Caulobacter crescentus* was found to have the highest identity with that from *T. selenatis*, and the sequence from *P. denitrificans* was also returned as a close match. An alignment of some of the sequences returned is shown in figure 5.4. The sequence obtained from PCR of the *T. selenatis* putative QCR includes the highly conserved 'PEWY' loop which is present at the Q_o site, and is implicated in the mechanism of quinol oxidation (Osyczka *et al.*, 2006). The DNA sequence obtained has been submitted to the GenBank database, with accession number EU732596.

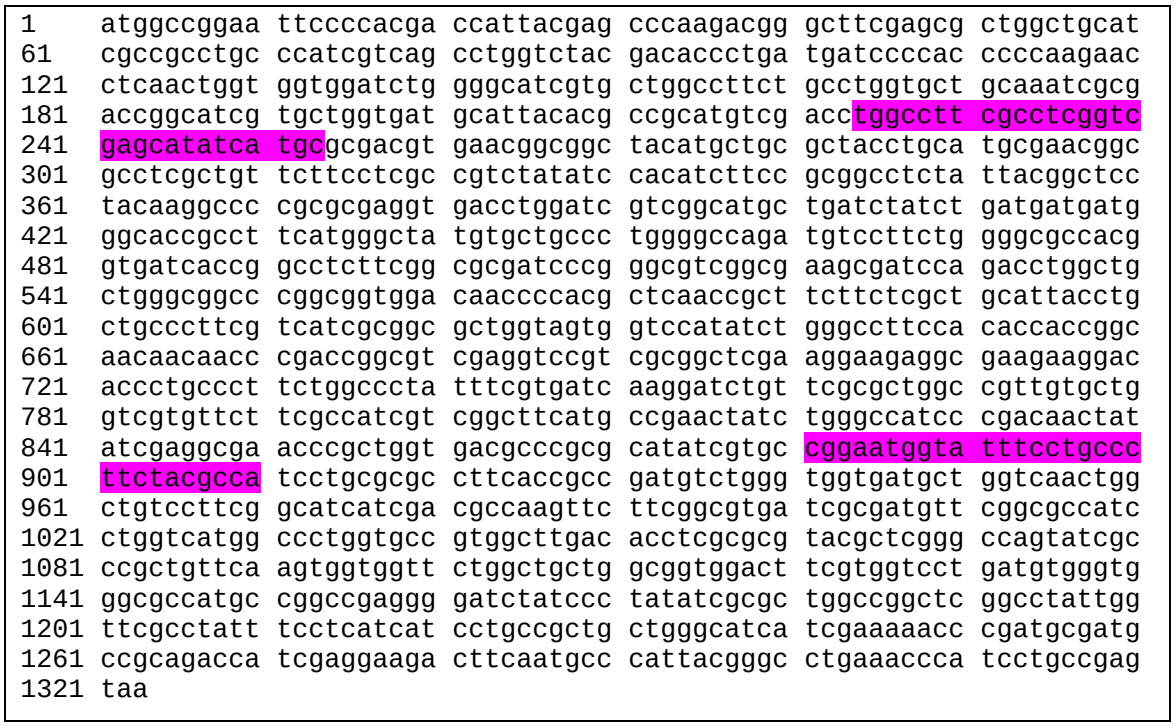

Figure 5.2: Primer design for amplification of partial QCR gene.

DNA sequence of cytochrome *b* gene of *P. denitrificans*, sites of primer binding are highlighted in pink.

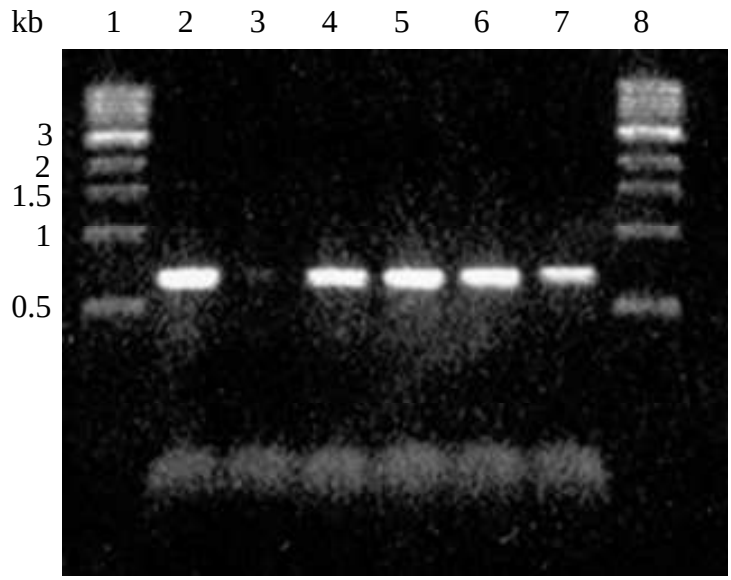

Figure 5.3: PCR amplification of partial QCR gene from *T. selenatis*.
Agarose gel electrophoresis of PCR products. Lanes 1 and 8 – Quick-Load 1 kb Ladder (NEB). Lane 2 – PCR reaction with annealing temperature 50.0ºC. Lane 3 – 50.8ºC. Lane 4 – 52.8ºC. Lane 5 – 54.1ºC. Lane 6 – 56.7ºC. Lane 7 – 59.5ºC.

Figure 5.4: Sequence alignments of QCRs with available sequence from *T. selenatis*.

Bacterial strains from which sequence data is taken are abbreviated as follows; Ts – *T. selenatis*, Cc – *C. crescentus*, Sa – *S. aggregata*, Pl – *P. lavamentivorans*, Ms – *Mesorhizobium sp*. BNC1, Rp – *R. palustris*, Pd – *P. denitrificans*, Mm – *M. magneticum* AMB-1, Mg – *M. gryphiswaldense* MSR-1. Conserved residues are highlighted in yellow, the conserved PEWY loop which forms part of the Q_o site is highlighted in red.

5.3. Respiratory inhibition of *T. selenatis* and *P. pantotrophus*

Confirming the presence of a QCR in *T. selenatis* is useful, but it does not necessarily mean that it is involved in selenate respiration. The QCR could be involved in passing electrons to terminal oxidase enzymes, such as cytochrome aa_3. As discussed earlier, there are a variety of membrane bound proteins capable of transferring electrons to terminal reductases, such as the NapC/NirT family of quinol dehydrogenases, or the NarG subunit of the respiratory nitrate reductase.

In order to investigate the involvement of a quinol: cytochrome c oxidoreductase in *T. selenatis*, classical inhibitors of respiratory chains, and QCRs in particular were used during selenate and nitrate respiration, and their effects measured by monitoring growth. The inhibitors used were myxothiazol, antimycin A and HQNO (2-n-heptyl-4-hydroxyquinoline N-oxide), and their structures are shown in figure 5.5. Myxothiazol is an antibiotic produced by the bacterium *Myxococcus fulvus* (Thierbach & Reichenbach, 1981), which binds to the Q_o site on the *b* haem subunit of the QCR (Zannoni, 2004). The Q_o site is where quinol is oxidised to quinone, and the binding of myxothiazol therefore stops electrons being transferred from the quinol pool, through the QCR to downstream electron acceptors. Antimycin A is produced by *Streptomyces* sp. and binds to the Q_i site of the QCR, inhibiting by out-competing the substrate (Gao *et al.*, 2003) and preventing the reduction of quinone to quinol. HQNO is a less specific quinone analogue which inhibits the QCR (Van Ark & Berden, 1977), the membrane bound nitrate reductase subunit NarI (Magalon *et al.*, 1998) and multi-haem quinol dehydrogenases such as NrfH from *Wolinella succinogenes* nitrite reductase (Simon, 2002).

Initial growth curves were conducted in 500 ml anaerobic bottles, and OD monitored hourly. *P. pantotrophus* was used as a control organism, as its electron transfer chain during denitrification has been studied extensively. *P. pantotrophus* was cultured with nitrate or nitrite as terminal electron acceptors, and 5 μM myxothiazol or 10 μM antimycin A. The growth curve data is shown in figure 5.6.

Nitrite respiration was completely inhibited by myxothiazol and antimycin A, a finding which fits with established knowledge; that nitrite reduction in *P. pantotrophus* by the cd_1 nitrite reductase is linked to the QCR, and is therefore blocked by both inhibitors

(Richardson, 2000). Nitrate respiration is severely inhibited, but not totally. Again, this fits with expected results, nitrate reduction under anaerobic conditions would be carried out by NarGHI, which releases protons from quinol oxidation into the periplasm and consumes cytoplasmic protons for reduction of nitrate, therefore contributing to Δp and supporting growth. Nitrite reduction is blocked, so the added Δp generated from this and other downstream denitrification enzymes such as nitric oxide reductase is lost, therefore limiting the growth. Additionally, the accumulation of toxic nitrite produced by NarGHI could be contributing to the retardation of growth.

To investigate the effect of myxothiazol on selenate respiration, growth curves were carried out as described above, with 10 mM selenate or 5 mM nitrite as electron acceptor and 5 μM myxothiazol as inhibitor (figure 5.7). The inhibitory effects in this case were much less clear. Growth with nitrite shows slight inhibition by myxothiazol, but selenate respiration does not seem to be significantly affected. As discussed in chapter 4, *T. selenatis* is believed to express a cd_1 nitrite reductase in its periplasm. In bacteria such as *P. pantotrophus*, this type of nitrite reductase receives its electrons from a QCR, via pseudoazurin and cytochrome *c* (550) (Richardson, 2000, Moir *et al*., 1993). If this electron transfer chain is similar in *T. selenatis*, myxothiazol should be able to effectively inhibit nitrite respiration, which we do not see here. It could be the case that the concentration is not high enough to inhibit *T. selenatis*. Growth on nitrite and selenate with 10 μM antimycin A showed a similar weak inhibition (data not shown).

A

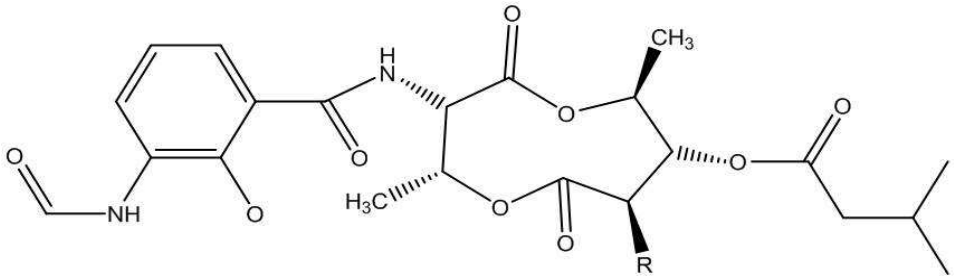

B

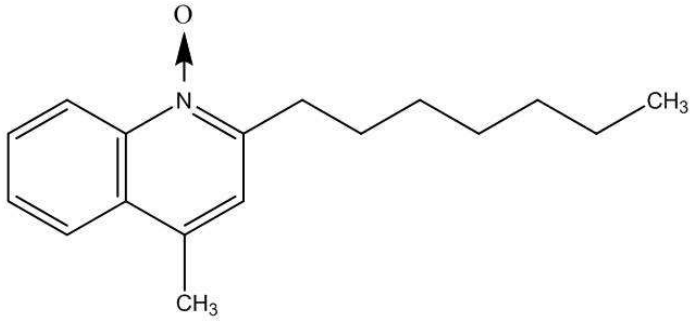

C

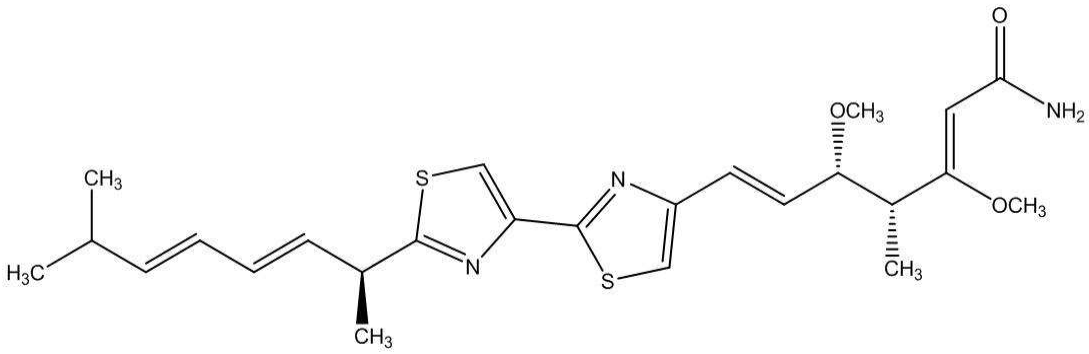

Figure 5.5: Chemical structures of respiratory chain inhibitors.

A: Antimycin A, B: HQNO, C: Myxothiazol.

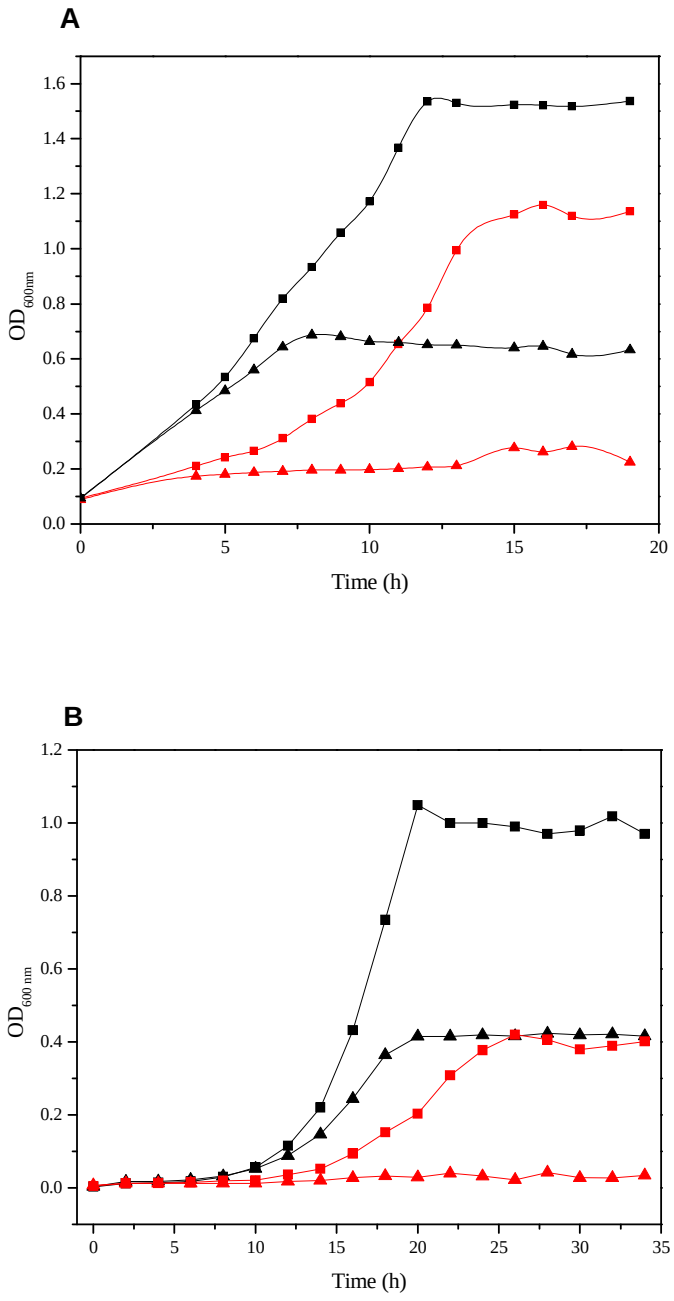

Figure 5.6: Anaerobic growth of *P. pantotrophus* with myxothiazol and antimycin A. Optical density of cultures with nitrate and nitrite as electron acceptor. Black lines indicate nitrate cultures (10 mM); red indicate those grown with nitrite (5 mM). Square points represent cultures in the absence of inhibitor; triangles represent those with inhibitor. In panel A, the inhibitor is 5 μM myxothiazol, in panel B, it is 10 μM antimycin A.

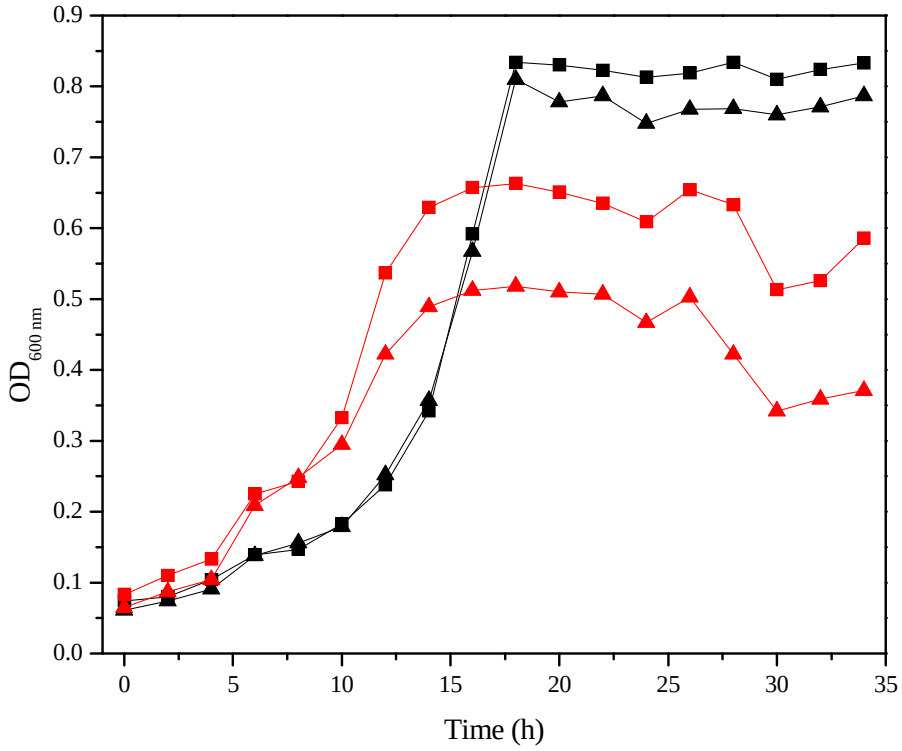

Figure 5.7: Anaerobic growth of *T. selenatis* with myxothiazol.

Optical density of cultures with selenate or nitrite as electron acceptors. Black lines indicate selenate cultures (10 mM); red indicate those grown with nitrite (5 mM). Square points represent cultures in the absence of inhibitor; triangles represent those with 5 μM myxothiazol.

5.4. Aerobic growth curves

For further elucidation of the *T. selenatis* electron transport chain, growth curves in aerobic shaking flasks were conducted in the presence of the QCR inhibitor antimycin A. As little or no inhibition of *T. selenatis* was observed with 10 µM antimycin, concentrations up to 100 µM were used. In *P. pantotrophus* (figure 5.8a), little or no inhibition was observed. This is because although two of the terminal oxidases are linked to the QCR (cytochrome cbb_3 and aa_3 types), one is not (cytochrome ba_3 type) (Otten *et al.*, 2001). Similarly, no inhibition is observed in *T. selenatis* growth curves (figure 5.8b), suggesting that at least one of the oxidases is also QCR independent.

5.5. Optimisation of growth curves

The large culture volumes used in previous growth curves limited inhibitor concentrations due to the amount of inhibitor available, but smaller batch cultures would not be large enough to remove 1 ml samples every hour. In order to culture *T. selenatis* under more reproducible conditions, and allow multiple replicates of growth curves for averages and error to be calculated, a method of culturing *T. selenatis* in a 96 well microplate was devised. The FLUOstar Optima microplate reader (BMG Labtech) was attached to an OFN source and degassed prior to use, and all media and supplements were also degassed to minimise the amount of oxygen present, which would affect the anaerobic growth curves. Optical density readings were taken at 15 minute intervals, after agitation to ensure cells were resuspended. The microplates were incubated at 30°C.

All growth conditions were replicated in 10 wells, allowing averaging of the optical densities over each time point. Before averaging, the optical density of a control set of wells of media with no bacterial culture was subtracted from the growth curves. In order to compare the effects of different conditions upon growth, a quantifiable factor was required. This was obtained by fitting all growth curves to the Gompertz equation using the OriginLab© graphing software, allowing the maximum gradient of the exponential section of the growth curve to be calculated (figure 5.9). The Gompertz equation (equation [9]) is routinely used to model bacterial growth curves (Zwietering *et al.*, 1990, Zwietering *et al.*, 1992, Banada *et al.*, 2000), and was shown to be a robust model when compared to other mathematical models (Zwietering *et al.*, 1990). When fitted to

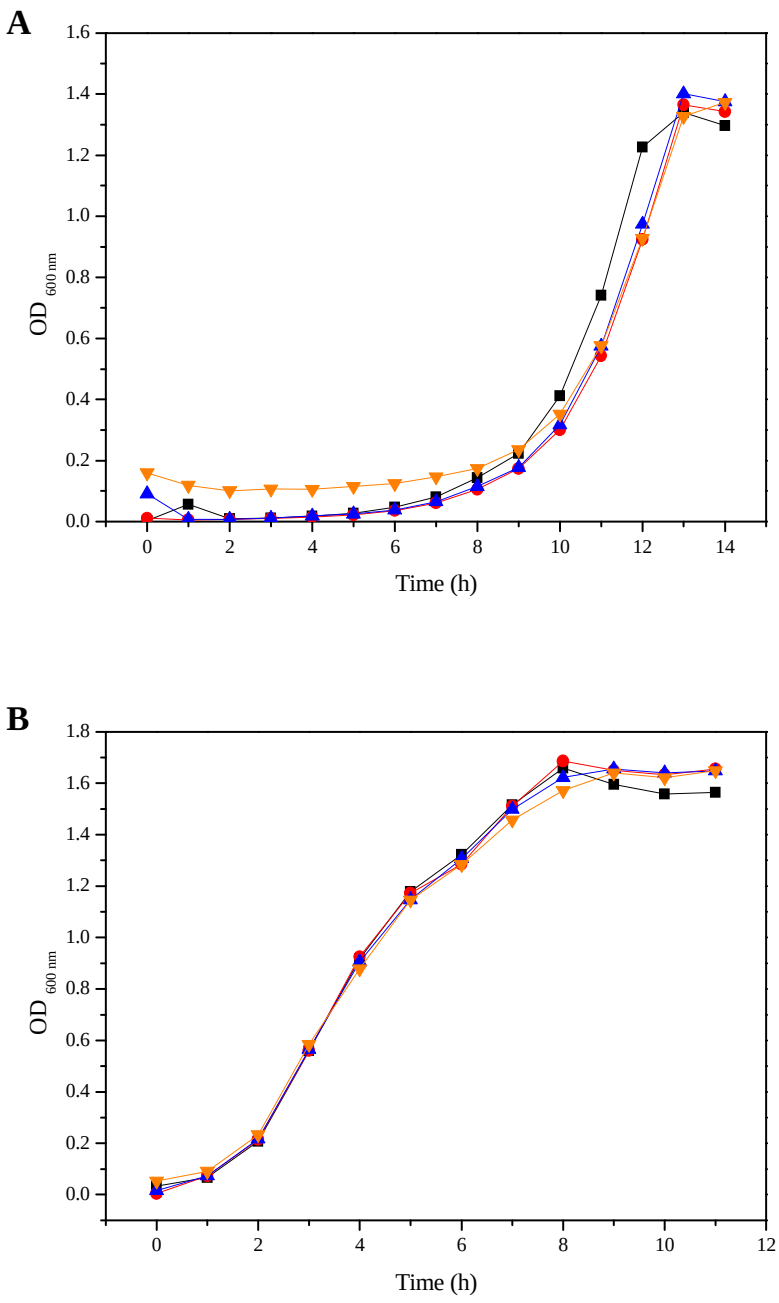

Figure 5.8: Aerobic growth curves of *P. pantotrophus* and *T. selenatis* with antimycin A.

Aerobic cultures grown at 30ºC with no inhibitor (black), 5 µM antimycin A (red), 10 µM (blue) or 100 µM (orange). A: *P. pantotrophus* growth curves. B: *T. selenatis* growth curves.

growth data using non-linear regression, the maximum growth rate of the culture can be calculated. This is termed the specific growth rate (μ) for the particular conditions of study (Kovarova-Kovar & Egli, 1998, Stanbury *et al.*, 1995). By varying a single condition of the growth medium, for example the concentration of electron acceptor, selenate, it is possible to measure μ at various concentrations and plot μ vs. substrate concentration. The relationship between substrate concentration and μ was originally described by Monod (see equation [10]) (Monod, 1942), where K_s is the affinity of the organism for a substrate, and s is substrate concentration.

$$y = a * e^{[-e^{(b-ct)}]} \quad [9]$$

(Where a is the upper asymptote, b is the gradient of the exponential phase and ct is the time at which b is reached.)

$$\mu = \mu_{max} \frac{s}{K_s + s} \quad [10]$$

This resembles an enzyme kinetic Michaelis-Menten equation; although it cannot be interpreted in exactly the same way, as enzyme kinetics necessarily describe a single enzyme, whereas growth rate is dependent upon many factors including uptake, transport and enzymatic activity. Nevertheless, a maximum specific growth rate (μ_{max}) can be calculated, and a value for K_s, the affinity of the whole organism for a substrate can be determined (the substrate concentration which allows the organism to reach a specific growth rate of half μ_{max}).

These values are very much dependent upon the particular culture conditions used, and have been shown to vary even in the same strain (Kovarova-Kovar & Egli, 1998). They are by no means definitive numbers, but here provide a useful tool to investigate the effects of inhibitors on the growth of *T. selenatis*.

A typical growth curve of *T. selenatis* cultured anaerobically with 10 mM selenate as electron acceptor was used to assess the fitting of the Gompertz curve (see figure 5.9). The Gompertz curve fitted to the data is also shown. The data deviates from the typical exponential curve in the lag phase of growth, where a small amount of growth can be seen before the exponential phase begins. This can be attributed to a small amount of oxygen being present in the media. Although every care was taken to minimize the level of oxygen, some will have been incorporated during pipetting media into the 96 well plate.

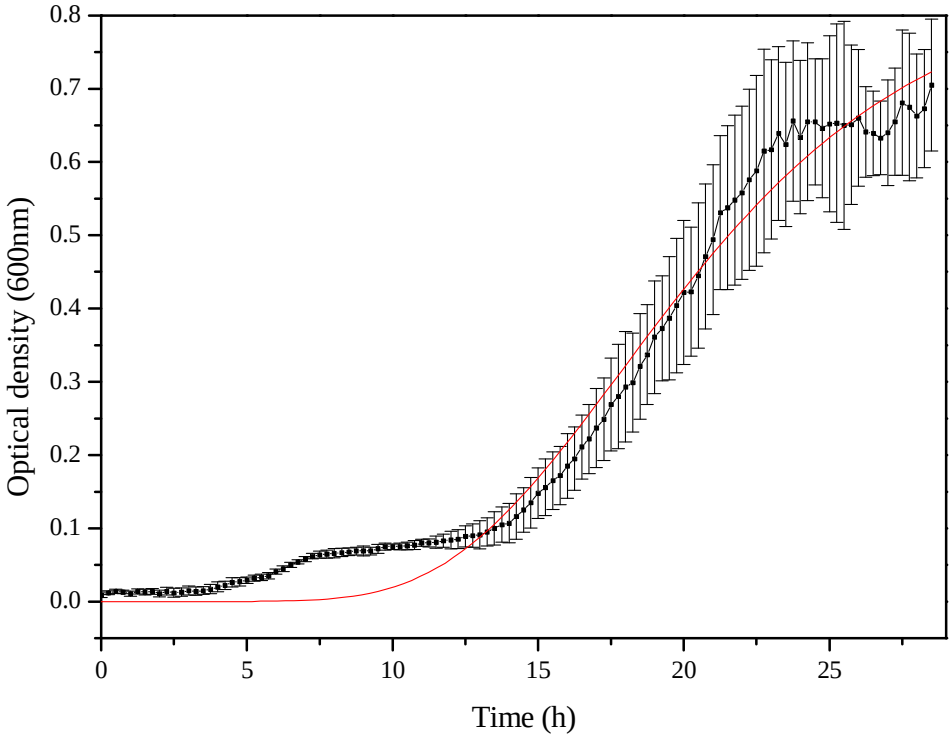

Figure 5.9: Preliminary microplate growth curve for *T. selenatis*.

Optical density of a *T. selenatis* anaerobic culture, containing 10 mM selenate as electron acceptor (black line). Error bars represent standard deviation from the average of 10 wells. The red line shows a Gompertz curve fitted to the data in OriginLab©. The Gompertz equation as specified in OriginLab© is $y = a*\exp(-\exp(-k*(x-x_c)))$, where a is the maximum OD of the culture, x_c is the time at maximum growth rate, and k is the maximum growth rate, μ.

5.6. Calculating K_s for selenate in *T. selenatis*

In order to determine an affinity constant (K_s) for selenate, *T. selenatis* was cultured in a 96 well microplate, under selenate respiring conditions as described previously, with varying concentrations of selenate. The average curves for each concentration were fitted to the Gompertz equation, and the μ values obtained were plotted against substrate concentration (figure 5.10). These data were then fitted to the Monod equation, and values for K_s and μ_{max} were determined. K_s was calculated to be 4.63± 1.41 mM, and μ_{max} at 0.32± 0.03 h^{-1}.

5.7. Inhibition of nitrite respiration by myxothiazol

In order to test whether the concentrations of inhibitor were high enough to inhibit *T. selenatis*, the microplate method was used to investigate the effect of myxothiazol on nitrite respiration, to see if complete inhibition could be achieved. A range of nitrite concentrations were used, with myxothiazol at 10 μM. Ten wells contained 5 mM nitrite, but no inhibitor. The resulting average growth curves for 5 mM nitrite ± myxothiazol can be seen in figure 5.11. Myxothiazol can be seen to inhibit nitrite respiration very effectively, so much so that the Gompertz curve cannot be fitted to the data successfully, so no measure of inhibited K_s is possible. This strengthens the evidence for the existence of a QCR in *T. selenatis*, and that nitrite reduction is carried out by a cd_1 nitrite reductase linked to the QCR. It also confirms that the concentration of myxothiazol used is sufficient to inhibit growth.

5.8. Inhibition of selenate respiration with myxothiazol

T. selenatis was cultured under selenate respiratory conditions, with varying concentrations of selenate and 10 μM myxothiazol. Ten wells contained 10 mM selenate but lacked myxothiazol, as a positive control. The resulting growth curves (figure 5.12a) indicate that selenate respiration is partially inhibited by myxothiazol, suggesting that the QCR is involved in this process. Analysis of the specific growth rates of the inhibited cultures (figure 5.12b) shows that the inhibited K_s is now 1.93± 1.58 mM, and the μ_{max} is 0.10± 0.02 h^{-1}. The K_s is not significantly altered when the error is taken into account, but the μ_{max} is 3 fold lower than that of uninhibited *T. selenatis*. It can be seen therefore, from the growth curves and analysis, that myxothiazol inhibits the growth of *T. selenatis* during selenate respiration, but does not completely prevent it.

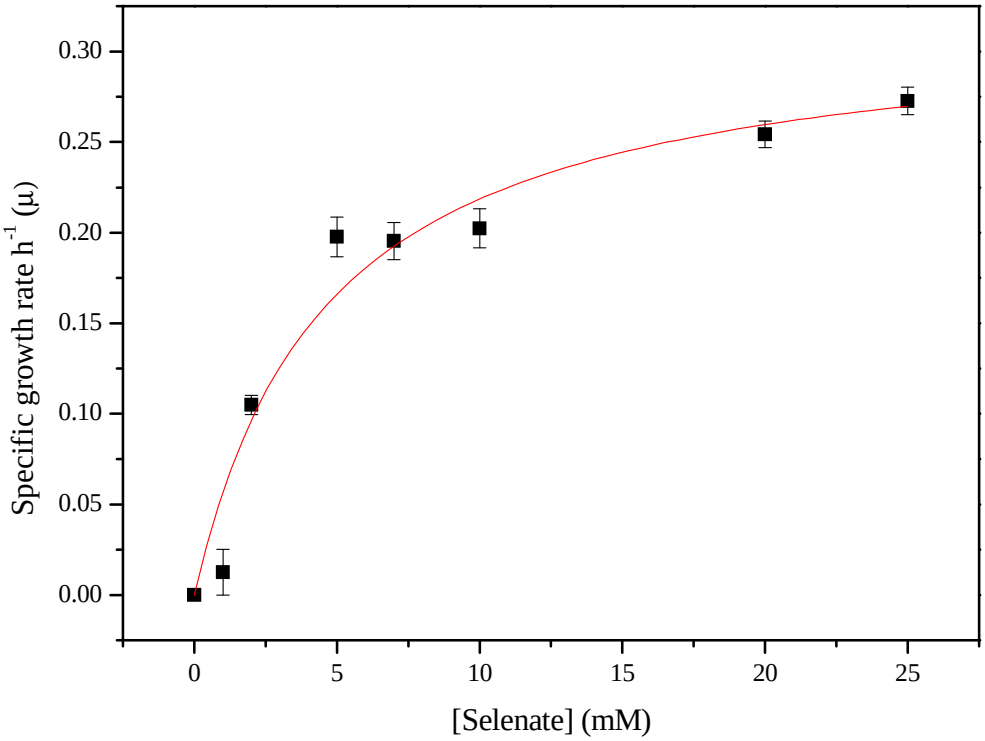

Figure 5.10: Selenate concentration dependence of the specific growth rate of *T. selenatis*.

The specific growth rate of *T. selenatis* in microplate wells (black squares) at different concentrations of selenate, fitted to the Monod equation (red line).

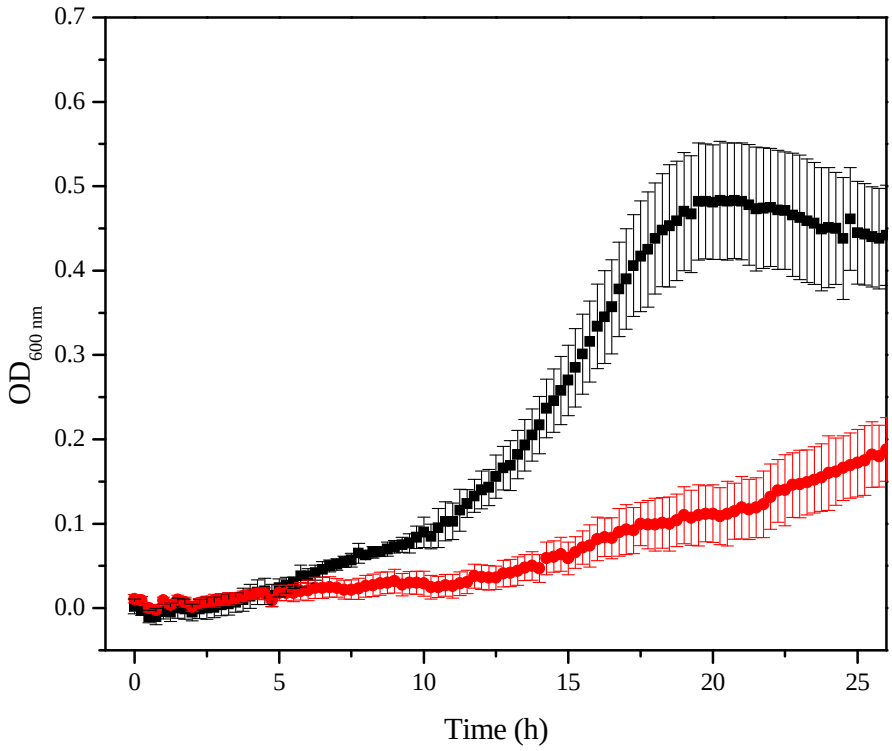

Figure 5.11: Inhibition of nitrite reduction by myxothiazol.

Optical density of *T. selenatis* cultures grown with 5 mM nitrite as electron acceptor. Black line indicates culture in the absence of inhibitor, red line shows culture with 10 µM myxothiazol. Error bars represent standard deviation of 10 cultures.

A

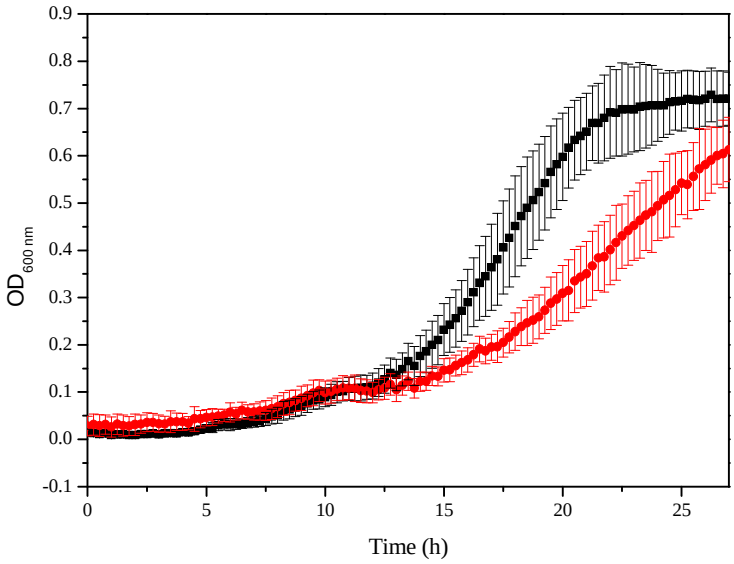

B

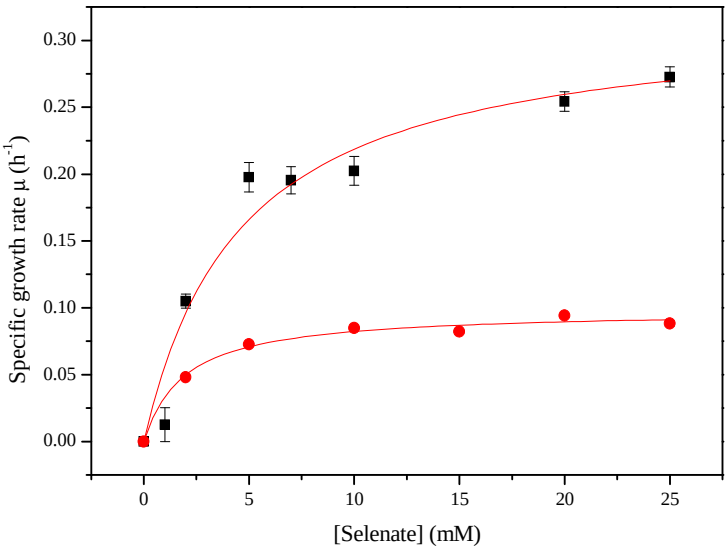

Figure 5.12: Inhibition of selenate respiration by myxothiazol.

A: Optical density of *T. selenatis* selenate (10 mM) respiring cultures ± myxothiazol. Black line indicates culture in the absence of myxothiazol, red with 10 µM myxothiazol.

B: Comparison of K_s and μ_{max} for selenate respiring cultures ± myxothiazol. Black squares - cultures in the absence of inhibitor, red circles - cultures with 10 µM myxothiazol

5.9. Inhibition of selenate respiration by HQNO

As myxothiazol has been shown to fully inhibit the QCR in nitrite reduction, but is only partially effective at inhibiting selenate respiration, HQNO was used as an inhibitor which affects a wider range of proteins with quinol dehydrogenase activity. An initial set of growth curves was carried out to find what concentration of HQNO would inhibit selenate respiration (figure 5.13). HQNO inhibits at concentrations as low as 2 µM, but maximum inhibition was reached at 20 µM, so this concentration was used for further experiments.

5.10. Inhibition of selenate respiration by HQNO and myxothiazol

Both HQNO and myxothiazol appear to partially inhibit selenate respiration, which could mean they are inhibiting different proteins. In order to test this theory, *T. selenatis* was cultured in the presence of both HQNO and myxothiazol, with varying concentrations of selenate. The results (figure 5.14) show complete inhibition of selenate respiration by combining these two inhibitors. This suggests that there is more than one route by which electrons can be transferred to selenate reductase; via the QCR which is inhibited by myxothiazol, and via another type of quinol dehydrogenase which is inhibited by HQNO.

5.11. Selenite respiration in *T. selenatis*

It has been proposed by Demolldecker and Macy (1993) that the nitrite reductase in *T. selenatis* is responsible for selenite reduction. Genetic (Etchebehere & Tiedje, 2005, Song & Ward, 2003) and now, biochemical evidence suggests that *T. selenatis* has a cd_1 nitrite reductase. If selenite is reduced by this enzyme, it should be able to support some growth, as the link to the QCR would provide a PMF. This would also account for a partial inhibition of selenate respiration by myxothiazol, if the inhibitor is blocking selenite reduction rather than selenate reduction.

T. selenatis was cultured with varying concentrations of selenite, to determine whether it could support growth. High concentrations of selenite can be toxic, but *T. selenatis* has been shown to grow in the presence of up to 1 mM selenite when selenate is also provided as an electron acceptor (Butler *et al*., unpublished). It can be seen from figure 5.15 that selenite does not support growth, and therefore casts doubt upon the assertion that selenite is reduced by the PMF-coupled enzyme cd_1 nitrite reductase. This is also

evidence to support the theory that the inhibitory effect of myxothiazol on selenate respiration is acting at the level of selenate reduction.

5.12. Identifying candidate membrane bound cytochromes

As we have established that electron transport to selenate reductase seems to occur via more than one pathway, it is important to consider what the alternative electron donors may be. The prediction made by McEwan *et al*., (2002) that SerABC receives electrons from a QCR via a high-potential *c*-type cytochrome seems to be confirmed by the data thus far, but the identity of the HQNO sensitive alternative membrane bound donor is unclear. There are two main possibilities; a *b*-haem cytochrome similar to NarI, or a tetra-*c*-haem quinol dehydrogenase of the NapC/NirT family. As discussed in chapter 4, the related *D. aromatica* chlorate reductase is adjacent to a NapC/NirT type cytochrome, but it is not known whether such an enzyme is present in the *T. selenatis* genome. We can look for evidence however, in the haem stained gels of membrane fractions from selenate respiring cultures shown in figure 4.1. Two cytochromes, cyt*c*3 and cyt*c*5, seem to be highly expressed during selenate respiration, and have molecular masses of ~30 and ~20 kDa respectively. The size of cytochromes of the NapC/NirT family varies; NapC of *P. pantotrophus* is around 30 kDa, NirT from *P. stutzeri* is around 25 kDa and the *D. aromatica* cytochrome is just below 20 kDa (These values are predicted from sequence information and include four haem groups at approximately 600 Da/haem). These differing molecular weights mean that both cyt*c*3 and cyt*c*5 could be candidates for quinol dehydrogenase enzymes.

Attempts were made to purify cyt*c*3 and cyt*c*5 from the membrane fraction of cells grown under selenate respiring conditions by solubilising proteins using detergent (see figure 5.16), but neither of the proteins was stable enough to survive further purification steps (data not shown).

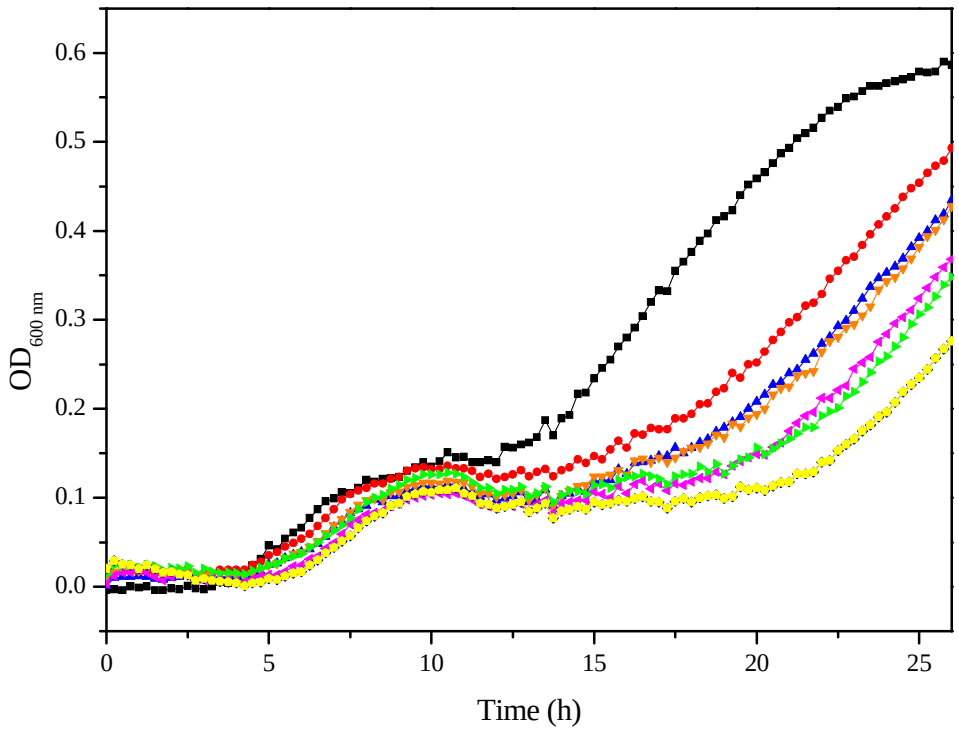

Figure 5.13: Titration of HQNO to inhibit selenate respiration.
Optical density of *T. selenatis* cultures containing 10 mM selenate and varying concentrations of HQNO. Black squares – positive control (10 mM selenate, no inhibitor), red – 2 μM HQNO, blue – 5 μM, orange – 7 μM, pink – 10 μM, green – 15 μM, dark blue – 20 μM, yellow – 25 μM.

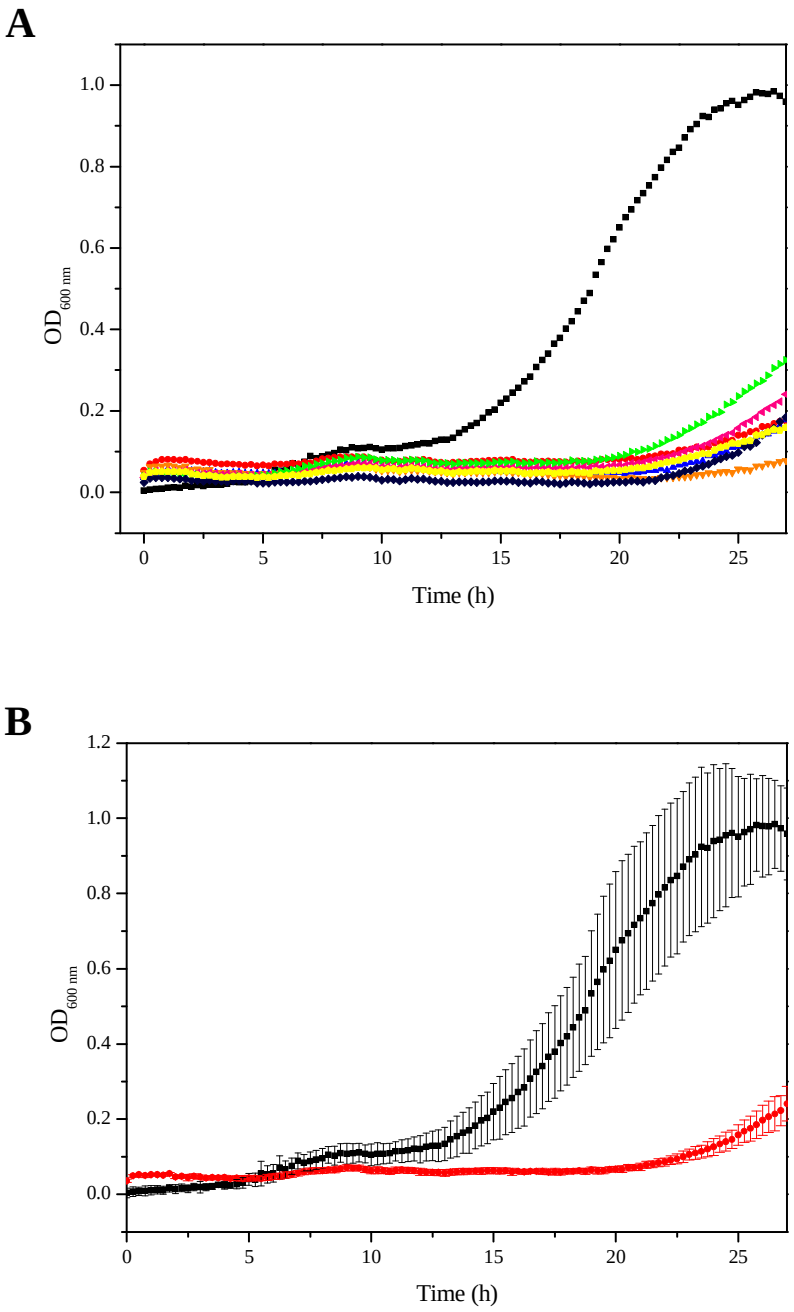

Figure 5.14: Inhibition of selenate respiration by myxothiazol and HQNO.

Optical density of *T. selenatis* cultures containing 10 µM myxothiazol, 20 µM HQNO and varying concentrations of selenate. A: Black squares – positive control (10mM selenate, no inhibitors), red – 2 mM selenate, blue – 5 mM, orange – 7 mM, pink – 10 mM, green – 15 mM, dark blue – 20 mM, yellow – 25 mM. B: 10 mM selenate with (red) and without (black) myxothiazol and HQNO. Error bars represent the standard deviation of ~ 10 cultures.

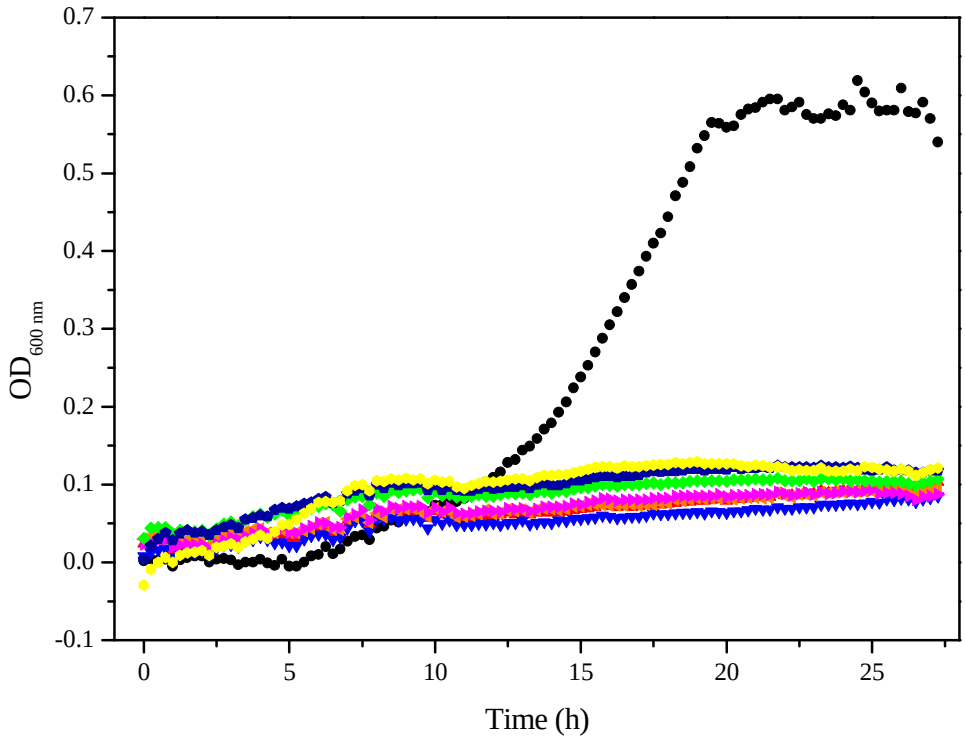

Figure 5.15: Growth of *T. selenatis* with selenite as electron acceptor.

Optical density of *T. selenatis* cultures containing varying concentrations of selenite. Black squares – 10 mM selenate as a positive control, red – 50 µM, blue – 100 µM, orange – 200 µM, pink – 500 µM, green – 1 mM, dark blue – 2 mM and yellow – 5 mM.

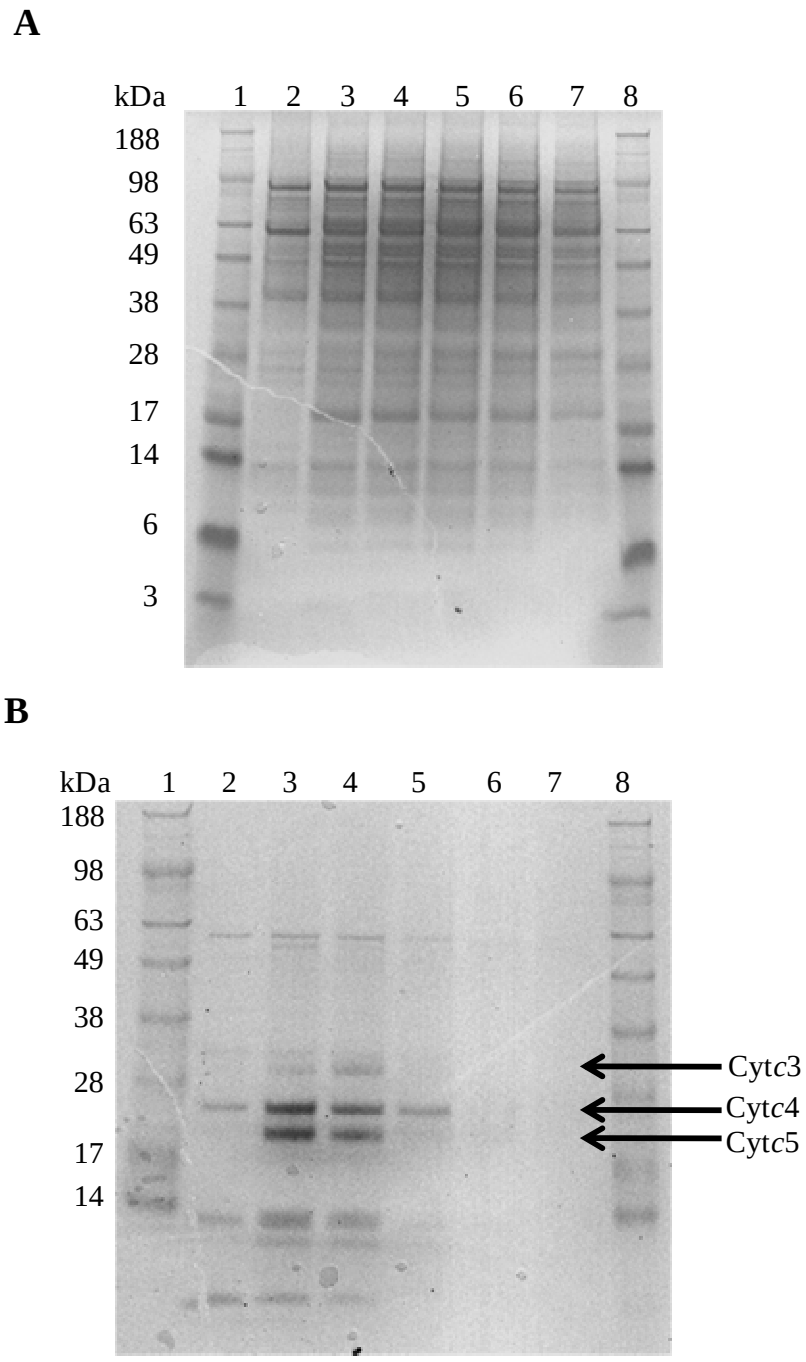

Figure 5.16: Solublisation of cytochromes from membranes of *T. selenatis*.

SDS-PAGE gels of membrane fraction from selenate grown cultures solubilised with Thesit detergent by shaking for 1 hour at room temperature. A: stained for total protein, B: haem stained for *c*-type cytochromes. The same samples were run on both gels. Lanes 1 and 8 –Invitrogen SeeBlue Plus Prestained Standard, lane 2 – 0% Thesit, lane 3 – 0.5%, lane 4 – 1%, lane 5 – 1.5%, lane 6 – 2%, lane 7 – 2.5%.

5.13. Discussion

The aim of this chapter was to discover the identity of any membrane bound cytochromes involved in selenate respiration. PCR with degenerate primers showed that *T. selenatis* possesses at least part of the gene cluster coding for a quinol: cytochrome *c* oxidoreductase, which appears very similar to those of other related proteobacteria. The sequence obtained was for the cytochrome *b* subunit of the QCR, so no information is available for the Rieske protein or cytochrome c_1 subunits. Can a protein corresponding to cytochrome c_1 be identified in the membrane of *T. selenatis*? The *C. crescentus* cytochrome c_1 protein has a predicted mass of ~28 kDa, whereas that from *P. denitrificans* is approximately 45 kDa. The previously identified cyt*c*3 fits in between this range and is a possible candidate for cytochrome c_1. The identification of a QCR in *T. selenatis* helps to expand our knowledge of the electron transport chain, and shows it has similarities to that of *Paracoccus sp.*, in that *T. selenatis* also possesses a QCR, and has at least one oxidase which is not linked to the QCR, like the cytochrome ba_3 oxidase of *P. denitrificans* (Otten *et al*., 2001). *T. selenatis* has detectable nitrate reductase activity in the membrane, suggesting it possesses a Nar type nitrate reductase (Rech & Macy, 1992). It is also able to utilise a wide variety of carbon sources, and is capable of denitrification (Macy *et al.*, 1993). A representation of the known/deduced respiratory pathways in *T. selenatis* is shown in figure 5.17.

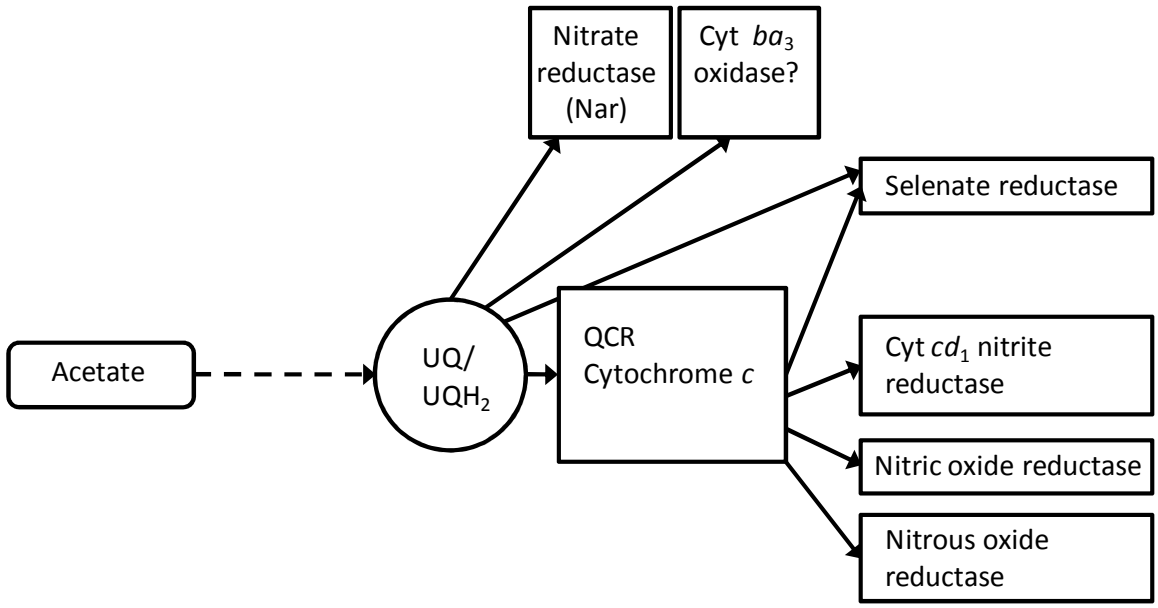

Figure 5.17: Electron transport chain in *T. selenatis*.

In order to determine the involvement of the QCR in selenate respiration, inhibitors of the respiratory chain were used during growth on various substrates. The microplate growth method which was developed to aid this analysis allowed reproducible measurements of growth under various conditions, and aided quantitative analysis of the data. As described earlier, *T. selenatis* expresses a cd_1 type nitrite reductase (Song & Ward, 2003) which has been shown in other bacteria to receive electrons from the QCR via a cytochrome *c* or copper protein intermediate (Moir *et al*., 1993, Pearson *et al.*, 2003). A similar organisation of the respiratory chain seems to be likely in *T. selenatis*, as we have shown that nitrite respiration is almost totally inhibited by myxothiazol and electron flow is therefore occurring through a QCR. The identity of the soluble electron-transferring intermediates is not known in this case however. This work also shows that 10 µM myxothiazol is sufficient to inhibit the QCR of *T. selenatis* and therefore can be utilised to investigate selenate respiration. The substrate affinity constant for selenate was determined to be 4.63± 1.41 mM, and when inhibited by myxothiazol the K_s was not significantly altered, but the maximum specific growth rate μ_{max} is decreased from 0.32± 0.03 h^{-1} to 0.10± 0.02 h^{-1}, an approximate three fold reduction. As the affinity of the selenate reductase enzyme is much greater (16 µM) than the affinity of the whole organism for selenate, it is clear that the substrate affinity is dependent upon a number of other factors such as selenate uptake. Considering that even in areas highly contaminated with selenate the environmental concentration is in the micro molar range, the affinity of *T. selenatis* for selenate is rather low, and may depend upon the higher affinity of the selenate reductase enzyme to scavenge the selenate that is available. It is important to note that the K_s value should not be over-interpreted, as it is highly dependent upon the conditions of culture and has been shown to vary by as much as three orders of magnitude for *E. coli* grown with glucose as the sole carbon source (Kovarova-Kovar & Egli, 1998).

The inhibition of anaerobic selenate respiration is less clear-cut, as myxothiazol only partially inhibits growth under these conditions. The less specific inhibitor HQNO also partially inhibits selenate respiration, but in combination, HQNO and myxothiazol completely inhibit growth on selenate, which suggests a branched pathway of electron transport to the selenate reductase. Myxothiazol acts to inhibit the QCR, while HQNO blocks electron flow through another membrane bound enzyme. The identity of this other enzyme is not known, although further study of membrane fractions from selenate respiring cultures showed two *c*-type cytochromes of a size consistent with the

NapC/NirT tetra-haem quinol dehydrogenases, known to donate electrons to a variety of periplasmic oxidoreductases. Confirmation of either of these cytochromes as a member of this family is not yet possible, as they are difficult to purify. NapC, for example was characterised spectroscopically by expressing a soluble truncated form of the protein (Roldan *et al.*, 1998). The lack of sequence information for *T. selenatis* means that a similar approach cannot be taken until the genome of this bacterium is fully sequenced.

The initial growth observed in some data from the microtitre plates has been attributed to oxygen present in the media, and could not be totally removed, even with extensive degassing of the media prior to inoculation. There is a lag of approximately 5 hours before this growth is noted, presumably because the cells were grown under anaerobic conditions prior to inoculation and had to upregulate oxidase enzymes for aerobic metabolism. This 'bump' in the growth curve is insensitive to HQNO or myxothiazol inhibition, but is absent when both are combined, suggesting that a number of oxidases are present in *T. selenatis*, both QCR dependent and independent.

It has also been confirmed that *T. selenatis* cannot respire selenite as the sole electron acceptor, making previous claims that selenite reduction is carried out by the QCR linked nitrite reductase unlikely (Demolldecker & Macy, 1993), unless the turnover of selenite is so low that it is not sufficient to generate enough PMF for cell growth without another electron acceptor available. Previous work has shown that a threshold PMF is required for significant ATP synthesis, and that a Δp below this threshold may lead to resources being devoted to maintenance of the cell rather than growth (Taylor & Jackson, 1985). A comparable situation was proposed for the membrane bound selenate reductase of *E. cloacae* SLD1-a1, which is unable to support growth in the absence of nitrate (Watts *et al.*, 2003), but recent continuous culture experiments have shown that the selenate reductase supports slow growth using selenate when nitrate is depleted under wash-out conditions (Leaver *et al.*, 2008). Similar experiments could be performed with *T. selenatis*, to investigate if selenite reduction can provide enough Δp for maintenance when nitrite is depleted. It has been shown however, that the cd_1 type nitrite reductase from *P. denitrificans* does not have any selenite reductase activity (Dr James Allen, personal communication), which is evidence against the nitrite reductase acting as a selenite reductase.

The linking of selenate reductase to the QCR shows similarities with the organisation of subunits predicted for the archaeal pNar enzymes. The pNarGH subunits are not associated with a *narI* gene in the *nar* gene clusters of *Haloferax mediterranei* and *H. marismortui*, instead genes named *narC* and *narB* code for a dihaem cytochrome *b* protein and a predicted Rieske [2Fe-2S] protein respectively (Lledo *et al.*, 2004, Yoshimatsu *et al.*, 2007). These genes have marked similarity to the QCR cytochrome *b* and Rieske subunits, and are postulated to be involved in a similar Q-cycle mechanism, translocating protons and providing a PMF linked to nitrate reduction in the periplasm.

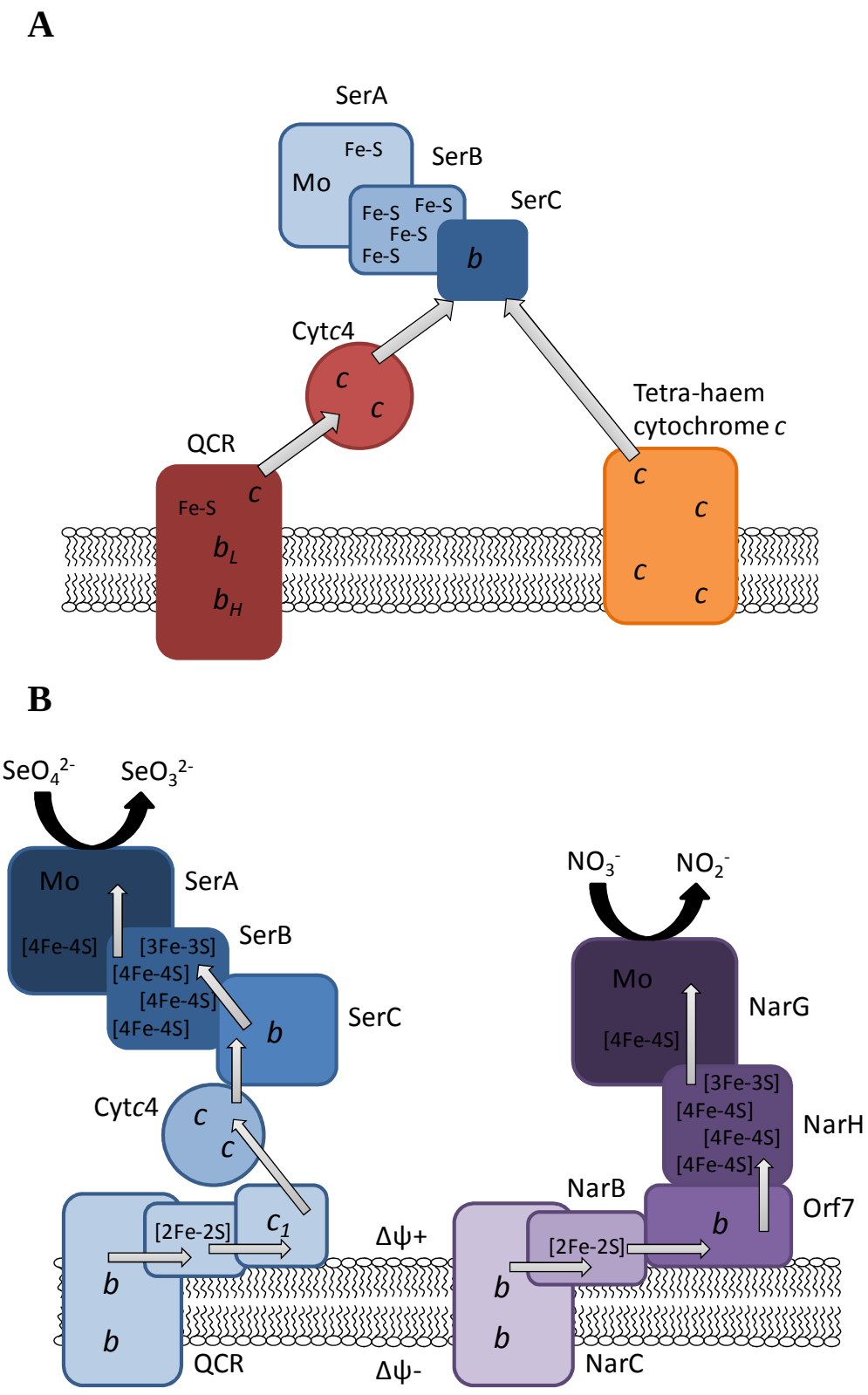

Figure 5.18: Cartoon representation of electron transfer route to selenate reductase. A: Predicted 'branched pathway' of electron transport to SerABC. B: Comparison between Ser and pNar predicted subunit topology.

6. Conclusions and future work

6.1. Conclusions

The work presented within this thesis has added to our knowledge of the selenate respiratory chain in *T. selenatis*, and how selenate reduction can contribute to the PMF. The selenate reductase from *T. selenatis* is the only respiratory selenate reductase to be characterised, so information about its ETC is valuable in understanding selenate respiration in general. The redox potential of the SerC subunit of selenate reductase was determined to be +234 mV (see figure 6.1), similar to those determined for EbdC and DdhC, which means it is likely that the unusual lysine and methionine ligands seen in EbdC and conserved in the amino acid sequences are ligands to the haem in SerC also. As the reductase and dehydrogenases are so similar in their potentials, the question of why they act as a dehydrogenase or a reductase must be raised. It seems as though the pivotal point is the potential of the substrate, a high potential substrate such as selenate is able to overcome the high potential of the γ-subunit and therefore electrons pass from SerC to the *bis*MGD cofactor, whereas the low reduction potentials of DMSO/DMS or 1-(S)-phenylethanol/ethylbenzene are not sufficient to pull the electrons in the reductive direction.

A profile of the *c*-type cytochromes expressed in *T. selenatis* showed a number of cytochromes which were highly expressed during selenate respiration. One of these, cyt*c*4 was shown to be able to donate electrons to SerABC *in vitro*. Spectroscopic characterisation and sequence analysis of cyt*c*4 has shown it to be a high-potential (+282 mV), di-haem cytochrome, of the cytochrome c_4 family. This represents the first role in anaerobic metabolism for a member of the cytochrome c_4 family. Although no strong interaction between cyt*c*4 and SerABC could be detected, it could be that the interaction is weak, or that binding could be more easily observed using just SerC instead of the large SerABC complex.

The presence of a quinol: cytochrome *c* oxidoreductase in *T. selenatis* was confirmed by PCR and sequencing, and its role in the respiratory chain investigated by using inhibitors. The development of a microplate growth curve method allowed analysis of growth curves under different conditions. Aerobic metabolism was unaffected by the QCR inhibitor antimycin A, suggesting *T. selenatis* has at least one oxidase that is not

linked to the QCR. In contrast, nitrite respiration was inhibited by myxothiazol, and therefore the nitrite reductase does receive electrons from the QCR. The inhibition of selenate respiration by myxothiazol was partial, which suggests that the pathway of electron transport to selenate reductase involves the QCR, but is branched and another electron donor may also be implicated. Passage of electrons from the QCR to cyt*c*4 and on to SerABC would be electrogenic due to the Q-cycle of the QCR, which therefore allows selenate to support anaerobic growth. Total inhibition of selenate respiration was achieved by combining myxothiazol with HQNO, a more general inhibitor. This means that an alternative HQNO sensitive electron donor exists, possibly a multi-haem quinol dehydrogenase of the NapC/NirT family, and candidate cytochromes have been identified from haem stained gels. These enzymes are not electrogenic, as the two protons released in the periplasm by quinol oxidation would be consumed by the reduction of selenate to selenite. The reason that *T. selenatis* can still grow, although at a reduced rate, when the proton-motive QCR is inhibited must be due to a primary dehydrogenase. The preferred carbon source for *T. selenatis* during selenate respiration is acetate, which is most likely metabolised through the TCA (tri-carboxylic acid) cycle, although until genome sequence is available it is difficult to know whether *T. selenatis* possesses the enzymes for a complete TCA cycle. This would produce NADH, which enters the electron transport chain via a proton pumping NADH dehydrogenase, therefore contributing to the PMF at the rate of $4H^+/2e^-$ (Nicholls & Ferguson, 2002).

The question of why *T. selenatis* would have a branched pathway to selenate reductase is interesting. If, as we predict, the alternative electron donor to SerABC is a member of the NapC/NirT family, then the role of this alternative pathway may be to detoxify selenate from the environment when another, preferred electron acceptor such as nitrate is also present (Rech & Macy, 1992) and is sufficient to generate a PMF. When no other electron acceptor is present, the selenate reductase can be linked to the QCR to provide a pmf, along with the Δp generated by NADH dehydrogenase. This branched pathway to a terminal reductase is an unusual occurrence, and we have been unable to find other examples in the literature, although some enzymes such as cd_1 nitrite reductase can receive electrons from both a *c*-type cytochrome and a copper protein.

The route of electron transfer to SerABC via a QCR represents a novel pathway within the DMSO reductase family, although it is commonly found for other enzymes such as oxidases. The implication of a member of the cytochrome c_4 family in selenate

respiration means that their roles may be much more varied than first thought, and not confined to aerobic metabolism. We have shown in this work how selenate respiration is linked to the pmf, and electron transport may occur via an unusual branched pathway, enhancing our knowledge of the only selenate respiring bacteria to be studied in any detail.

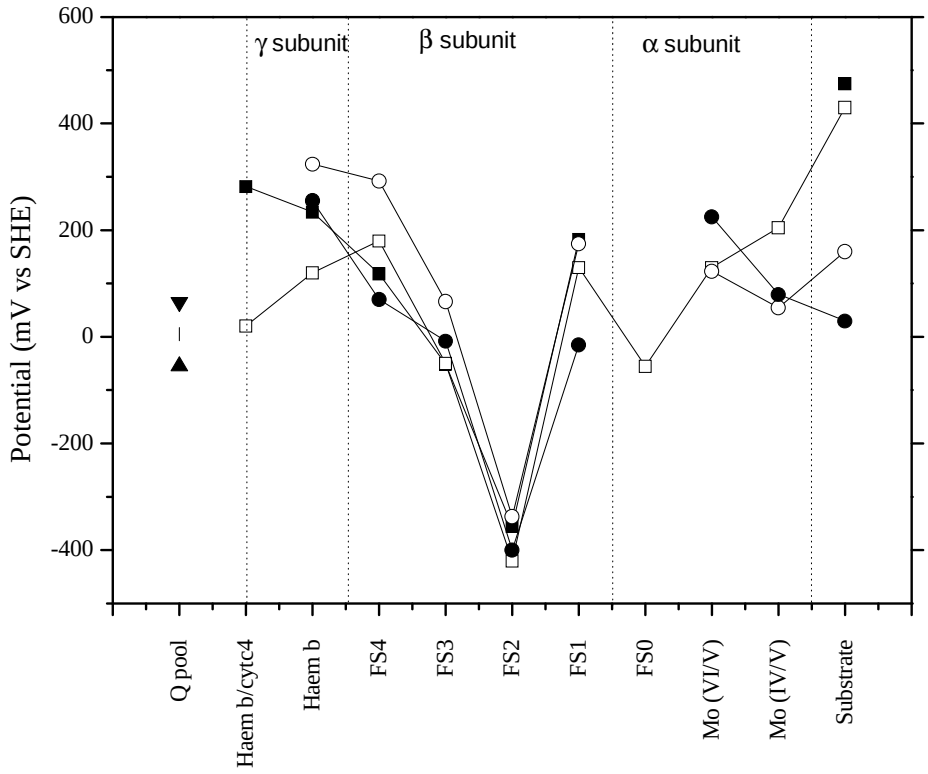

Figure 6.1: Midpoint potentials of redox centres of some type II DMSO reductase family enzymes.

■= SerABC,○ = DdhABC, ● = EbdABC, □ = NarGHI. Updated figure includes the values for SerC and cyt*c*4 determined within this work.

6.2. Future work

There are a number of ways in which this work could be continued. Our knowledge of the redox centres with SerABC could be completed by obtaining the redox potentials of the predicted FS0 centre and the molybdenum couples using EPR-monitored potentiometry.

In order to confirm the role of cyt*c*4 in the selenate respiratory chain, a mutant could be constructed in which the cyt*c*4 gene has been inactivated, and the mutated strains

growth under selenate respiring conditions could be monitored. If, as we predict, there is an alternative electron donor in the membrane, there may be little or no effect on growth. The alternative electron donor, possibly a multi-haem quinol dehydrogenase needs to be identified, and a mutant constructed in which this protein is inactivated. If the 'branched pathway' hypothesis is correct, strains in which both cyt*c*4 and the alternative donor are mutated should be unable to respire selenate, and those lacking the alternative electron donor only should be unable to respire selenate when treated with myxothiazol. The most sensible way to identify target proteins would be to sequence the genome of *T. selenatis*, which would reveal whether any NapC/NirT family proteins are present in the genome, and also provide the complete sequence of cyt*c*4.

To produce soluble SerC for investigating the interaction with cyt*c*4, the expression system will need to be changed. The peptide leader sequence of the *T. selenatis* gene could be replaced with an *E. coli* leader sequence, to see if processed protein is obtained. Alternatively, SerC could be expressed attached to a fusion protein to aid solubility.

To test the hypothesis that nitrite reductase is responsible for selenite reduction, this enzyme needs to be purified and tested for selenite reductase activity. Even if the cd_1 nitrite reductase does not possess activity, continuous culture experiments with nitrite as the electron acceptor could be carried out, in which selenite is washed in while nitrite is washed out. This would show whether selenite reduction is capable of providing a PMF sufficient to maintain cell viability in the absence of the preferred electron acceptor, even if it cannot support growth.

Selenate respiration differs from other respiratory pathways because the product is insoluble Se, compared to the diffusible products of denitrification and oxidative phosphorylation, N_2 and H_2O. It would be interesting to investigate the formation of Se nanospheres by *T. selenatis*, and how they are excreted from the cell. The particles are around 200 nm in size, and are therefore presumably very difficult to remove from the cell. It is not known whether excretion of Se nanospheres is ATP dependent, but if it is, selenate respiration would need to provide enough ATP for both growth and removal of selenate. The first step would be to determine whether the selenite is reduced in the periplasm, by cd_1 nitrite reductase for example, or in the cytoplasm, where perhaps an

assimilatory nitrite reductase reduces selenite to selenide. It is possible that the selenide is then exported to the periplasm and oxidised to produce elemental selenium.

As the genome sequence of *T. selenatis* is unavailable, it is not known how many selenoproteins are present in the genome, but it would be useful to determine whether any of the selenate provided for respiration is assimilated into selenoproteins. This could be achieved by providing *T. selenatis* with radiolabelled selenium in the form of selenate, then harvesting proteins and identifying any which contain radioactive Se. This could also provide information about where selenite is reduced in the cell.

Further investigation of the bioenergetics of selenate respiration and formation of the unusual selenium nanoparticles is important both from a biochemical point of view, and for future applications of selenate respiring bacteria, such as bioremediation of selenate/selenite contaminated areas and possible uses of Se nanoparticles.

7. References

Abergel, C., Nitschke, W., Malarte, G., Bruschi, M., Claverie, J. M. & Giudici-Orticoni, M. T., (2003) The structure of *Acidithiobacillus ferrooxidans* c(4)-cytochrome: a model for complex-induced electron transfer tuning. *Structure* **11**: 547-555.

Abrahams, J. P., Leslie, A. G., Lutter, R. & Walker, J. E., (1994) Structure at 2.8 Å resolution of F1-ATPase from bovine heart mitochondria. *Nature* **370**: 621-628.

Ahuja, U. & Thony-Meyer, L., (2005) CcmD is involved in complex formation between CcmC and the heme chaperone CcmE during cytochrome *c* maturation. *J Biol Chem* **280**: 236-243.

Alami, M., Luke, I., Deitermann, S., Eisner, G., Koch, H. G., Brunner, J. & Muller, M., (2003) Differential interactions between a twin-arginine signal peptide and its translocase in *Escherichia coli*. *Mol Cell* **12**: 937-946.

Allen, J. W., Barker, P. D., Daltrop, O., Stevens, J. M., Tomlinson, E. J., Sinha, N., Sambongi, Y. & Ferguson, S. J., (2005) Why isn't 'standard' heme good enough for *c*-type and d_1-type cytochromes? *Dalton Trans*: 3410-3418.

Arakawa, T., Tsumoto, K., Kita, Y., Chang, B. & Ejima, D., (2007) Biotechnology applications of amino acids in protein purification and formulations. *Amino Acids* **33**: 587-605.

Arnoux, P., Sabaty, M., Alric, J., Frangioni, B., Guigliarelli, B., Adriano, J. M. & Pignol, D., (2003) Structural and redox plasticity in the heterodimeric periplasmic nitrate reductase. *Nat Struct Biol* **10**: 928-934.

Banada, P. P., Liu, Y., Yang, L., Bashir, R. & Bhunia, A. K., (2000) Performance evaluation of a low conductive growth medium (LCGM) for growth of healthy and stressed *Listeria monocytogenes* and other common bacterial species. *Int J Food Microbiol* **111**: 12-20.

Baymann, F., Lebrun, E. & Nitschke, W., (2004) Mitochondrial cytochrome c_1 is a collapsed di-heme cytochrome. *Proc Natl Acad Sci U S A* **101**: 17737-17740.

Bender, K. S., Shang, C., Chakraborty, R., Belchik, S. M., Coates, J. D. & Achenbach, L. A., (2005) Identification, characterization, and classification of genes encoding perchlorate reductase. *J Bacteriol* **187**: 5090-5096.

Berks, B. C., (1996) A common export pathway for proteins binding complex redox cofactors? *Mol Microbiol* **22**: 393-404.

Berks, B. C., Palmer, T. & Sargent, F., (2005) Protein targeting by the bacterial twin-arginine translocation (Tat) pathway. *Curr Opin Microbiol* **8**: 174-181.

Berks, B. C., Sargent, F. & Palmer, T., (2000) The Tat protein export pathway. *Mol Microbiol* **35**: 260-274.

Bertero, M. G., Rothery, R. A., Palak, M., Hou, C., Lim, D., Blasco, F., Weiner, J. H. & Strynadka, N. C., (2003) Insights into the respiratory electron transfer pathway from the structure of nitrate reductase A. *Nat Struct Biol* **10**: 681-687.

Bertsova, Y. V. & Bogachev, A. V., (2002) Operation of the *cbb*$_3$-type terminal oxidase in *Azotobacter vinelandii*. *Biochemistry (Mosc)* **67**: 622-626.

Blasco, F., Dos Santos, J. P., Magalon, A., Frixon, C., Guigliarelli, B., Santini, C. L. & Giordano, G., (1998) NarJ is a specific chaperone required for molybdenum cofactor assembly in nitrate reductase A of *Escherichia coli*. *Mol Microbiol* **28**: 435-447.

Blasco, F., Guigliarelli, B., Magalon, A., Asso, M., Giordano, G. & Rothery, R. A., (2001) The coordination and function of the redox centres of the membrane-bound nitrate reductases. *Cell Mol Life Sci* **58**: 179-193.

Boekema, E. J. & Braun, H. P., (2007) Supramolecular structure of the mitochondrial oxidative phosphorylation system. *J Biol Chem* **282**: 1-4.

Boyer, P. D., (1997) The ATP synthase-a splendid molecular machine. *Annu Rev Biochem* **66**: 717-749.

Boyington, J. C., Gladyshev, V. N., Khangulov, S. V., Stadtman, T. C. & Sun, P. D., (1997) Crystal structure of formate dehydrogenase H: catalysis involving Mo, molybdopterin, selenocysteine, and an Fe4S4 cluster. *Science* **275**: 1305-1308.

Bradford, M. M., (1976) A rapid and sensitive method for the quantitation of microgram quantities of protein utilizing the principle of protein-dye binding. *Anal Biochem* **72**: 248-254.

Branca, R. M., Bodo, G., Bagyinka, C. & Prokai, L., (2007a) De novo sequencing of a 21-kDa cytochrome *c*(4) from *Thiocapsa roseopersicina* by nanoelectrospray ionization ion-trap and Fourier-transform ion-cyclotron resonance mass spectrometry. *J Mass Spectrom* **42**: 1569-1582.

Branca, R. M., Bodo, G., Varkonyi, Z., Debreczeny, M., Osz, J. & Bagyinka, C., (2007b) Oxygen and temperature-dependent structural and redox changes in a novel cytochrome *c*(4) from the purple sulfur photosynthetic bacterium *Thiocapsa roseopersicina*. *Arch Biochem Biophys* **467**: 174-184.

Brondijk, T. H., Nilavongse, A., Filenko, N., Richardson, D. J. & Cole, J. A., (2004) NapGH components of the periplasmic nitrate reductase of *Escherichia coli* K-12: location, topology and physiological roles in quinol oxidation and redox balancing. *Biochem J* **379**: 47-55.

Brown, K., Nurizzo, D., Besson, S., Shepard, W., Moura, J., Moura, I., Tegoni, M. & Cambillau, C., (1999) MAD structure of *Pseudomonas nautica* dimeric cytochrome *c*552 mimicks the *c*4 Dihemic cytochrome domain association. *J Mol Biol* **289**: 1017-1028.

Bushnell, G. W., Louie, G. V. & Brayer, G. D., (1990) High-resolution three-dimensional structure of horse heart cytochrome *c*. *J Mol Biol* **214**: 585-595.

Butler, C. S., Charnock, J. M., Bennett, B., Sears, H. J., Reilly, A. J., Ferguson, S. J., Garner, C. D., Lowe, D. J., Thomson, A. J., Berks, B. C. & Richardson, D. J., (1999) Models for molybdenum coordination during the catalytic cycle of periplasmic nitrate reductase from *Paracoccus denitrificans* derived from EPR and EXAFS spectroscopy. *Biochemistry* **38**: 9000-9012.

Cavazza, C., Giudici-Orticoni, M. T., Nitschke, W., Appia, C., Bonnefoy, V. & Bruschi, M., (1996) Characterisation of a soluble cytochrome *c*4 isolated from *Thiobacillus ferrooxidans*. *Eur J Biochem* **242**: 308-314.

Christensen, H. E., (1994) Cloning and characterisation of the gene encoding cytochrome *c*4 from *Pseudomonas stutzeri*. *Gene* **144**: 139-140.

Craske, A. & Ferguson, S. J., (1986) The respiratory nitrate reductase from *Paracoccus denitrificans*. Molecular characterisation and kinetic properties. *Eur J Biochem* **158**: 429-436.

Creevey, N. L., McEwan, A. G., Hanson, G. R. & Bernhardt, P. V., (2008) Thermodynamic characterization of the redox centers within dimethylsulfide dehydrogenase. *Biochemistry* **47**: 3770-3776.

DeLano, W. L., (2002) The PyMOL Molecular Graphics System.

Demolldecker, H. & Macy, J. M., (1993) The Periplasmic Nitrite Reductase of *Thauera selenatis* May Catalyze the Reduction of Selenite to Elemental Selenium. *Archives of Microbiology* **160**: 241-247.

Dias, J. M., Than, M. E., Humm, A., Huber, R., Bourenkov, G. P., Bartunik, H. D., Bursakov, S., Calvete, J., Caldeira, J., Carneiro, C., Moura, J. J., Moura, I. & Romao, M. J., (1999) Crystal structure of the first dissimilatory nitrate reductase at 1.9 Å solved by MAD methods. *Structure* **7**: 65-79.

Dong, X., Stothard, P., Forsythe, I. J. & Wishart, D. S., (2004) PlasMapper: a web server for drawing and auto-annotating plasmid maps. *Nucleic Acids Res* **32**: W660-664.

Dridge, E. J., (2007) Molecular analysis of the type II molybdo-enzymes from *Thauera selenatis* and *Archaeoglobus fulgidus*. Newcastle University PhD Thesis, Faculty of Medical Sciences pp. 191.

Dridge, E. J., Watts, C. A., Jepson, B. J., Line, K., Santini, J. M., Richardson, D. J. & Butler, C. S., (2007) Investigation of the redox centres of periplasmic selenate reductase from *Thauera selenatis* by EPR spectroscopy. *Biochem J* **408**: 19-28.

Driessen, A. J., Fekkes, P. & van der Wolk, J. P., (1998) The Sec system. *Curr Opin Microbiol* **1**: 216-222.

Dutton, P. L., (1978) Redox potentiometry: Determination of midpoint potentials of oxidation-reduction components of biological electron-transfer systems. In: Methods in enzymology; Biomembranes E, specialized techniques. S. Fleischer & L. Packer (eds). New York ; London: Academic Press, pp. 411-435.

Dyall, S. D., Brown, M. T. & Johnson, P. J., (2004) Ancient invasions: from endosymbionts to organelles. *Science* **304**: 253-257.

Ellis, P. J., Conrads, T., Hille, R. & Kuhn, P., (2001) Crystal structure of the 100 kDa arsenite oxidase from *Alcaligenes faecalis* in two crystal forms at 1.64 Å and 2.03 Å. *Structure* **9**: 125-132.

Emsley, P. & Cowtan, K., (2004) Coot: model-building tools for molecular graphics. *Acta Crystallogr D Biol Crystallogr* **60**: 2126-2132.

Etchebehere, C. & Tiedje, J., (2005) Presence of two different active nirS nitrite reductase genes in a denitrifying *Thauera* sp. from a high-nitrate-removal-rate reactor. *Appl Environ Microbiol* **71**: 5642-5645.

Futagami, T., Goto, M. & Furukawa, K., (2008) Biochemical and genetic bases of dehalorespiration. *Chem Rec* **8**: 1-12.

Gadsby, P. M., Hartshorn, R. T., Moura, J. J., Sinclair-Day, J. D., Sykes, A. G. & Thomson, A. J., (1989) Redox properties of the diheme cytochrome *c*4 from *Azotobacter vinelandii* and characterisation of the two hemes by NMR, MCD and EPR spectroscopy. *Biochim Biophys Acta* **994**: 37-46.

Gao, X., Wen, X., Esser, L., Quinn, B., Yu, L., Yu, C. A. & Xia, D., (2003) Structural basis for the quinone reduction in the bc_1 complex: a comparative analysis of crystal structures of mitochondrial cytochrome bc_1 with bound substrate and inhibitors at the Q_i site. *Biochemistry* **42**: 9067-9080.

Giudici-Orticoni, M. T., Leroy, G., Nitschke, W. & Bruschi, M., (2000) Characterization of a new dihemic *c*(4)-type cytochrome isolated from *Thiobacillus ferrooxidans*. *Biochemistry* **39**: 7205-7211.

Goldman, B. S., Gabbert, K. K. & Kranz, R. G., (1996) Use of heme reporters for studies of cytochrome biosynthesis and heme transport. *J Bacteriol* **178**: 6338-6347.

Gonzalez, P. J., Correia, C., Moura, I., Brondino, C. D. & Moura, J. J., (2006) Bacterial nitrate reductases: Molecular and biological aspects of nitrate reduction. *J Inorg Biochem* **100**: 1015-1023.

Hanahan, D., (1985). In: DNA cloning : a practical approach. D. M. Glover (ed). Oxford: IRL Press, pp. 3 v.

Hartshorne, R. S., Jepson, B. N., Clarke, T. A., Field, S. J., Fredrickson, J., Zachara, J., Shi, L., Butt, J. N. & Richardson, D. J., (2007) Characterization of *Shewanella oneidensis* MtrC: a cell-surface decaheme cytochrome involved in respiratory electron transport to extracellular electron acceptors. *J Biol Inorg Chem* **12**: 1083-1094.

Hille, R., (1996) The Mononuclear Molybdenum Enzymes. *Chem Rev* **96**: 2757-2816.

Hoffmann, T., Troup, B., Szabo, A., Hungerer, C. & Jahn, D., (1995) The anaerobic life of *Bacillus subtilis*: cloning of the genes encoding the respiratory nitrate reductase system. *FEMS Microbiol Lett* **131**: 219-225.

Howard, J. B. & Rees, D. C., (2006) How many metals does it take to fix N_2? A mechanistic overview of biological nitrogen fixation. *Proc Natl Acad Sci U S A* **103**: 17088-17093.

Huang, L. S., Sun, G., Cobessi, D., Wang, A. C., Shen, J. T., Tung, E. Y., Anderson, V. E. & Berry, E. A., (2006) 3-nitropropionic acid is a suicide inhibitor of mitochondrial respiration that, upon oxidation by complex II, forms a covalent adduct with a catalytic base arginine in the active site of the enzyme. *J Biol Chem* **281**: 5965-5972.

Iverson, T. M., Arciero, D. M., Hsu, B. T., Logan, M. S., Hooper, A. B. & Rees, D. C., (1998) Heme packing motifs revealed by the crystal structure of the tetra-heme cytochrome *c*554 from *Nitrosomonas europaea*. *Nat Struct Biol* **5**: 1005-1012.

Jepson, B. J., Mohan, S., Clarke, T. A., Gates, A. J., Cole, J. A., Butler, C. S., Butt, J. N., Hemmings, A. M. & Richardson, D. J., (2007) Spectropotentiometric and structural analysis of the periplasmic nitrate reductase from *Escherichia coli*. *J Biol Chem* **282**: 6425-6437.

Jetten, M. S., Cirpus, I., Kartal, B., van Niftrik, L., van de Pas-Schoonen, K. T., Sliekers, O., Haaijer, S., van der Star, W., Schmid, M., van de Vossenberg, J., Schmidt, I., Harhangi, H., van Loosdrecht, M., Gijs Kuenen, J., Op den Camp, H. & Strous, M., (2005) 1994-2004: 10 years of research on the anaerobic oxidation of ammonium. *Biochem Soc Trans* **33**: 119-123.

Jormakka, M., Byrne, B. & Iwata, S., (2003) Protonmotive force generation by a redox loop mechanism. *FEBS Lett* **545**: 25-30.

Jormakka, M., Richardson, D., Byrne, B. & Iwata, S., (2004) Architecture of NarGH reveals a structural classification of Mo-*bis*MGD enzymes. *Structure* **12**: 95-104.

Jormakka, M., Tornroth, S., Byrne, B. & Iwata, S., (2002) Molecular basis of proton motive force generation: structure of formate dehydrogenase-N. *Science* **295**: 1863-1868.

Kadziola, A. & Larsen, S., (1997) Crystal structure of the dihaem cytochrome c_4 from *Pseudomonas stutzeri* determined at 2.2 Å resolution. *Structure* **5**: 203-216.

Kapust, R. B. & Waugh, D. S., (1999) *Escherichia coli* maltose-binding protein is uncommonly effective at promoting the solubility of polypeptides to which it is fused. *Protein Sci* **8**: 1668-1674.

Karlsson, J. & Nilsson, T., (2005) The C subunit of *Ideonella dechloratans* chlorate reductase: expression, purification, refolding, and heme reconstitution. *Protein Expr Purif* **41**: 306-312.

Kengen, S. W., Rikken, G. B., Hagen, W. R., van Ginkel, C. G. & Stams, A. J., (1999) Purification and characterization of (per)chlorate reductase from the chlorate-respiring strain GR-1. *J Bacteriol* **181**: 6706-6711.

Kessi, J. & Hanselmann, K. W., (2004) Similarities between the abiotic reduction of selenite with glutathione and the dissimilatory reaction mediated by *Rhodospirillum rubrum* and *Escherichia coli*. *J Biol Chem* **279**: 50662-50669.

Kirillova, O., Chruszcz, M., Shumilin, I. A., Skarina, T., Gorodichtchenskaia, E., Cymborowski, M., Savchenko, A., Edwards, A. & Minor, W., (2007) An extremely SAD case: structure of a putative redox-enzyme maturation protein from *Archaeoglobus fulgidus* at 3.4 Å resolution. *Acta Crystallogr D Biol Crystallogr* **63**: 348-354.

Kisker, C., Schindelin, H., Baas, D., Retey, J., Meckenstock, R. U. & Kroneck, P. M., (1998) A structural comparison of molybdenum cofactor-containing enzymes. *FEMS Microbiol Rev* **22**: 503-521.

Kloer, D. P., Hagel, C., Heider, J. & Schulz, G. E., (2006) Crystal structure of ethylbenzene dehydrogenase from *Aromatoleum aromaticum*. *Structure* **14**: 1377-1388.

Kniemeyer, O. & Heider, J., (2001) Ethylbenzene dehydrogenase, a novel hydrocarbon-oxidizing molybdenum/iron-sulfur/heme enzyme. *J Biol Chem* **276**: 21381-21386.

Knight, V. V. & Blakemore, R., (1998) Reduction of diverse electron acceptors by *Aeromonas hydrophila*. *Arch Microbiol* **169**: 239-248.

Kovarova-Kovar, K. & Egli, T., (1998) Growth kinetics of suspended microbial cells: from single-substrate-controlled growth to mixed-substrate kinetics. *Microbiol Mol Biol Rev* **62**: 646-666.

Krafft, T., Bowen, A., Theis, F. & Macy, J. M., (2000) Cloning and sequencing of the genes encoding the periplasmic-cytochrome *b*-containing selenate reductase of *Thauera selenatis*. *DNA Seq* **10**: 365-377.

Krissinel, E. & Henrick, K., (2004) Secondary-structure matching (SSM), a new tool for fast protein structure alignment in three dimensions. *Acta Crystallogr D Biol Crystallogr* **60**: 2256-2268.

Lanciano, P., Vergnes, A., Grimaldi, S., Guigliarelli, B. & Magalon, A., (2007) Biogenesis of a respiratory complex is orchestrated by a single accessory protein. *J Biol Chem* **282**: 17468-17474.

Lange, C. & Hunte, C., (2002) Crystal structure of the yeast cytochrome bc_1 complex with its bound substrate cytochrome *c*. *Proc Natl Acad Sci U S A* **99**: 2800-2805.

Leaver, J. T., (2008) The enzymology and physiology of nitrate and selenate reduction/respiration in *Enterobacter cloacae* SLD1a-1 and *Aeromonas hydrophila* ATCC7966. University of Newcastle PhD Thesis, Faculty of Medical Sciences pp. 238.

Leaver, J. T., Richardson, D. J. & Butler, C. S., (2008) *Enterobacter cloacae* SLD1a-1 gains a selective advantage from selenate reduction when growing in nitrate-depleted anaerobic environments. *J Ind Microbiol Biotechnol*.

Leitch, F. A., Brown, K. R. & Pettigrew, G. W., (1985) Complexity in the redox titration of the dihaem cytochrome *c*4. *Biochim Biophys Acta* **808**: 213-218.

Lie, T. J., Godchaux, W. & Leadbetter, E. R., (1999) Sulfonates as terminal electron acceptors for growth of sulfite-reducing bacteria (*Desulfitobacterium* spp.) and sulfate-reducing bacteria: effects of inhibitors of sulfidogenesis. *Appl Environ Microbiol* **65**: 4611-4617.

Lledo, B., Martinez-Espinosa, R. M., Marhuenda-Egea, F. C. & Bonete, M. J., (2004) Respiratory nitrate reductase from haloarchaeon *Haloferax mediterranei*: biochemical and genetic analysis. *Biochim Biophys Acta* **1674**: 50-59.

Lloyd, J. R. & Lovley, D. R., (2001) Microbial detoxification of metals and radionuclides. *Curr Opin Biotechnol* **12**: 248-253.

Lortie, L., Gould, W. D., Rajan, S., McCready, R. G. & Cheng, K. J., (1992) Reduction of Selenate and Selenite to Elemental Selenium by a *Pseudomonas stutzeri* Isolate. *Appl Environ Microbiol* **58**: 4042-4044.

Losi, M. E. & Frankenberger, W. T., (1997) Reduction of Selenium Oxyanions by *Enterobacter cloacae* SLD1a-1: Isolation and Growth of the Bacterium and Its Expulsion of Selenium Particles. *Appl Environ Microbiol* **63**: 3079-3084.

Louie, T. M. & Mohn, W. W., (1999) Evidence for a chemiosmotic model of dehalorespiration in *Desulfomonile tiedjei* DCB-1. *J Bacteriol* **181**: 40-46.

Lovley, D. R., Holmes, D. E. & Nevin, K. P., (2004) Dissimilatory Fe(III) and Mn(IV) reduction. *Adv Microb Physiol* **49**: 219-286.

Macy, J. M., Michel, T. A. & Kirsch, D. G., (1989) Selenate reduction by a *Pseudomonas species*: a new mode of anaerobic respiration. *FEMS Microbiol Lett* **52**: 195-198.

Macy, J. M., Rech, S., Auling, G., Dorsch, M., Stackebrandt, E. & Sly, L. I., (1993) Thauera selenatis gen. nov., sp. nov., a member of the beta subclass of Proteobacteria with a novel type of anaerobic respiration. *International journal of systematic bacteriology* **43**: 135-142.

Magalon, A., Rothery, R. A., Lemesle-Meunier, D., Frixon, C., Weiner, J. H. & Blasco, F., (1998) Inhibitor binding within the NarI subunit (cytochrome b_{nr}) of *Escherichia coli* nitrate reductase A. *J Biol Chem* **273**: 10851-10856.

Malarte, G., Leroy, G., Lojou, E., Abergel, C., Bruschi, M. & Giudici-Orticoni, M. T., (2005) Insight into molecular stability and physiological properties of the diheme cytochrome CYC_{41} from the acidophilic bacterium *Acidithiobacillus ferrooxidans*. *Biochemistry* **44**: 6471-6481.

Martinez-Espinosa, R. M., Dridge, E. J., Bonete, M. J., Butt, J. N., Butler, C. S., Sargent, F. & Richardson, D. J., (2007) Look on the positive side! The orientation, identification and bioenergetics of 'Archaeal' membrane-bound nitrate reductases. *FEMS Microbiol Lett* **276**: 129-139.

McCrindle, S. L., Kappler, U. & McEwan, A. G., (2005) Microbial dimethylsulfoxide and trimethylamine-N-oxide respiration. *Adv Microb Physiol* **50**: 147-198.

McDevitt, C. A., Hanson, G. R., Noble, C. J., Cheesman, M. R. & McEwan, A. G., (2002a) Characterization of the redox centers in dimethyl sulfide dehydrogenase from *Rhodovulum sulfidophilum*. *Biochemistry* **41**: 15234-15244.

McDevitt, C. A., Hugenholtz, P., Hanson, G. R. & McEwan, A. G., (2002b) Molecular analysis of dimethyl sulphide dehydrogenase from *Rhodovulum sulfidophilum*: its place in the dimethyl sulphoxide reductase family of microbial molybdopterin-containing enzymes. *Mol Microbiol* **44**: 1575-1587.

McEwan, A. G., Ferguson, S. J. & Jackson, J. B., (1983) Electron flow to dimethylsulphoxide or trimethylamine-N-oxide generates a membrane potential in *Rhodopseudomonas capsulata*. *Arch Microbiol* **136**: 300-305.

McEwan, A. G., Ridge, J. P., McDevitt, C. A. & Hugenholtz, P., (2002) The DMSO reductase family of microbial molybdenum enzymes; Molecular properties and role in the dissimilatory reduction of toxic elements. *Geomicrobiology Journal* **19**: 3-21.

Moir, J. W., Baratta, D., Richardson, D. J. & Ferguson, S. J., (1993) The purification of a cd_1-type nitrite reductase from, and the absence of a copper-type nitrite reductase from, the aerobic denitrifier *Thiosphaera pantotropha*; the role of pseudoazurin as an electron donor. *Eur J Biochem* **212**: 377-385.

Monod, J., (1942) *Recherches sur la croissance des cultures bactâeriennes,* p. [211]. Hermann, Paris.

Najmudin, S., Gonzalez, P. J., Trincao, J., Coelho, C., Mukhopadhyay, A., Cerqueira, N. M., Romao, C. C., Moura, I., Moura, J. J., Brondino, C. D. & Romao, M. J., (2008) Periplasmic nitrate reductase revisited: a sulfur atom completes the sixth coordination of the catalytic molybdenum. *J Biol Inorg Chem* **13**: 737-753.

Nakagawa, S., Nakamura, S., Inagaki, F., Takai, K., Shirai, N. & Sako, Y., (2004) *Hydrogenivirga caldilitoris* gen. nov., sp. nov., a novel extremely thermophilic, hydrogen- and sulfur-oxidizing bacterium from a coastal hydrothermal field. *Int J Syst Evol Microbiol* **54**: 2079-2084.

Narasingarao, P. & Haggblom, M. M., (2006) *Sedimenticola selenatireducens,* gen. nov., sp. nov., an anaerobic selenate-respiring bacterium isolated from estuarine sediment. *Syst Appl Microbiol* **29**: 382-388.

Nicholls, D. G. & Ferguson, S. J., (2002) *Bioenergetics,* p. 288. Academic Press.

Oremland, R. S., Blum, J. S., Culbertson, C. W., Visscher, P. T., Miller, L. G., Dowdle, P. & Strohmaier, F. E., (1994) Isolation, Growth, and Metabolism of an

Obligately Anaerobic, Selenate-Respiring Bacterium, Strain SES-3. *Appl Environ Microbiol* **60**: 3011-3019.

Oremland, R. S., Herbel, M. J., Blum, J. S., Langley, S., Beveridge, T. J., Ajayan, P. M., Sutto, T., Ellis, A. V. & Curran, S., (2004) Structural and spectral features of selenium nanospheres produced by Se-respiring bacteria. *Appl Environ Microbiol* **70**: 52-60.

Osyczka, A., Zhang, H., Mathe, C., Rich, P. R., Moser, C. C. & Dutton, P. L., (2006) Role of the PEWY glutamate in hydroquinone-quinone oxidation-reduction catalysis in the Q_o Site of cytochrome bc_1. *Biochemistry* **45**: 10492-10503.

Otten, M. F., Stork, D. M., Reijnders, W. N., Westerhoff, H. V. & Van Spanning, R. J., (2001) Regulation of expression of terminal oxidases in *Paracoccus denitrificans*. *Eur J Biochem* **268**: 2486-2497.

Page, C. C., Moser, C. C., Chen, X. & Dutton, P. L., (1999) Natural engineering principles of electron tunnelling in biological oxidation-reduction. *Nature* **402**: 47-52.

Palmer, K. L., Brown, S. A. & Whiteley, M., (2007) Membrane-bound nitrate reductase is required for anaerobic growth in cystic fibrosis sputum. *J Bacteriol* **189**: 4449-4455.

Pearson, I. V., Page, M. D., van Spanning, R. J. & Ferguson, S. J., (2003) A mutant of *Paracoccus denitrificans* with disrupted genes coding for cytochrome c_{550} and pseudoazurin establishes these two proteins as the in vivo electron donors to cytochrome cd_1 nitrite reductase. *J Bacteriol* **185**: 6308-6315.

Pettigrew, G. W. & Brown, K. R., (1988) Free and membrane-bound forms of bacterial cytochrome *c*4. *Biochem J* **252**: 427-435.

Pettigrew, G. W. & Moore, G. R., (1987) *Cytochromes c : biological aspects*, p. 282p. Springer, Berlin.

Pittman, M. S. & Kelly, D. J., (2005) Electron transport through nitrate and nitrite reductases in *Campylobacter jejuni*. *Biochem Soc Trans* **33**: 190-192.

Potter, L., Angove, H., Richardson, D. & Cole, J., (2001) Nitrate reduction in the periplasm of gram-negative bacteria. *Adv Microb Physiol* **45**: 51-112.

Pugsley, A. P., (1993) The complete general secretory pathway in gram-negative bacteria. *Microbiol Rev* **57**: 50-108.

Qiu, Y., Zhang, R., Binkowski, T. A., Tereshko, V., Joachimiak, A. & Kossiakoff, A., (2008) The 1.38 Å crystal structure of DmsD protein from *Salmonella typhimurium*, a proofreading chaperone on the Tat pathway. *Proteins* **71**: 525-533.

Rainey, F. A., Kelly, D. P., Stackebrandt, E., Burghardt, J., Hiraishi, A., Katayama, Y. & Wood, A. P., (1999) A re-evaluation of the taxonomy of *Paracoccus denitrificans* and a proposal for the combination *Paracoccus pantotrophus* comb. nov. *International Journal of Systematic Bacteriology* **49**: 645-651.

Rech, S. A. & Macy, J. M., (1992) The terminal reductases for selenate and nitrate respiration in *Thauera selenatis* are two distinct enzymes. *J Bacteriol* **174**: 7316-7320.

Richardson, D. & Sawers, G., (2002) Structural biology. PMF through the redox loop. *Science* **295**: 1842-1843.

Richardson, D. J., (2000) Bacterial respiration: a flexible process for a changing environment. *Microbiology* **146 (Pt 3)**: 551-571.

Richardson, D. J., Berks, B. C., Russell, D. A., Spiro, S. & Taylor, C. J., (2001) Functional, biochemical and genetic diversity of prokaryotic nitrate reductases. *Cell Mol Life Sci* **58**: 165-178.

Richardson, D. J. & Watmough, N. J., (1999) Inorganic nitrogen metabolism in bacteria. *Curr Opin Chem Biol* **3**: 207-219.

Ridley, H., Watts, C. A., Richardson, D. J. & Butler, C. S., (2006a) Development of a viologen-based microtiter plate assay for the analysis of oxyanion reductase activity: application to the membrane-bound selenate reductase from *Enterobacter cloacae* SLD1a-1. *Anal Biochem* **358**: 289-294.

Ridley, H., Watts, C. A., Richardson, D. J. & Butler, C. S., (2006b) Resolution of distinct membrane-bound enzymes from *Enterobacter cloacae* SLD1a-1 that are responsible for selective reduction of nitrate and selenate oxyanions. *Appl Environ Microbiol* **72**: 5173-5180.

Robertson, L. A. & Kuenen, J. G., (1983) *Thiosphaera-Pantotropha* Gen-Nov Sp-Nov, a Facultatively Anaerobic, Facultatively Autotrophic Sulfur Bacterium. *Journal of General Microbiology* **129**: 2847-2855.

Rodrigue, A., Chanal, A., Beck, K., Muller, M. & Wu, L. F., (1999) Co-translocation of a periplasmic enzyme complex by a hitchhiker mechanism through the bacterial tat pathway. *J Biol Chem* **274**: 13223-13228.

Roldan, M. D., Sears, H. J., Cheesman, M. R., Ferguson, S. J., Thomson, A. J., Berks, B. C. & Richardson, D. J., (1998) Spectroscopic characterization of a novel multiheme *c*-type cytochrome widely implicated in bacterial electron transport. *J Biol Chem* **273**: 28785-28790.

Rothery, R. A., Bertero, M. G., Cammack, R., Palak, M., Blasco, F., Strynadka, N. C. & Weiner, J. H., (2004) The catalytic subunit of *Escherichia coli* nitrate reductase A contains a novel [4Fe-4S] cluster with a high-spin ground state. *Biochemistry* **43**: 5324-5333.

Sabaty, M., Avazeri, C., Pignol, D. & Vermeglio, A., (2001) Characterization of the reduction of selenate and tellurite by nitrate reductases. *Appl Environ Microbiol* **67**: 5122-5126.

Sambasivarao, D., Scraba, D. G., Trieber, C. & Weiner, J. H., (1990) Organization of dimethyl sulfoxide reductase in the plasma membrane of *Escherichia coli*. *J Bacteriol* **172**: 5938-5948.

Santini, C. L., Ize, B., Chanal, A., Muller, M., Giordano, G. & Wu, L. F., (1998) A novel sec-independent periplasmic protein translocation pathway in Escherichia coli. *EMBO J* **17**: 101-112.

Sargent, F., Bogsch, E. G., Stanley, N. R., Wexler, M., Robinson, C., Berks, B. C. & Palmer, T., (1998) Overlapping functions of components of a bacterial Sec-independent protein export pathway. *EMBO J* **17**: 3640-3650.

Sazanov, L. A. & Hinchliffe, P., (2006) Structure of the hydrophilic domain of respiratory complex I from *Thermus thermophilus*. *Science* **311**: 1430-1436.

Schindelin, H., Kisker, C., Hilton, J., Rajagopalan, K. V. & Rees, D. C., (1996) Crystal structure of DMSO reductase: redox-linked changes in molybdopterin coordination. *Science* **272**: 1615-1621.

Schroder, I., Rech, S., Krafft, T. & Macy, J. M., (1997) Purification and characterization of the selenate reductase from *Thauera selenatis*. *J Biol Chem* **272**: 23765-23768.

Schutz, M., Brugna, M., Lebrun, E., Baymann, F., Huber, R., Stetter, K. O., Hauska, G., Toci, R., Lemesle-Meunier, D., Tron, P., Schmidt, C. & Nitschke, W., (2000) Early evolution of cytochrome *bc* complexes. *J Mol Biol* **300**: 663-675.

Sears, H. J., Sawers, G., Berks, B. C., Ferguson, S. J. & Richardson, D. J., (2000) Control of periplasmic nitrate reductase gene expression (*napEDABC*) from *Paracoccus pantotrophus* in response to oxygen and carbon substrates. *Microbiology* **146 (Pt 11)**: 2977-2985.

Sellars, M. J., Hall, S. J. & Kelly, D. J., (2002) Growth of *Campylobacter jejuni* supported by respiration of fumarate, nitrate, nitrite, trimethylamine-N-oxide, or dimethyl sulfoxide requires oxygen. *J Bacteriol* **184**: 4187-4196.

Seshadri, R., Joseph, S. W., Chopra, A. K., Sha, J., Shaw, J., Graf, J., Haft, D., Wu, M., Ren, Q., Rosovitz, M. J., Madupu, R., Tallon, L., Kim, M., Jin, S., Vuong, H., Stine, O. C., Ali, A., Horneman, A. J. & Heidelberg, J. F., (2006) Genome sequence of *Aeromonas hydrophila* ATCC 7966T: jack of all trades. *J Bacteriol* **188**: 8272-8282.

Simon, J., (2002) Enzymology and bioenergetics of respiratory nitrite ammonification. *FEMS Microbiol Rev* **26**: 285-309.

Song, B. & Ward, B., (2003) Nitrite reductase genes in halobenzoate degrading denitrifying bacteria. *FEMS Microbiol Ecology* **43**: 349-357.

Stanbury, P. F., Whitaker, A. & Hall, S. J., (1995) *Principles of fermentation technology*, p. xviii, 357. Pergamon, Oxford.

Stanley, N. R., Sargent, F., Buchanan, G., Shi, J., Stewart, V., Palmer, T. & Berks, B. C., (2002) Behaviour of topological marker proteins targeted to the Tat protein transport pathway. *Mol Microbiol* **43**: 1005-1021.

Stevens, J. M., Daltrop, O., Allen, J. W. & Ferguson, S. J., (2004) *C*-type cytochrome formation: chemical and biological enigmas. *Acc Chem Res* **37**: 999-1007.

Stevens, J. M., Uchida, T., Daltrop, O. & Ferguson, S. J., (2005) Covalent cofactor attachment to proteins: cytochrome *c* biogenesis. *Biochem Soc Trans* **33**: 792-795.

Stock, D., Gibbons, C., Arechaga, I., Leslie, A. G. & Walker, J. E., (2000) The rotary mechanism of ATP synthase. *Curr Opin Struct Biol* **10**: 672-679.

Stock, D., Leslie, A. G. & Walker, J. E., (1999) Molecular architecture of the rotary motor in ATP synthase. *Science* **286**: 1700-1705.

Stolz, J. F., Basu, P., Santini, J. M. & Oremland, R. S., (2006) Arsenic and selenium in microbial metabolism. *Annu Rev Microbiol* **60**: 107-130.

Stolz, J. F. & Oremland, R. S., (1999) Bacterial respiration of arsenic and selenium. *FEMS Microbiol Rev* **23**: 615-627.

Stroh, A., Anderka, O., Pfeiffer, K., Yagi, T., Finel, M., Ludwig, B. & Schagger, H., (2004) Assembly of respiratory complexes I, III, and IV into NADH oxidase supercomplex stabilizes complex I in *Paracoccus denitrificans*. *J Biol Chem* **279**: 5000-5007.

Swank, R. T. & Burris, R. H., (1969) Purification and properties of cytochromes *c* of *Azotobacter vinelandii*. *Biochim Biophys Acta* **180**: 473-489.

Switzer Blum, J., Burns Bindi, A., Buzzelli, J., Stolz, J. F. & Oremland, R. S., (1998) *Bacillus arsenicoselenatis*, sp. nov., and *Bacillus selenitireducens*, sp. nov.: two haloalkaliphiles from Mono Lake, California that respire oxyanions of selenium and arsenic. *Arch Microbiol* **171**: 19-30.

Takai, K., Hirayama, H., Sakihama, Y., Inagaki, F., Yamato, Y. & Horikoshi, K., (2002) Isolation and metabolic characteristics of previously uncultured members of the order *Aquificales* in a subsurface gold mine. *Appl Environ Microbiol* **68**: 3046-3054.

Takai, K., Kobayashi, H., Nealson, K. H. & Horikoshi, K., (2003) *Sulfurihydrogenibium subterraneum* gen. nov., sp. nov., from a subsurface hot aquifer. *Int J Syst Evol Microbiol* **53**: 823-827.

Tavares, P., Pereira, A. S., Moura, J. J. & Moura, I., (2006) Metalloenzymes of the denitrification pathway. *J Inorg Biochem* **100**: 2087-2100.

Taylor, M. A. & Jackson, J. B., (1985) Threshold dependence of bacterial growth on the protonmotive force. *FEBS Letters* **192**: 199-203.

Thierbach, G. & Reichenbach, H., (1981) Myxothiazol, a new inhibitor of the cytochrome *b*-c_1 segment of the respiratory chain. *Biochim Biophys Acta* **638**: 282-289.

Thony-Meyer, L., (1997) Biogenesis of respiratory cytochromes in bacteria. *Microbiol Mol Biol Rev* **61**: 337-376.

Thony-Meyer, L., (2002) Cytochrome *c* maturation: a complex pathway for a simple task? *Biochem Soc Trans* **30**: 633-638.

Thorell, H. D., Stenklo, K., Karlsson, J. & Nilsson, T., (2003) A gene cluster for chlorate metabolism in *Ideonella dechloratans*. *Appl Environ Microbiol* **69**: 5585-5592.

Tomcova, I., Branca, R. M., Bodo, G., Bagyinka, C. & Smatanova, I. K., (2006) Cross-crystallization method used for the crystallization and preliminary diffraction analysis of a novel di-haem cytochrome *c*4. *Acta Crystallogr Sect F Struct Biol Cryst Commun* **62**: 820-824.

Tranier, S., Iobbi-Nivol, C., Birck, C., Ilbert, M., Mortier-Barriere, I., Mejean, V. & Samama, J. P., (2003) A novel protein fold and extreme domain swapping in the dimeric TorD chaperone from *Shewanella massilia*. *Structure* **11**: 165-174.

Tsukihara, T., Aoyama, H., Yamashita, E., Tomizaki, T., Yamaguchi, H., Shinzawa-Itoh, K., Nakashima, R., Yaono, R. & Yoshikawa, S., (1996) The whole structure of the 13-subunit oxidized cytochrome *c* oxidase at 2.8 A. *Science* **272**: 1136-1144.

Van Ark, G. & Berden, J. A., (1977) Binding of HQNO to beef-heart sub-mitochondrial particles. *Biochim Biophys Acta* **459**: 119-127.

van de Pas, B. A., Smidt, H., Hagen, W. R., van der Oost, J., Schraa, G., Stams, A. J. & de Vos, W. M., (1999) Purification and molecular characterization of ortho-chlorophenol reductive dehalogenase, a key enzyme of halorespiration in *Desulfitobacterium dehalogenans*. *J Biol Chem* **274**: 20287-20292.

Vinceti, M., Wei, E. T., Malagoli, C., Bergomi, M. & Vivoli, G., (2001) Adverse health effects of selenium in humans. *Rev Environ Health* **16**: 233-251.

Watts, C. A., Ridley, H., Condie, K. L., Leaver, J. T., Richardson, D. J. & Butler, C. S., (2003) Selenate reduction by *Enterobacter cloacae* SLD1a-1 is catalysed by a molybdenum-dependent membrane-bound enzyme that is distinct from the membrane-bound nitrate reductase. *FEMS Microbiol Lett* **228**: 273-279.

Weiner, J. H., Bilous, P. T., Shaw, G. M., Lubitz, S. P., Frost, L., Thomas, G. H., Cole, J. A. & Turner, R. J., (1998) A novel and ubiquitous system for membrane targeting and secretion of cofactor-containing proteins. *Cell* **93**: 93-101.

Weingarten, R. A., Grimes, J. L. & Olson, J. W., (2008) Role of Campylobacter jejuni respiratory oxidases and reductases in host colonization. *Appl Environ Microbiol* **74**: 1367-1375.

Yee, N. & Kobayashi, D. Y., (2008) Molecular genetics of selenate reduction by *Enterobacter cloacae* SLD1a-1. *Adv Appl Microbiol* **64**: 107-123, 102 p following 264.

Yoshida, M., Masuda, S., Nagashima, K. V., Vermeglio, A., Shimada, K. & Matsuura, K., (2001) In vitro and in vivo electron transfer to the triheme cytochrome subunit bound to the photosynthetic reaction center complex in the purple bacterium *Rhodovulum sulfidophilum*. *Biochim Biophys Acta* **1506**: 23-30.

Yoshimatsu, K., Araya, O. & Fujiwara, T., (2007) *Haloarcula marismortui* cytochrome *b*-561 is encoded by the narC gene in the dissimilatory nitrate reductase operon. *Extremophiles* **11**: 41-47.

Zannoni, D., (2004) *Respiration in archaea and bacteria*, p. 2 v. Kluwer Academic, Dordrecht ; London.

Zwietering, M. H., Jongenburger, I., Rombouts, F. M. & Van't Riet, K., (1990) Modeling of the bacterial growth curve. *Appl Environ Microbiol* **56**: 1875-1881.

Zwietering, M. H., Rombouts, F. M. & Van't Riet, K., (1992) Comparison of definitions of the lag phase and the exponential phase in bacterial growth. *J Appl Bacteriol* **72**: 139-145.

8. Appendix

Luria-Bertani (LB) Broth	g/L
Tryptone	10
Yeast extract	5
NaCl	5

Hungates Media	g/10 L
NaCl	12
KCl	3
NH_4Cl	3
KH_2PO_4	2
Na_2SO_4	3
$NaHCO_3$	6
Yeast extract	10

SL8 Trace elements	mg/L
EDTA-2Na	5200
$FeCl_3.H_2O$	1500
$ZnCl_2$	70
$MnCl_2.4H_2O$	100
H_3BO_3	62
$CoCl_2.6H_2O$	190
Na_2MoO_4	36
$CuCl_2.2H_2O$	17
$NiCl_2.6H_2O$	24

Vitamin solution for Hungates	mg/L
Folic acid	2
Riboflavin	5
Thiamine-HCl	5
Pantothenate	5
Nicotinamide	5
Vitamin B_{12}	0.1
Biotin	5
Pyridoxine-HCl	2
P-aminobenzoate	5

Minimal media #356	g/L
Na_2HPO_4	7.9
KH_2PO_4	1.5
NH_4Cl	0.3
$MgSO_4.7H_2O$	0.1

Yeast extract	1

SL10 Trace elements	mg/L
$ZnCl_2$	70
$MnCl_2.4H_2O$	100
H_3BO_3	6
$CoCl_2.6H_2O$	190
Na_2MoO_4	36
$CuCl_2.2H_2O$	2
$NiCl_2.6H_2O$	24

Then add 1.5 g $FeCl_2.4H_2O$ in 10 ml 23% HCl.

TFB1	g/100 ml
$C_2H_3O_2Na$	0.25
$CaCl_2$	0.14
$MnCl_2$	0.99
$RbCl_2$	1.21
Glycerol	15 ml

pH to 5.8 with acetic acid.

TFB2	g/100 ml
$CaCl_2$	1.07
$RbCl_2$	0.12
Glycerol	15 ml
MOPS (1M stock)	1 ml

pH to 6.5 with KOH.

5 x TBE	g/L
Tris	54
Boric acid	27.5
0.5 M EDTA, pH 8	20 ml

10 x CAPS buffer	g/L
CAPS	22.13

pH to 11 with 2 M NaOH.

SDS-PAGE gels - resolving layer

30% Acrylamide	5 ml
Water	2.3 ml
1.5M Tris pH 8.8	2.5 ml
10% SDS	100 µl
TEMED	5 µl
APS	100 µl

SDS-PAGE gels – stacking layer

30% Acrylamide	415 µl
Water	1.7 ml
0.5M Tris pH 6.8	315 µl
10% SDS	25 µl
TEMED	2 µl
APS	20 µl

SDS running buffer	g/L
Tris	15.1
Glycine	94
10% SDS	50 ml

Native gels

30% Acrylamide	5 ml
Water	2.4 ml
1.5M Tris pH 8.8	2.5 ml
TEMED	8 µl
APS	100 µl

Native running buffer as SDS running buffer but without SDS.

Native loading dye

1 M Tris pH 8.5	62.5 µl
Glycerol	200 µl
H_2O	687 µl
1% bromophenol blue	10 µl

Posters and presentations

EBEC European Bioenergetics Conference, Moscow, Russia, 2006 Abstract and poster presentation:

Lowe EC, Watts CA, Richardson DJ, Santini JM, Singleton I, Butler CS.

The bioenergetics of selenate respiration in *Thauera selenatis*. Published in Biochimica et Biophysica Acta – Bioenergetics. 2006: 203-203 Supplement: S

International Nitrogen Cycle Meeting, York, UK, 2007. Abstract and presentation – Electron transfer during selenate respiration in *Thauera selenatis*.